Assessment of Corn and Starch Based Biochar as Reinforcing Fillers in the Rubber Composite Industry

By
Nicole Bélanger

Department of Bioresource Engineering
Faculty of Agriculture and Environmental Sciences
Macdonald Campus of McGill University
Sainte-Anne-de-Bellevue, Québec, Canada

Fall 2022

A thesis submitted to McGill University in partial fulfilment of the requirements for the degree of Master of Science.

Copyright © Nicole Bélanger 2022

Abstract

Fillers are essential in rubber-based materials, providing enhanced physical, mechanical, thermal and barrier properties, thereby improving the performance and durability of the resulting rubber products. For over a century, carbon black, a highly processed petrochemical derived material has been the filler of choice. Though it has desirable physicochemical traits which allow it to bind effectively with rubber, it is also carcinogenic and problematic for the environment. Thus, the search continues for suitable filler alternatives, as the rubber industry seeks to green their operations and products.

Biochar is one material with potential to be effective as a green, biodegradable filler. It is produced from heating bio-based feedstocks in a low oxygen environment, which increases its carbon content while reducing the volatile matter. Since biochar can be synthesized from renewable feedstocks which are often by-products of other industries, its application as a reinforcing filler has potential to both reduce waste and avoid use of petrochemical materials. However, the physicochemical properties of biochar are highly dependent on the feedstock and pyrolysis parameters.

In the first study, corn-based feedstocks were evaluated and compared to N772 grade carbon black to determine their suitability as reinforcing fillers in styrene butadiene rubber (SBR). Corn cob, corn stover and corn starch were pyrolyzed at 700 °C for 1 h, at a heating rate of 50 °C min^{-1} under nitrogen gas and refined prior to blending with SBR. The biochar was evaluated in terms of size, structure, surface chemistry and composition and its performance in SBR was evaluated in terms of cure characteristics, tensile properties, and dynamic mechanical properties. Of all biochar fillers studied, corn stover based biochar had the greatest reinforcing effect in SBR. However, there was relatively little difference between the performance of stover and cob biochar, suggesting the two feedstocks could be blended without significant loss in performance. Meanwhile, biochar from corn starch was also an effective filler with a high degree of crosslinking, though the composites were more brittle compared to cob, stover and N772. Though the biochar filled composites had lower dispersion and refinement indexes compared to N772 carbon black composites, all showed a marked improvement in reinforcement compared to unfilled rubber, highlighting their potential to become effective fillers with further engineering.

A subsequent study, on starch-based biochar was then conducted with 2 objectives. The first objective was to examine the effects of the ratio of amylose (linear structure) to amylopectin

(branched structure) type starch on the properties of the biochar. The second goal was to evaluate the performance of starch-based biochar treated through different physical activations, which have been known to improve the performance of biochar in other applications. Thus, three sets of biochar from high amylose, high amylopectin, and regular blend (73/27 amylopectin to amylose ratio) starch were produced and activated via 4 different physical activation processes. The processes involved pyrolysis with (1) N_2 only, (2) steam and N_2, (3) a biochar-water slurry (SteamT2) and (4) CO_2 only. The results indicated that the ratio of amylose-amylopectin had little effect on the physicochemical properties and performance of the biochar. The activations, however, had a significant impact on the physicochemical properties, mainly the pore size, and the carbon, oxygen and ash content of the biochar. Composites filled with biochar activated with steam and with N_2 only pyrolysis had the most consistent performance while several composites from CO_2 activated biochar outperformed the N772 filled composites. Conversely, composites with SteamT2 activated biochar were highly brittle and performed poorly, despite the biochar having a high carbon content (>90%) and a low ash content (<2%).

Résumé

Les charges sont essentielles dans les matériaux caoutchouc car elles confèrent des propriétés physiques accrue. Le noir de carbone, un matériau dérivé de la pétrochimie hautement transformé, est la charge de choix. Bien qu'il présente des caractéristiques physicochimiques permettant de se lier au caoutchouc, il est également cancérigène et problématique pour l'environnement.

Le biochar est un matériau qui pourrait s'avérer efficace comme charge verte et biodégradable. Il est produit en chauffant des matières premières biosourcées dans un environnement pauvre en oxygène, ce qui augmente sa teneur en carbone tout en réduisant les matières volatiles. Comme il peut être synthétisé à partir de matières renouvelables, son application comme charge de renforcement a le potentiel de réduire les déchets et d'éviter l'utilisation de matériaux pétrochimiques. Cependant, leurs propriétés physico-chimiques dépendent fortement de la matière première et des paramètres de pyrolyse.

Dans la première étude, les matières premières à base de maïs ont été évaluées et comparées au noir de carbone N772 afin de déterminer leur aptitude à servir de charge de renforcement dans le caoutchouc styrène-butadiène (SBR). L'épi de maïs, la canne de maïs et l'amidon de maïs ont été pyrolysés à 700 °C pendant 1 h, à une vitesse de chauffage de 50 °C min^{-1} sous N_2, et raffinés avant d'être mélangés au SBR. Les 3 types de biochar sont désignés par la présente sous les noms Cob$_{700}$, Stover$_{700}$ et Starch$_{700}$. Ils ont été évalués en termes de taille, de structure, de chimie de surface et de composition, et leur performance dans le SBR a été évaluée en termes de caractéristiques de durcissement, de propriétés de traction et de propriétés mécaniques dynamiques. Parmi les charges de biochar étudiées, le Stover$_{700}$ a eu le plus grand effet de renforcement dans le SBR. Cependant, il y avait peu de différence entre les performances du Stover$_{700}$ et du Cob$_{700}$, ce qui suggère que leurs matières premières pourraient être mélangées sans perte significative de performance. Parallèlement, les composites de Starch$_{700}$ avaient un degré élevé de réticulation, mais ils étaient également les plus fragiles parmi tous. Bien que les composites de biochar présentent des indices de dispersion et de raffinement inférieurs à ceux des composites de N772, tous ont montré une amélioration du renforcement par rapport au caoutchouc non chargé, ce qui souligne leur potentiel à devenir des charges efficaces.

Une dernière étude sur le biochar à base d'amidon a été menée avec deux objectives : (1) d'examiner les effets du rapport amylose (structure linéaire) et amylopectine (structure ramifié) sur les propriétés du biochar, et (2) d'évaluer la performance du biochar à base d'amidon traité par différentes activations physiques. Trois types de biochars provenant d'amidon ~99% amylose, ~99% amylopectine et d'un mélange régulier (ratio amylopectine/amylose 73/27) ont été produits et activés par 4 processus d'activation physique différents. Ces processus impliquaient la pyrolyse avec (1) N_2 seulement, (2) vapeur et N_2, (3) une boue de biochar - eau (SteamT2) et (4) CO_2 seulement. Les résultats ont indiqué que le rapport amylose-amylopectine avait peu d'effet sur les propriétés physicochimiques et la performance du biochar. Les activations, cependant, ont eu un impact significatif sur les propriétés, principalement la taille des pores, et la teneur en carbone, oxygène et cendres du biochar. Les composites de charges de biochar activées par la vapeur et N_2 et par la pyrolyse N_2 seulement ont eu les performances les plus cohérentes, tandis que plusieurs composites de biochar activé par CO_2 ont surpassé les composites de N772. À l'inverse, les composites de biochar activé par SteamT2 étaient très fragiles et avaient une performance médiocre, bien que le biochar ait une teneur élevée en carbone (>90%) et faible en cendres (<2%).

Table of Contents

List of Tables

List of Figures

Acknowledgements

I would like to begin with expressing my sincere gratitude to my supervisor, Professor Marie-Josée Dumont, for her support and encouragement throughout my graduate studies. I was and continue to be inspired by her research and am grateful to have had the opportunity to collaborate with her on this project. I would also like to thank my co-supervisor, Professor Shiv Prasher, for his involvement in the project and his input in the review process.

I am grateful towards Mr. Yvan Gariépy for the excellent technical support he provided, helping the experimental process remain efficient and effective. A thanks to Dr. Jiby Kudakasseril Kurian as well, for teaching me to use the experimental equipment and for providing helpful advice on the graduate research process. I would also like to extend my thanks to Ms. Aleksandra Djuric, for performing the BET surface area experiments and the laser diffraction particle size analysis and to the Laboratoire d'Analyse de la Biomasse, des Bioproduits et des Bioprocédés (LAB) (Sherbrooke University) for performing the elemental analysis. Thanks to Dr. Hatem Titi for training me in powder XRD and to the Facility for Electron Microscopy Research (McGill University) for providing some of the SEM imaging.

I would like to thank the team at Michelin in Greenville, South Carolina for their work synthesizing and testing the rubber composites at their facility. A sincere thank you to Dr. Constantine Y. Khripin and Dr. Jeremy J. Mehlem for their expert advice and contributions to the manuscript review process.

I am thankful for the financial contributions which made this project possible, provided by Michelin Inc. and the Natural Science and Engineering Research council of Canada (NSERC) through the Collaborative Research and Development Grants (CRD).

Finally, I would like to thank my family and partner for their full support and encouragement of me pursuing graduate studies.

Contribution of Authors

This thesis is submitted as a manuscript-based thesis. The candidate, Nicole Bélanger, developed and conducted experiments, specifically the production and characterization of the biochar fillers. She also performed data analysis on the biochar and rubber composites and wrote the manuscripts forming the thesis. Professor Marie-Josée Dumont provided the resources for the research project, including funding acquisition, the research planning and supervision and the editing and review of the manuscripts and thesis prior to submission. As co-supervisor, Professor Shiv Prasher was also responsible for the review and editing of the manuscripts and thesis. Mr. Yvan Gariépy ensured the functioning of the experimental equipment related to biochar production. Heidi Macek was involved in the experimental work and manuscript writing for the study in Chapter 3. Dr. Constantine Y. Khripin and Dr. Jeremy J. Mehlem provided technical expertise and feedback on the manuscripts. Matthew S. Francis, Reyda Lizette Bazan Cornejo and Shreya Thammana were involved in the rubber composite formation process. The reference information for the manuscripts currently published, or submitted for publication are included below:

1. N. Bélanger, S. Prasher, and M.-J. Dumont, 'Tailoring biochar production for use as a reinforcing bio-based filler in rubber composites: a review', *Polymer Plastics Technology and Materials*, pp. 1–22, Jun. 2022, doi: 10.1080/25740881.2022.2089584.
2. N. Bélanger, H. Macek, Y. Gariépy, M. Francis, S. Prasher, C.Y Khripin, J.J. Mehlem and M.-J. Dumont 'Evaluating Corn-based Biochar as an Alternative to Carbon Black in Styrene-Butadiene Rubber Composites', Jul. 2022 Submitted for publication.
3. N. Bélanger, H. Macek, Y. Gariépy, M. Francais, S. Prasher, R.L.B. Cornejo, S. Thammana, M. Francis, C.Y. Khripin, J.J. Mehlem and M.-J. Dumont 'Assessing Starch Based Biochar as a Renewable Filler in Styrene-Butadiene Rubber Composites', Jul. 2022

List of Abbreviations

Abbreviaton	**Definition**
Cob_{700}	Biochar produced from corn cob
DPG	diphenyl guanidine
FTIR	Fourier transform infrared spectroscopy
HA-CS	Biochar from high amylose cornstarch
HA -CS_{700}	Biochar from high amylose cornstarch, normal pyrolysis under N_2
$\text{HA-CS}_{700+CO2}$	Biochar from high amylose cornstarch, pyrolysis under CO_2
$\text{HA-CS}_{700+steam}$	Biochar from high amylose cornstarch, pyrolysis under Steam
$\text{HA-CS}_{700+steamT2}$	Biochar from high amylose cornstarch, pyrolysis under Steam (Type 2)
HAP-CS	Biochar from high amylopectin cornstarch
HAP-CS_{700}	Biochar from high amylopectin cornstarch, normal pyrolysis under N_2
$\text{HAP-CS}_{700+CO2}$	Biochar from high amylopectin cornstarch, pyrolysis under CO_2
$\text{HAP-CS}_{700+steam}$	Biochar from high amylopectin cornstarch, pyrolysis under Steam
$\text{HAP-CS}_{700+steamT2}$	Biochar from high amylopectin cornstarch, pyrolysis under Steam (Type 2)
N772	N772 carbon black
6PPD	N-(1,3-dimethylbutyl)-N’-phenyl-1,4-benzenediamine
R-CS	Biochar from regular cornstarch
R-CS_{700}	Biochar from regular cornstarch, normal pyrolysis under N_2
$\text{R-CS}_{700+CO2}$	Biochar from regular cornstarch, pyrolysis under CO_2
$\text{R-CS}_{700+steam}$	Biochar from regular cornstarch, pyrolysis under Steam
$\text{R-CS}_{700+steamT2}$	Biochar from regular cornstarch, pyrolysis under Steam (Type 2)
SAD	stearic acid
SBR	Styrene Butadiene Rubber
Starch_{700}	Biochar produced from cornstarch (regular cornstarch)
Steam	Steam activation
SteamT2	Steam slurry activation
Stover_{700}	Biochar produced from corn stover
TGA	Thermogravimetric Analysis
XRD	X Ray Diffraction
ZnO	zinc oxide

Chapter 1

Introduction

1.1 General Introduction

From tires to gaskets and seals, to gloves and protective footwear, rubber is in many of the products modern society depends on. The reliability of these important rubber materials is largely influenced by fillers, which enhance their strength and durability. The most common filler associated with rubber reinforcement is carbon black. Though carbon black has been produced since prehistoric times, its modern counterpart, produced from natural gas has beginnings dating back to 1870 [1]. Its rubber reinforcing properties were reportedly discovered in 1904 and it has been considered an essential component in most rubber formulations ever since [1]. It is produced though heating a hydrocarbon fuel with limited combustion at high temperatures, resulting in nanosized, spherical particles of carbon. These particles, when mixed with rubber, form crosslinks leading to the formation of bound rubber, which is critical in rubber reinforcement. Though it is an incredibly convenient material with decades of field research backing its performance, it has negative environmental implications, as it is produced from non-renewable petrochemical feedstocks and is a known carcinogen [2].

With climate change at the forefront and the rise of the circular economy movement, industries are incentivized to adapt their products and services to keep pace with the changing world. Several key players in the rubber industry have mentioned ambitious environmental targets. Michelin aims to develop a tire made from 100% sustainable materials by 2050 [3] while growth in the global green tires market is projected to increase from USD 89 billion to 196 billion by 2027 [4]. Fillers such as carbon black are among the many rubber components that could be replaced with greener alternatives. The industry has been actively exploring alternative biobased fillers, mainly derived from lignocellulosic sources. However, there are several compatibility issues with bio-based fillers which prevent them from becoming widespread in the rubber industry.

One bio-based material which has the potential to behave more like carbon black is biochar. Biochar is produced by heating bio-based feedstocks at elevated temperatures in low oxygen environments, reducing their volatile matter while increasing their carbon content. In addition to being synthesized from renewable feedstock, biochar production can be energy efficient, through reusing the generated syngas to form a continuous production process**.** Though biochar appears to share similar characteristics with carbon black, complications can arise as biochar properties are highly dependent on the feedstock material and the pyrolysis parameters used.

Previous studies from the last decade indicate that biochar produced from lignocellulosic feedstocks with low ash and high carbon content performs better than others [5–7]. The studies described in this thesis use corn and starch-based feedstocks. Corn was selected as it is a highly relevant crop in North America with an abundant source of lignocellulosic material, having 7.1-8.1 tonnes available per hectare of production [8, 9]. It has been studied before in reinforcing filler applications, through under different pyrolysis conditions. Starch has also shown interesting reinforcing properties in rubber but to the author’s knowledge, starch-based biochar has never before been tested in rubber. Starch is highly refined with a low ash content, which may provide beneficial properties upon increasing its carbon content through pyrolysis.

1.2 Study Objectives

The rubber industry needs to develop greener filler alternatives as part of their transition to more sustainable product development. Biochar is a material with the potential to perform well as a filler, however there is much to discover about the material, as its properties are highly dependent on the feedstock material and pyrolysis conditions. This thesis focuses on evaluating biochar produced from corn and starch-based sources to determine what the strengths and limitations are in using these feedstocks. In addition, physical activation methods are studied to determine whether they have a positive effect on the physicochemical properties of the biochar and its reinforcing capabilities in SBR. As such, the specific objectives of this study are:

1. To comprehensively review the literature on the production and treatment of biochar to determine the extent it can be tailored to have desirable filler characteristics
2. To examine and compare the performance of corn-based biochar from both refined corn starch and unrefined lignocellulosic parts of the corn plant (stalk and cob)
3. To study the influence of starch structure (amylose vs amylopectin) on the physicochemical properties of the resulting biochar and whether that impacts its performance in SBR composites

4. To study of influence of physical activations (using steam and/or CO_2) on the physicochemical properties of starch-based biochar, and whether that impacts its performance in SBR composites.

1.3 Organization of the Thesis

Chapter 2 provides a comprehensive literature review on the current understanding of rubber filler reinforcement. It also identifies potential tailoring processes on biochar to improve its physicochemical properties for the rubber filler industry, satisfying the first research objective. The three areas of focus for optimization include the particle size, the structure and surface chemistry of biochar, as ideal characteristics in these three areas are key to effective rubber reinforcement. Chapter 3 follows with a detailed comparison of the physicochemical and performance differences between biochar fillers derived from corn cob, corn stover and corn starch, satisfying the second research objective. Research objectives 3 and 4 are then covered in the study in Chapter 4. The concluding chapter, Chapter 5, reviews the findings and identifies future research opportunities for this field.

Chapter 2.

Tailoring Biochar Production for Use as a Reinforcing Filler in Rubber Composites: a Review

Abstract

Biochar is gaining popularity as a reinforcing filler in composite manufacturing. Applied to rubber composites, biochar shows potential as a greener filler, but is not yet a drop-in substitute for fillers like carbon black. Through optimizing the pyrolysis process, biochar may be engineered to have ideal filler characteristics. This review identifies the key properties of highly reinforcing filler materials as particle size, structure, and surface activity. It subsequently focuses on the techniques to optimize biochar for applications as a rubber-reinforcing filler. Finally, the mechanical performance of biochar as a filler in rubber is reviewed and compared with industry-adopted reinforcing fillers.

Keywords: biochar; rubber composites; reinforcement

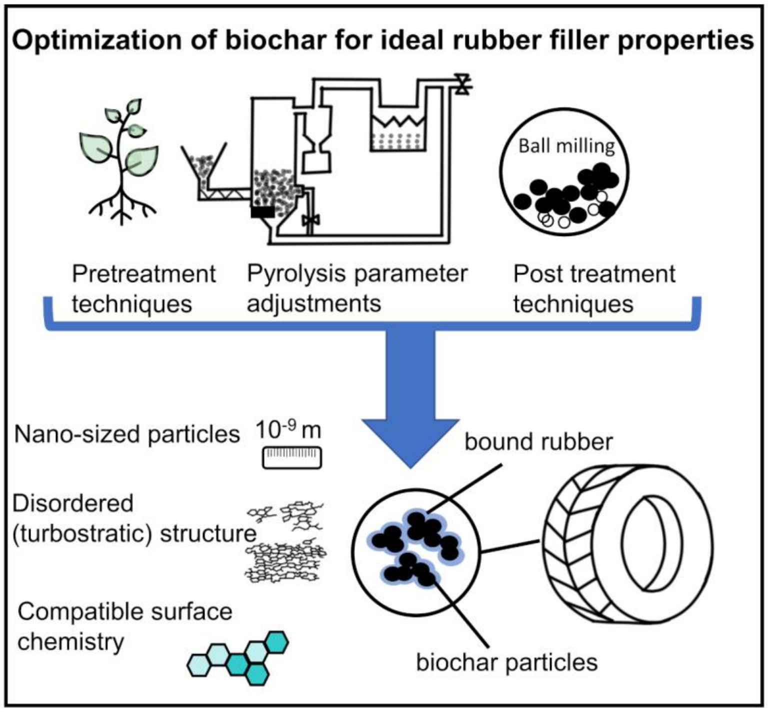

2.1 Introduction

Filler materials are a key component in the rubber industry to enhance the durability and safety of rubber products. One of the most ubiquitous filler materials is carbon black, which is manufactured from the incomplete combustion of heavy aromatic oils. Though it remains a formidable material which provides enhanced physical, mechanical, thermal and barrier properties to rubber, it is non-renewable and is considered a group 2B carcinogen [2]. Therefore, it is important to continue research into other materials with similar abilities to enhance rubber compounds.

Since the 1970s, a wide range of materials have been examined as potential fillers for the rubber industry. Examples of non-renewable fillers examined in literature include graphene [10], clay-based minerals montmorillonite, kaolin and organoclay [11–14], and carbon nanotubes [15]. Renewable filler sources have also been studied, including cornstarch [6], chitosan [16], cellulose [17], lignin [18–21] and soy proteins [22]. Though progress has been made in exploring the potential of these fillers, their lower carbon content, large particle size and hydrophilic properties make it challenging to apply them at a large scale in rubber composites.

Of increasing interest is the potential use of biochar as a reinforcing filler. Biochar is already a popular material with several prospective applications including water treatment, soil amendment, and environmental remediation [23–27] . It is formed through pyrolysis of biomass under a limited amount of oxygen at relatively low temperatures (>250 °C) [28]. The thermal decomposition results in a material with a high fixed carbon content, with potential similarities to carbon black. Unlike carbon black however, it can be made with low cost and renewable waste streams. Lignocellulosic waste streams such as those derived from forestry or agriculture serve as a popular feedstock option. Studies have been done on rubber composites reinforced by biochar produced from corn stover [6], woody biomass [7, 29–31], rice husk ash [32], rice bran [33] and coconut shell [34, 35]. The challenges with using biochar as a rubber filler lie within the complex variation between and within feedstocks, and the need to optimize pyrolysis and post processing treatments to tailor biochar to have the ideal particle size, surface activity, and structure for effective reinforcement capabilities.

Recent reviews have focused on the physicochemical comparison between carbon black and biochar, noting the potential for biochar to become a drop in substitute for carbon black [36]. Depending on the feedstock and processing techniques, biochar-based fillers may behave like other filler materials such as silica or clay, which require different treatments to be effective reinforcing fillers. As such, it is useful to identify the key areas that affect the reinforcing mechanisms of different fillers materials.

This review begins with the identification and justification of filler particle size, filler structure and filler surface activity as the key areas that contribute to effective rubber reinforcement mechanisms. Next, the review examines in more depth how biochar can be tailored to have an effective reinforcement mechanism when added to rubber. Literature pertaining to tailoring biochar for other industrial applications is also reviewed, as the same treatment techniques may prove advantageous to biochar applied in the rubber filler industry. Finally, the current performance of biochar as a filler in rubber is summarized and compared against more established fillers. This will indicate to what degree biochar can be optimized for use as a reinforcing filler in greener rubber composite manufacturing.

2.2 Advantageous Physicochemical Traits of Rubber Fillers

Fillers act as a reinforcing agent in rubber, which is observed in the marked increase in tensile strength, tear resistance, abrasion resistance and modulus of filled rubber composites as compared to their unfilled counterparts. Consensus indicates that the three most significant properties affecting the degree of reinforcement a filler can provide are its primary particle size, its structure, and its surface activity. There is a strong interplay between these three factors as the filler surface activity is influenced by both the filler particle size and the filler structure. This section of the review will focus on the effect of these properties in different commercial fillers and how they contribute to different reinforcement mechanisms. The primary focus will be on carbon black, as it accounts for most of the rubber filler market. However, the reinforcement mechanisms of other non-black fillers will be touched on as biochar may have physicochemical similarities to these materials as well.

2.2.1 Particle Size/ Surface Area

Early on in the 20th century, researchers identified small particle size as an essential characteristic of a highly reinforcing rubber filler [37]. The trend originally observed in carbon black is that rubber reinforcement increases as the filler particle size decreases. This observation has led to an enormous body of research into nanofillers for composite applications both within and outside of the rubber industry [12, 15, 38–42].

In the rubber industry, different grades of carbon black are suitable for different applications. The ASTM classification for carbon black grades is based on particle surface area [43]. The classification is a 4-character code. The first character is “S” or “N”, depending on the rate of cure. The S character represents a slower cure rate and was used more often when channel blacks were in regular circulation as they were modified to reduce the curing rate of rubber [43]. N types indicate normal cure rates and are typical of furnace blacks that have not been modified to influence the rate of cure. The second character is a number from 1 to 9, meant to designate the average surface area, as defined by the BET nitrogen adsorption technique which also accounts for porosity. The remaining 3rd and 4th characters are arbitrarily assigned digits.

For fillers that are more spherical in shape, a smaller particle size generally means a higher surface area, which provides more room for physical and chemical interactions with the rubber matrix [44]. This property works hand in hand with the filler concentration, as increasing the concentration also increases the filler particle surface area available for filler-polymer interactions. Table 2.1 presents an example of 4 grades of carbon black and the influence of their particle size on their applications and mechanical performance.

Table 2.1 Example of 4 Carbon Black Grades and Their Mechanical Properties in SBR Rubber (Table adapted from **[45]**)

ASTM Group	ASTM Classification and Name	Average Nitrogen Surface Area (m^2/g) (ASTM D1765)	Applications [46]	Shore A Hardness	Stress at Break (MPa)	Strain at Break (MPa)	Resilience (%)
1	N110 Super Abrasion Furnace Black	121-150	Tread compounds	69 ± 1	23.0 ± 1.4	480 ± 36	38 ± 1
3	N330 High Abrasion Furnace Black	70-99	Tread compounds, inner tire, conveyor belts, rubber mechanical goods	66 ± 1	23.9 ± 0.9	520 ± 23	39 ± 1
5	N550 Fast Extruding Furnace Black	40-49	Tire carcass (framework) and tire inner liner, hoses, seals and cable jackets	64 ± 1	19.8 ± 0.5	510 ± 25	44 ± 1
9	N990 Medium Thermal Black	0-10	Sponge rubber, gaskets, wiper blades, hoses, o-rings	55 ± 1	11.9 ± 2.7	640 ± 75	51 ± 1

Carbon black grades in groups 1-3 are considered highly reinforcing and have an average primary particle size between 15 -36 nm while grades in groups 5-7 are considered semi reinforcing with an average primary particle size of 50 nm-90 nm [46].

Using fillers with particle sizes greater than 3 micrometers (3000 nm) can lead to weakened rubber composites due to stress localizations, causing defects such as tears and fracturing. Larger particle sizes also lower the maximum packing fraction of the filler which means that failure can occur at lower filler concentrations [7, 47]. For added reference, carbon black 990 is considered a low reinforcing black and its particle size ranges from 250-350 nm [46].

2.2.2 Filler Structure

Equally important to the primary particle size is the structure that the particles form. The filler structure can be described as the degree of irregularity of the filler unit [44]. The higher the structure, the greater the irregularity. Fillers with higher structures, such as carbon black, tend to have better reinforcement capabilities. The filler structure influences the restrictive motion of the elastomer chains under strain, contributing to the stiffness of the filled composite [44].

Primary carbon black particles are believed to be spherical and formed from a turbostratic (disordered, non-uniform interlaying spacing) arrangement of graphene sheets. During the carbon black forming process, primary particles may fuse together to form aggregate structures. High structure carbon blacks have a high number of primary particles per aggregate while low structure blacks have weaker aggregations. Sometimes aggregates can loosely join together via van der Waals forces to form agglomerates [44]. The empty space or void volume between the aggregates is often the basis for comparing the structures of different carbon black grades and is commonly evaluated through determining the oil absorption number (OAN). This is done by dripping oil at a constant rate into a rotating cylinder full of a single grade of carbon black. The torque of the cylinder is measured until it reaches the maximum torque value when the oil has filled all the void space between the carbon black particles. Larger grades of carbon black generally have lower OAN values than smaller/finer grades [48]. These values only hold for carbon blacks outside of the rubber compound as their aggregate structure will change during the mixing process with rubber. Figure 2.1 depicts the structure of the carbon black including its turbostratic primary particles, its aggregate formation and the possible functional groups on its surface.

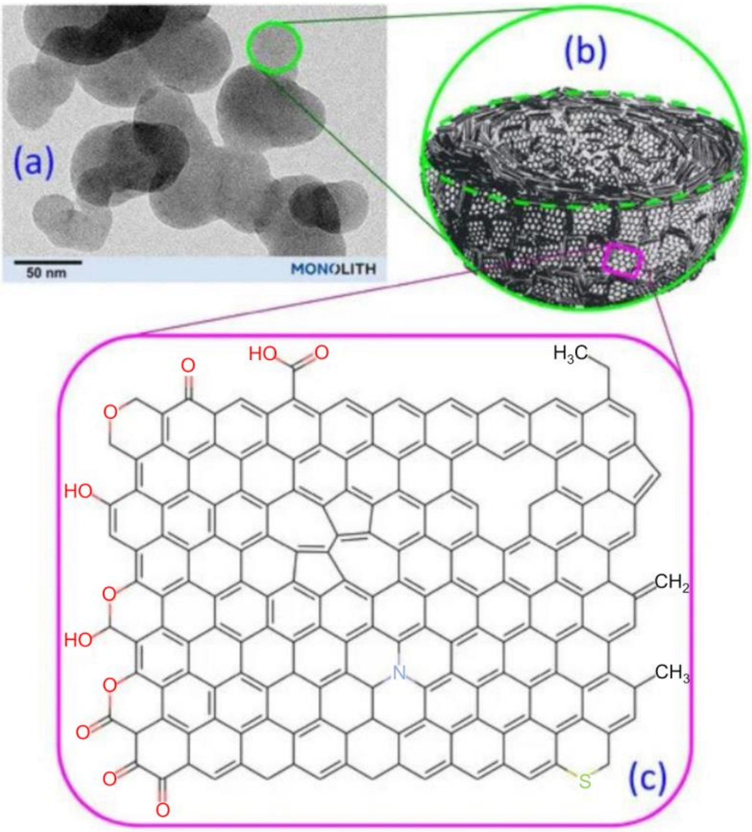

Figure 2.1 Reprinted from [48] showing (a) the turbostratic layers in carbon black primary particles, (b) the aggregate structure of primary particles and (c) various possible functional groups presented counter clockwise from top in red: carboxylic acid, carbonyl, ether, phenol, lactol, ester and quinone

The origin of the turbostratic nature of the primary particles is believed to be due to the highly controlled rapid reaction time in the furnace, causing rough-surfaced particles to form from disordered graphene layers with exposed edges [49]. However, further structural changes are made during the incorporation into the rubber matrix. Literature indicates that the shearing forces of the mixer fracture the aggregates and generate delocalized electrons from the graphene plane edges, forming carbon free radicals [48, 50].

Early 1950s research supports the notion that rubber reinforcement by carbon black has origins in free radical chemistry. The studies focused on free radicals on the surface of carbon black particles using electron spin resonance. The principle behind this is that the two spin states of individual electrons can be split under a strong magnetic field, and radiation can be subsequently used to determine the amount of unpaired electrons [48, 51]. Interestingly, [52] found that the addition of carbon black in rubber stabilizes the rubber polymer free radicals that are also formed during the mixing process. This suggests that the nature of carbon black reinforcement may partially exist based on delocalized electrons within the carbon black particles combining with the polymer free radicals to form a stable complex, the bound rubber layer. Conversely, when carbon black is heated at high temperatures above 1400 °C, studies have found that its reinforcing properties decrease significantly. In studies emphasizing free radical chemistry, this has been attributed to heat induced aggregate growth, which stabilizes unpaired pi electrons through resonance configurations with electronegative groups like quinone oxygen [53]. As the growth continues, the larger molecules begin to merge and the stabilization sites combine which decreases the concentration of unpaired electrons, reducing the reinforcement potential [53, 54]. Other studies are in agreement, citing that temperatures between 1500°C and 2700°C increase the size and the order of the nanocrystalline structures that form the primary particles, altering the microstructure and reducing the number of high energy sites on the crystallite edges [55].

In contrast, non-carbon-black fillers like silica and clay, may have different reinforcing mechanisms due to elements such as porosity, shape, and surface chemical groups. There are limited studies on the impact of filler porosity on rubber composite reinforcement, however general findings are that the size of the rubber chains are within the mesoporous (2-50 nm) to macroporous range (> 50 nm), so increasing the microporosity of fillers does not improve reinforcement [56]. When fillers contain larger sized pores, studies show that reinforcing results can be favorable. Mesoporous silica has been described as an effective filler, partially due to the porosity which increases the likelihood of chemical interactions between the rubber and the filler as the rubber chains can access the interior of the filler pores [57]. Most common fillers are thought to have spherical shaped primary particles. By contrast, nanokaolin, a clay-based filler, has a sheet like structure that can bond to large rubber chains in two dimensions, giving composites better tensile performance than composites with precipitated silica. However, the diameter of the sheets is large (several hundred nanometers), which causes weaker binding forces between the filler layers, reducing the tear strength of the composites as compared with silica composites, which have a spherical shape that can combine with rubber chains in three dimensions [12]. The surface chemical groups, such as silanol groups on silica also have a large impact on filler structure, which will be explained in the following section.

2.2.3 Filler Surface Activity

Surface activity is the most significant factor influencing filler-filler and filler-polymer interactions, and the activity can be physical or chemical in nature. Favorable surface activity means increasing the filler-polymer interactions as the strength of the filler-polymer network is responsible for the reinforcement of the composite. Surface activity is affected by the filler particle size, structure and the presence or absence of surface functional groups. Surface functional groups influence the surface activity by affecting the hydrophobicity and pH of the filler, which impacts its ability to disperse in the rubber matrix as well as the amount of crosslinking that occurs during the curing process.

Carbon black particles have oxygen-containing functional groups such as carboxyls, lactones and quinones among others, allowing it to have high affinity with rubber [48]. On the other hand, some fillers contain surface groups that can cause compatibility issues. For instance, the functional groups on the surfaces of silicas (siloxane and silanol) and other fillers such as kaolin clay (OH groups), can lead to excessive particle-particle interactions. They also make the filler more acidic [58] and moisture adsorbing [59]. Several studies show that while alkali groups on fillers increase the cure rate, acidic groups tend to slow down the curing rate which can have negative repercussions on the crosslinking density [60–62]. As a result, bifunctional organosilanes, (coupling agents), are required to control the filler surface activity to improve its reinforcing capacity [62].

Surface functional groups can also influence the reinforcement through forming covalent bonds with the rubber polymer strands. For instance, though not the primary reinforcement mechanism, the covalent interactions between rubber chains and quinonic groups on carbon black is believed to enhance the reinforcing properties of the filler [63]. With fillers requiring coupling agents like silica, the case of reinforcement through covalent bonding is even stronger, as a layer of bound rubber develops through chemical bonds between the polymer chains and the organosilane coupling agents attached to the filler surface. As seen in Figure 2.2a, the organosilanes (such as TESPT), hydrophobize the silica, allowing its network to be broken down at lower strains, leading to better dispersion in the rubber matrix. Thus, at low strains, the strong silica-silica network causes part of the matrix rubber to be immobilized or occluded. Yet, at high strains, this occluded rubber is gradually lost as the network is broken apart. However, the layer of rubber chemically bound to the silica surface through the organosilane molecule remains immobilized and provides the reinforcement at high strains [44, 64, 65].

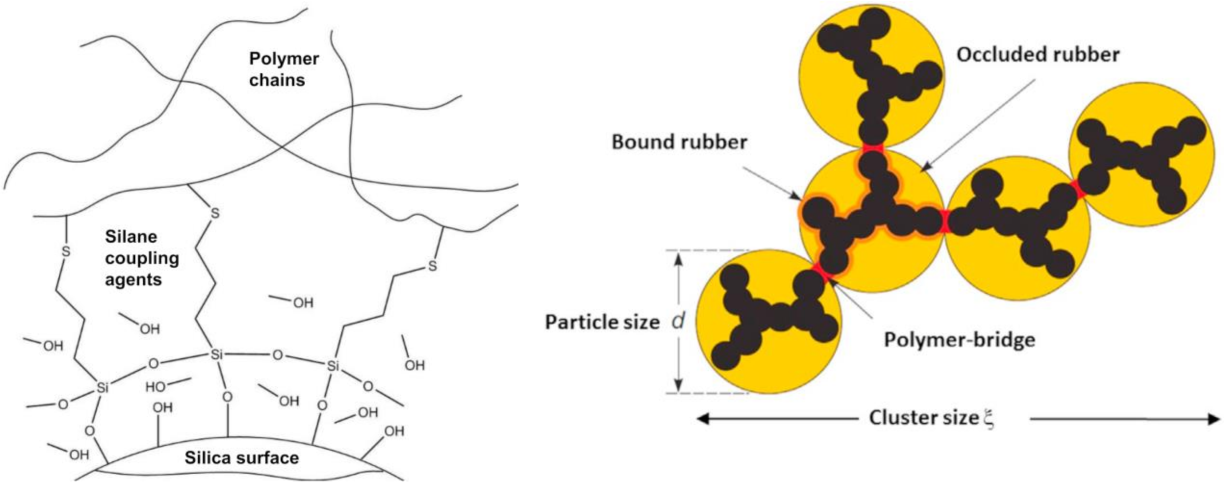

Figure 2.2 Showing (a) Simplified Model of the Reinforcement mechanism for Silica + bifunctional silane coupling agents [64] and (b) Simplified Model of carbon black showing reinforcement through physical adsorption/van der Waals forces and covalent bonding [66]

2.2.4 Reinforcement Behaviour at Low and High Strains

To better understand the interplay of these 3 factors, it is important to distinguish between the filled composite behaviour at low strains and at high strains.

Low strain Modulus Behaviour (<<5%)

At low strains, the complex modulus indicates the strength of the filler-filler network. In general, the higher the filler loading, the stronger the filler-filler network. The network strength also improves with increasing the surface area or decreasing size of the filler particles. The interaggregate distance becomes smaller in both scenarios, leading to a higher chance of filler-filler interactions. High surface activity on the other hand leads to a decrease in filler – filler networking due to increasing filler-polymer interaction, as filler-filler and filler-polymer interactions are inversely related [44].

The Payne effect [67], illustrated in Figure 2.3a, describes the behaviour of the composite at low strains/small deformations. It is not observable in unfilled elastomers but in filled elastomers experiencing small oscillations, there is typically a decrease in the storage modulus, G’ (and an increase in the loss modulus, G”), corresponding with higher amplitudes of oscillation. Figure 2.3b depicts the complex modulus G* and its relationship to the storage modulus, loss modulus and tan δ values.

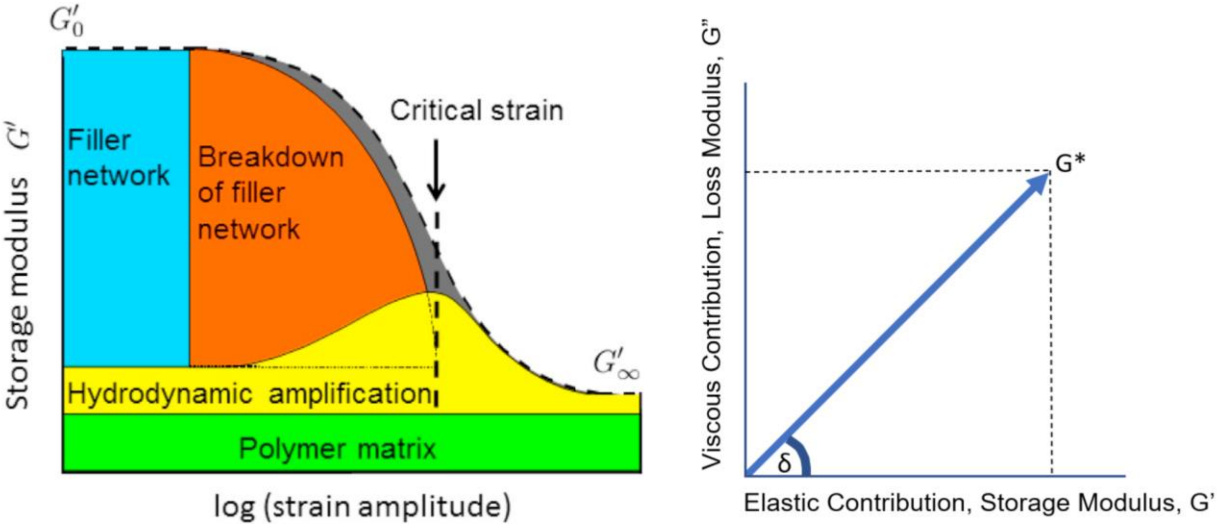

Figure 2.3 Showing (a) Graphical Depiction of the Payne Effect [66] and (b) Graphical depiction of the relationship between the storage modulus, loss modulus and tan δ

High Strain Modulus Behaviour (>30%)

Under high strains, the filler structure may no longer be fully intact. The high strain modulus is enhanced only if the structure of the filler inside the rubber (the in-rubber filler structure) is high, and the surface activity is high. The Mullins effect [68], illustrated in Figure 2.4, is observed under high strains/deformations. It is an instantaneous and irreversible softening of the stress strain curve, reportedly due to filler particles debonding from each other or from the polymer chains. [44].

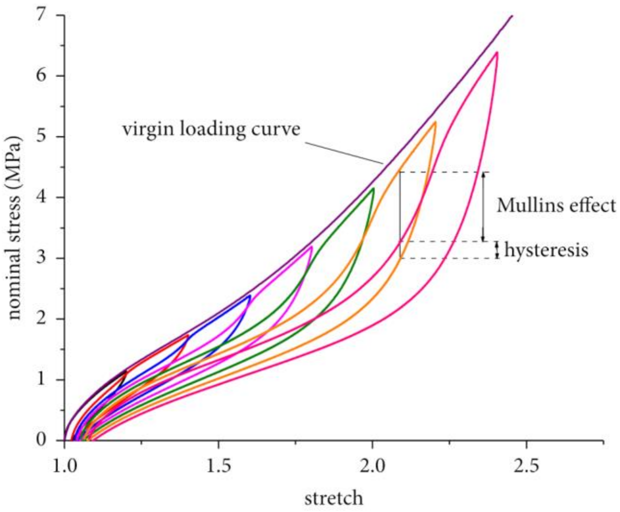

Figure 2.4 Graphical Depiction of the Mullins Effect [69]

2.3 Refining Physicochemical Traits of Biochar for its Use as A Green Rubber Composite Filler

Following the identification of key physicochemical traits of highly reinforcing rubber fillers, this section focuses on studies involving biochar as fillers. A summary of techniques to optimize biochar is presented, namely in terms of its particle size, surface activity and structure for applications in rubber composite reinforcement

2.3.1 Optimizing the Filler Particle Size/Surface Area

As mentioned in the previous section, carbon black is known to have particle sizes on the nanoscale due to the carefully controlled process parameters. One study has shown the potential for bio-oil to be used in a process similar to furnace black. Results of the study yielded a material that is macroscopically similar to carbon black, though unfortunately the material's mechanical performance was not tested and thus this technique has yet to be validated [70]. When considering biochar- derived filler as opposed to bio-oil derived filler, both pyrolysis techniques and post pyrolysis treatments have the greatest impact on the particle size. A recent review on nano biochar processing techniques reveals that current processes mainly involve combinations of mechanical milling, sonication, filtration, centrifugation and sieving [40] .

2.3.1.1 Ball Milling

Ball milling is currently the most popular post-processing technique to reduce the size of biochar, likely owing to its simplicity and low-cost process. Several parameters can be adjusted to achieve the desired properties including milling material, co-milling material, solvents and the milling atmosphere, among others. There are several types of milling machines, including planetary ball mills, tumbler ball mills, vibrational tube mills and attrition mills [71]. Planetary ball milling is particularly effective through the use of both shear and impact forces to break down biochar [72]. They are also compact in size and can be filled with artificial atmospheres. Milling can be done wet or dry. In wet milling, a solvent is used to reduce agglomeration of particles, allowing for better dispersion. The most important parameters affecting surface area and particle size is the mass ratio of milling media to biochar, with the ideal ratio in literature at 100:1 [73]. Common solvents include acetone, ethanol, hexane, heptane and water [73]. With dry milling, co-milling materials such as salt or sugar can effectively migrate into interstitial areas between the rigid milling material, (such as YSZ or stainless steel spheres), introducing shearing forces which further reduction in biochar's particle size [74, 75]. Building on this concept, [75] found that biochar milled with YSZ and 0.16 wt% nanosilica for 1 hour was able to replace 40% of the carbon black (CB) with equal tensile strength, and improved elongation and toughness by 31% and 24% respectively. Nanosilica has a further advantage since it does not need to be removed from the biochar and only requires small amounts to be effective, as higher concentrations cause agglomerations due to intermolecular hydrogen bonding between hydroxyl groups The atmosphere during ball-milling can also affect the morphology and functional groups of biochar. Ball milling in nitrogen or vacuum atmosphere prevents oxygen containing functional group formation and lead to further reduction in biochar size compared to air [76]. Another treatment that enhances the ball-milling process is the cryogenic conditioning of samples. [77] found that biochar held 24 hours at -20 °C was reduced to a particle size of 102.5 nm, while biochar at −80 °C was reduced to 60 nm. Ultimately, the cryogenic treatment inhibited particle agglomeration during milling and produced particle sizes comparable to carbon black with optimized milling parameters of 1.6 hours at 575 rpm with a 4.5g/g ball: powder ratio. It also increased the surface area by a factor of 15 as compared to raw biochar. Table 2.2 provides a summary of various milling parameters on biochar and their effects on filler particle size and surface area.

Though ball milling is a powerful technique in particle size reduction, it requires careful process optimization and may need to be combined with other techniques to sufficiently reduce biochar's particle size. For instance, as seen in Figure 2.5, even after ball milling with silica, Paulownia biochar particle sizes (Figure 2.5b) are not as uniform as carbon black (Figure 2.5a) with some particle sizes appearing larger than 3 microns, which can cause defects in the rubber composite.

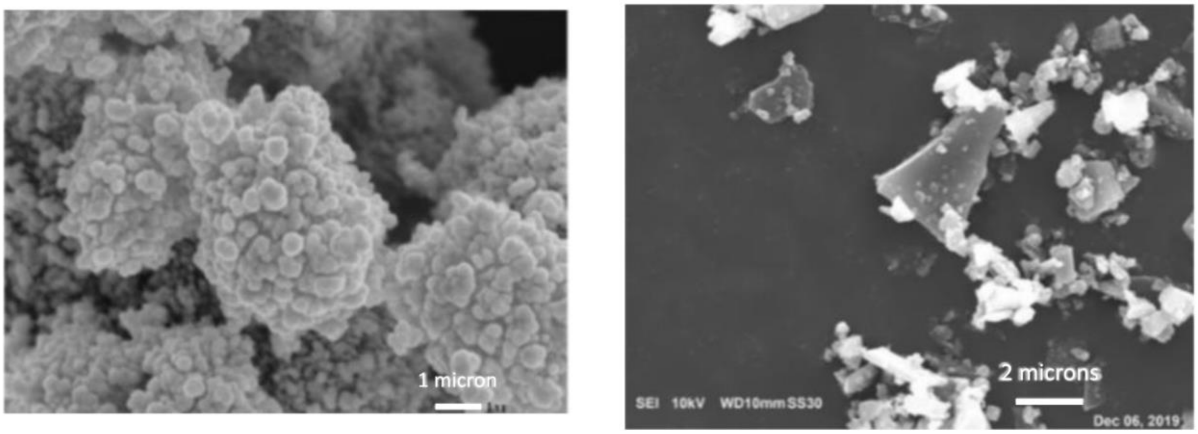

Figure 2.5 (a) Carbon black at 10,000X magnification [29] and (b) Paulownia biochar at 7500X magnification post silica milling [29]

Table 2.2 Summary of Ball-Milling Parameters and Their Effects on the Surface Area and Mean Particle Size of Biochar

Biochar Conditions	Milling Conditions	Milling Speed and Time	Particle Size	Surface Area	References
Feedstock: corn stover Temperature: - Heating Rate: - Time: - Environment: -	Wet milling Solvents used: ethanol, hexane, and heptane, 5g Milling media: 3 mm yttria-stabilized zirconia (YSZ) spheres Mass ratio of YSZ:biochar: 100:1	6 h	0.89mm (number average) and 7.72mm (volume average),	Micropore surface area 92-95 m^2/g Increased SA by 60 times from 3 m^2/g to 194 m^2/g	[73]
Feedstock: Straw and newspaper Temperature: 900 °C Heating Rate: 5°C/min Time: 2h Environment: nitrogen Other Treatments: feedstock ball milled, freeze dried, oxidized as a slurry with deionizing water TEMPO, NaBr, NaClO and NaOH, freeze dried again	Dry milling Milling media: 200g agate ball Mass ratio of milling media to biochar: -	2h, 300 rpm	n/a	specific surface areas reaching up to 871.5m^2/g and 1065 m^2/g	[78]
Feedstock: Hickory chip, ground into 0.5-1mm powder Temperature: 600°C Heating Rate: 5°C/min Time: 2h Environment: nitrogen	Dry milling Different atmospheres used: air, N2, vacuum Milling media: 6 mm 180 g steel balls Machine Type: Planetary ball mill Mass ratio of milling media to biochar: -	12h, 300 rpm.	Air: 223 nm N2: 155 nm Vacuum: 140 nm	Air: 382 m^2/g N2: 317 m^2/g Vacuum: 330 m^2/g	[76]
Feedstock: pine white wood Temperature: 525°C Heating Rate: - Time: 2 min Environment: nitrogen	Cryogenic conditioning (sample held at -80°C for 24 hours) Milling Media: 2.4 mm stainless steel balls Machine Type: Planetary ball mill Mass ratio of milling media to biochar: 4.5:1	1.6 h, 575 rpm	Average particle size of 60 nm (volume mean)	47.25 m^2/g	[77]
Feedstock: silver maple landscape wood waste Temperature: Heating Rate: Time: Environment:	Co-milled with 0.16 wt% nanosilica (12 nm particle size) Milling Media: 3 mm YSZ balls Machine Type: Planetary ball mill Mass ratio of milling media to biochar: 4.5:1	1 h, 400 rpm	Mean particle size just over 1 μm with 30% of particles < 1 μm	-	[75]

Other: feedstock pre-milled in tumbling mill with stainless steel spheres for 3 h and passed through 325 mesh (≤ 44 µm)					
Feedstock: Pine and wheat straw based biochar Temperature: 600°C Heating Rate: 4°C/min Time: 30 min Environment: nitrogen	Milling Media: 5 mm ZrO_2 balls Machine Type: Planetary ball mill Mass ratio of milling media to biochar: 50:1	3h, 500 rpm	<4 µm with majority of particles <1.5µm	Pine 337 m^2/g, Wheat Straw 278 m^2/g Pulp Sludge 50 m^2/g Switchgrass 338 m^2/g Hemp 295 m^2/g	[79]
Feedstock: bamboo Temperature: 450°C Heating Rate: - Time: - Environment: nitrogen	Dry milling Milling Media: 5 × 20 mm and 10 × 10 mm agate balls Machine Type: Planetary ball mill Mass ratio of milling media to biochar: 10:1	12 h, 500 rpm	No exact particle size but was nano-sized	298.6 m^2/g post ball milling (18.2 m^2/g pre ball milling)	[80]
Feedstock: Rice husk Temperature: - Heating Rate: - Time: - Environment: -	Wet milling with water (WM) or ethanol (EM) as solvent Dry milling control (DM) Milling Media: 450 g zirconia spheres and Machine Type: Planetary ball mill Mass ratio of milling media to biochar: - Ball to biochar ratio of 10:1	12h, (30 min on/off), 400 rpm	DM: 5.81 EM: ~ 2 WM: ~ 2	DM: 157.2 EM: 179.2 WM: 202.3	[81]

2.3.1.2 Ultrasonication

Increasing biochar's adsorption capacity through ultrasonic treatment is well documented in literature [27, 82]. It has demonstrated the ability to exfoliate and leach minerals from biochar, while enhancing the porosity and surface area. [27] described a method where biochar was mixed with deionized water and subjected to ultrasound at 100% amplitude and 20 kHz for 30 seconds. The resulting impacts on the biochar was an increase of 40% in the microporous surface area, from 110.13 to 154.96 m^2/g. The increase was attributed to micro-jets and shock waves induced by the ultrasound, which could open blocked pores and generate new ones while exfoliating the biochar. It can also be used to synthesize nano-sized biochar. In a process described by [83], ultrasonic vibration can be used to disperse biochar in a water solution and subsequently the suspension can be sieved and centrifuged to extract the resulting nanoparticles. Overall this method has the advantage of consuming less energy, being environmentally friendly, and could potentially cost less than other methods if applied at large scale [84].

2.3.1.3 Other Techniques

Though less common and potentially cost prohibitive, studies have indicated other techniques which can be used to synthesize nano-sized biochar particles. One novel technique established by [85] involves a high temperature thermal-chemical flash exfoliation process applied to pretreated biomass that has been pyrolyzed under nitrogen. The study used corn cob feedstock (pith removed), soaked in dilute acid (HNO_3), dried and then pyrolyzed under nitrogen, followed by soaking in concentrated HNO_3 before a 45 second flash heat treatment in a muffle furnace at 950 °C. The resulting material is nanosized carbon particles composed of agglomerated thin carbon sheets resembling dry graphene powder. The dilute acid pre-treatment removed the amorphous carbon allowing the flash process to exfoliate and reveal the inner carbon layers. Another study involved biomass pre-treatment with HNO_3 and H_2SO_4 in combination with a high-pressure hydrothermal reactor, followed by filtration and drying. The resulting median particle sizes were 5 nm and 4 nm respectively, for soybean straw biochar and cattle manure biochar [86].

2.3.2 Optimizing the Filler Structure

The structure of biochar is primarily influenced by feedstock selection but can be refined by carefully controlling the pyrolysis temperature, the feedstock particle size, the pressure conditions and the removal of exogeneous sources of ash.

Even when the particle size is similar, the feedstock can affect the structure. In a study comparing nano biochar from different materials, it was found that nano biochar from wheat straw had a more amorphous structure than biochar from wicker, which was more crystalline. In miscanthus based nano biochar, there were larger spherical particles that formed less concentrated aggregates as compared to the other two. The nano biochar in general showed graphene like structures surrounded by amorphous carbon with disordered structure dominating the majority of the samples [83]. In addition to the structure, the feedstock selection affects several biochar properties including the overall carbon and fixed carbon contents, the elemental composition, the mineral concentration, and the ash content [87]. Woody biomass derived biochar are known for their higher carbon content as compared to biochar derived from animal litter or solid waste [88]. In terms of elemental composition, a separate study comparing biochar from different feedstocks showed that peanut-shell based biochar consistently had the highest amount of nitrogen, regardless of the pyrolysis temperature, given the higher nitrogen content in the feedstock [89]. Mineral concentration is also feedstock dependent as opposed to temperature dependent. In a study of 12 different feedstocks pyrolyzed at various temperatures, manure derived biochar tended to have more phosphorus as compared to crop residues derived biochar which had a higher potassium content [87]. The amount of minerals present in the feedstock strongly influences the ash content since the feedstock mineral content typically forms the ash content when pyrolyzed. For instance, rice straw biochar has an ash content of 38% which is higher than rape stalk biochar, which has 19% ash for the same pyrolysis conditions [90]. Therefore, biochar with higher amounts of minerals, like wastewater sludge char will likely have a higher ash content overall.

Most biochar is produced from lignocellulosic biomass, which is composed of lignin, cellulose, and hemicellulose fractions. These three fractions are often studied separately in pyrolysis kinetics given the theory that the superposition of the product yields of these individual components can determine the total yields for the entire pyrolysis process [91]. Other literature highlights the important role that secondary reactions play in biochar formation, citing that models of primary pyrolysis kinetics must be combined with models of homogeneous and heterogeneous secondary pyrolysis reactions along with models of heat and mass transfer to accurately predict biochar and fixed carbon yields [92]. The literature is generally in agreement that biochar yield is significantly affected by feedstock properties such as biomass type, moisture content and raw material size [93]. Different lignocellulosic feedstocks will have varying amounts of the three fractions which will influence the yield. The fractions are also highly linked with temperature due to their decomposition at different temperatures. In the case of low temperature (< 300 °C) pyrolysis, cellulose degradation will affect the char properties whereas with higher temperature (> 300 °C) pyrolysis, the effect of lignin decomposition will dominate the biochar properties [94].

Lignin is one of the most important components for biochar formation as it has the highest yield of all fractions due to a high number of benzene rings, which are the moieties that form the biochar [91]. A study comparing biochar produced from different biomass samples showed that feedstock with higher lignin content, such as pine cone and peanut shells, produced biochar with higher surface areas [95]. There have been several studies examining the reinforcing capabilities of lignin in the rubber industry. Using lignin in its raw form has been so far found to be complicated and not cost effective due to undesirable properties such as strong self-aggregation and poor interfacial interactions [18–20, 96, 97]. However, when lignin is pyrolyzed, the structure of lignin changes from loosely stacked, hollow, vesicular primary particles to closely stacked primary particles, still with a vesicular structure but with thickened walls [21]. The pyrolysis process reduced the oxygen containing functional groups that were contributing to hydrogen bonding and π-π stacking, while increasing the carbon content from 59 wt % in raw lignin to 84 wt% in the biochar [21]. Most impressively was the finding that the reinforcing effect of lignin biochar in SBR rubber was comparable to commercial N330 carbon black [21]. Compared to the carbon black control, the lignin biochar had a smaller mean aggregate size (474 nm vs 807 nm) as well as a higher level of disorder in the carbon framework, potentially indicating more active sites for filler-particle interactions [21]. Additionally, graphitic fractions were found dispersed in the material and the theory was that they could provide the flexibility and slippage of rubber chains while the active sites created from the disordered fractions could adsorb rubber through physical or chemical interactions (Fröhlich et al., 2005; Wang et al., 1994). The promising results from this study suggest that pre-treating biomass to separate the lignin fraction prior to its conversion to biochar may be an ideal route to achieving high performing biochar filler.

The interest in lignin extraction is not new and there are numerous papers describing the potential of biorefineries that can separate lignin fractions from the rest of the intake biomass [98–101]. Lignin is also available as a waste product from the pulp and paper industry. Techniques such as the acid sulfite pulping process and Kraft pulping have been employed since the mid to late 1800s in the paper making process. [21] used waste lignin isolated from black liquor, a coproduct from Kraft pulping. This process is already commercially available through the LignoBoost™ process which allows plants in North America and Europe to produce thousands of tons of Kraft lignin per year [99]. Additional refining techniques being explored among others include using alkali chemicals NaOH, NH_3 [102], dilute acid H_2SO_4, HCL [103], steam explosion [104], ethanol and water [105] and deep eutectic solvents [106].

Prewashing of lignocellulosic biomass is commonly done to remove exogenous ash sources that can impact biochar quality by affecting the degradation temperature and the gas product distributions from the pyrolysis process. A study testing the effects of washing on wheat straw found that ash is more effectively removed by washing the biomass prior to pyrolysis rather than washing the char [107]. This is attributed to the formation of an intermediate molten phase during pyrolysis, which traps the ash components making them harder to remove as the char is formed [108]. Through TGA, the study also found that washing increases the temperature at which devolatilization begins (242°C for washed straw vs 192°C for unwashed straw), improving its stability in an oxygen environment as there is less ash content to catalyze oxygen combustion. Yang et al., 2006 found similar effects of washing while investigating the effects of mineral content on pyrolysis of palm oil waste using TGA. Water washing raised the degradation temperature of the cellulose content of palm oil waste by 20 °C, leading to the appearance of two distinct decomposition temperatures for cellulose and hemicellulose. In contrast, when mineral content (K_2CO_3) was added to the biomass, the degradation temperature lowered for cellulose, and it was subsequently difficult to distinguish a different onset point between cellulose and hemicellulose degradation. This finding is further supported in a 2013 study on washing 6 different biomass materials, where washing caused further separation of the cellulose and hemicellulose degradation peaks observed with TGA. In terms of washing temperature, the general consensus is that hot water removes mineral content more efficiently than cold water [107, 110] . In addition to water, dilute acid is an effective washing agent. Aston et al., 2016 found that 95 wt% aqueous, dilute-acid leaching removed 97% of the alkali metals and alkaline earth metals in corn stover in the presence of the acid catalyst (sulfuric acid). In the absence of the acid catalyst, only 6.8% of the alkali metals and alkaline earth metals were removed. However, 88% of chloride was still able to be removed.

Regarding the effect of temperature, turbostratic carbon is formed at higher pyrolysis temperatures, which is confirmed in studies involving biochar. [112] found that pyrolysis of dead leaf biomass at 1000 °C produced a more irregular grain shape with a rougher surface as compared to the morphology at 550 °C. This was confirmed by Raman spectroscopy when the D band shifted to lower frequencies as the pyrolysis temperature increased, attributed to the increase in turbostratic carbon. The ratio of the D (disorder) band to G (graphite) band increased with increasing temperature across the range of 500 °C to 900 °C, indicating a larger disordered carbon structure. However, the ratio decreased from 1.13 at 900 °C to 0.92 at 1000 °C due to the removal of loose carbons, suggesting that there is a limit to the beneficial effect of high temperatures on the structure. This is in a way similar to the discovery that heat treatment of carbon black changes the morphology in an unfavorable manner past a certain point (1400 °C) [53].

Though not as significant as the other factors, feedstock particle size, and pressure conditions during pyrolysis can impact the carbon content of the biochar which can in turn, affect its structure. The importance of feedstock particle size has more often been discussed in fast pyrolysis systems due to the limited time the biomass spends in the pyrolysis unit. Particle size and shape have also been examined in developing effective models of biomass conversion through pyrolysis [113, 114]. On a practical scale, biomass has low thermal conductivity so smaller particle sizes can facilitate heat transfer into the individual particles. This is ideal in cases of fast pyrolysis where high heating rates are desired to maximize oil yield [115]. In the case of slow pyrolysis, several studies report higher fixed-carbon yields with larger particle sizes [92, 116–118] . Increasing the particle size can enhance the secondary reactions by prolonging the contact between the bio-oil vapor species with the solids at the interior of the particle, ultimately leading to an increase in fixed carbon yield [92].

Elevated pressure increases the fixed-carbon yield above what is possible with pyrolysis at atmospheric pressure. [92] postulated that increasing the pressure increases the saturation pressure and temperature of the liquid bio-oil, which keeps the material in a liquid phase for longer and increases the likelihood of liquid coking reactions which favor biochar formation. In addition, elevated pressure conditions increase the partial pressures of the tarry vapours in the pores of the biochar portion, which also enhances the biochar forming vapor-phase secondary reactions. Their experimental results confirmed this hypothesis with the fixed carbon yield of coarse oak wood sawdust increasing from 16.1 wt% at 1.14 MPa to 27.6% at 2.17 MPa. They found that an air pressurized flash carbonization process yielded the highest fixed carbon values. This is in agreement with results from previous studies on pressurized carbonization of miscanthus [119] and cellulose [120].

2.3.3 Optimizing the Filler Surface Activity

Apart from the particle size and structure, the filler surface activity is often affected by the surface functional groups on a filler. In the case of biochar, surface functional groups depend on the feedstock selection, the temperature during pyrolysis and the reaction with the atmosphere during and after pyrolysis. Chemical treatments can also be applied to alter the surface functional groups.

In terms of feedstock selection, the mineral content and the lignin content will influence the type of functional groups present. Rice based feedstock for instance, is known to contain higher amounts of silica, often leading to silanol groups on the surface [32, 33, 81, 121–123]. Meanwhile, biogas digestate, and chicken manure have higher proportions of ash, which is also related to basic functional groups [124]. Lignin based biomass contains aromatic carbon and aliphatic CH2 groups which are the last to degrade and are the most heat resistant [124].

The next factor affecting surface groups is the temperature during pyrolysis. [124] found that pyrolysis temperatures above 750 °C contributed to the loss of functional groups at all wavenumbers in the FTIR spectra of 13 different feedstocks. [125] found that biochar produced at ≤ 500°C may have more negatively charged carboxylic and phenolic functional groups while biochar produced at higher temperatures (≥ 700°C) tend to have more positively charged surface functional groups, such as oxonium groups.

The presence of different gases during pyrolysis and the natural aging process in atmosphere can also affect the surface functional groups. [126] report that pyrolysis with steam or with CO_2 has a large impact on the tar reforming reactions that occur during pyrolysis. With steam, these reactions tend to take place from the interior particles to the surface. Therefore, if there are alkali and alkaline earth metal species present in the biomass, activation with steam appears to concentrate these metals on the biochar surface. Under CO_2, the tar reformation takes place on the surface of the biochar and does not tend to bring out the alkali and alkaline species. In both cases, tar reformation decreases the surface graphite carbon (C-C and C=C), while increasing hydrocarbon (C-H) groups as the tar fraction is adsorbed onto the existing biochar surface and is reformed to expose unsaturated C elements. This leads to hydrocarbon bond formation from secondary pyrolysis reactions with H/O/OH radicals which are formed from the dissociation of CO_2, and H_2O. Activation with CO_2 or steam also increases the number of oxygen-containing groups (such as phenol, alcohol and ether) on the biochar surface. This result is more noticeable in activation with steam [126]. As for the effects of aging, a study involving chemical oxidation to simulate the effects of the atmosphere on biochar showed that exposure to atmosphere also introduces more oxygen-containing functional groups to the surface of the biochar, especially carboxyl groups [127].

The presence of surface chemical groups can affect the use of biochar as a reinforcing filler in rubber, mainly due to its impact on hydrophobicity and on the tendency to form aggregates through filler-filler interactions [121]. [128] found a strong correlation between hydrophobicity and aliphatic surface groups, which are usually found on biochar produced at lower temperatures (< 400 °C). A study by [129] is in agreement and attributes these aliphatic groups to possible pyrogenic tars and oils that were not fully reformed during the pyrolysis process [129, 130]. As these aliphatic groups are destroyed with higher pyrolysis temperatures, the biochar becomes more hydrophilic [129]. In their study, [129] compared the water to ethanol uptake in hazelnut shell and Douglas fir chip based biochar produced at low temperatures (370 °C) and higher temperatures (500 °C and 620 °C). They found that the low temperature biochar from both feedstocks took up less water than the higher temperatures ones, but both took up the same amount of ethanol. This further suggests that temperature affects the hydrophobicity of the surface through the presence or absence of certain functional groups.

Due to biochar's surface group related compatibility issues, several studies have been done on the use of coupling agents to improve its reinforcement capabilities in rubber composites. In a 2015 study, Zhang et al. used a method called latex compounding, involving the blending of different additives to improve the dispersion of rice bran filler in carboxylated SBR rubber. They tested several additives, including N-(2-aminoethyl)-3-aminopropyltrimethoxysilane (AAPTS), 3-mercaptopropyltrimethoxysilane (MPTMS), 4,4-methylene bis(phenyl isocyanate) (MDI) and ionic liquid 1-hexyl-3-methylimidazolium hexafluorophosphate (HMIMPF6). The use of MDI led to the greatest improvement in the reinforcement properties. The reported values for tensile strength and elastic modulus at 300% elongation were 16.43 and 16.33 MPa, respectively. These results are among the higher values reported for composites using pure biochar as a reinforcing filler. The reinforcing mechanism was attributed to the interaction of delocalized π electrons on MDI and XSBR benzene rings [122]. In a subsequent study, rice bran carbon was either left alone (RCBp), treated with acid (RCBa) or trimethoxysilane (silane functionalized) (RCBsi) and then mixed with styrene butadiene with excess 3-MPTMS to form composites. The results indicated that both RCBp and RCBsi were compactly embedded into the rubber matrix through covalent bonding with the addition of the excess 3-MPTMS, forming a filler-silane-matrix structure [123]. Rice husk ash biochar has improved interactions with rubber when phenolic formaldehyde (PF) resin is applied at 100 °C. It showed the highest tensile strength of 7.1 MPa compared to 6.5 MPa for N774 and 4.1 MPa for uncoated rice husk ash biochar [121].

Though there are limited studies on chemical activations on biochar for rubber reinforcement, they may prove to be advantageous to such applications and are thus briefly reviewed here. Reviewed chemical activation methods have been mainly used to modify the surface functional groups and, in some cases, the structure of the biochar. One study by [123] reports that rice bran carbon treated with HNO_3 and H_2SO_4 had a smoother surface with reduced amounts of impurities and amorphous carbon. The results from FTIR also showed that the biochar surface had an increased density of carboxylic acid (-COOH) and hydroxyl (-OH) functional groups. Rubber composites made with acid functionalized rice bran carbon showed an increase in modulus, but no improvement in tensile properties as compared to composites made with regular rice bran carbon was observed. The increase in modulus is believed to be due to the acid treatment which removed the impurities, increased its degree of crystallinity, and improved the incorporation of the filler in the matrix.

Other areas for improvement could focus on increasing the hydrophobicity of the biochar through chemical activation. Biochar is often chemically tailored for applications in environmental remediation, where it is used as an adsorbent for heavy oil, among other hydrophobic compounds. These chemical treatments may also be useful to test on biochar used in rubber filler applications as in both remediation and filler applications, biochar should be hydrophobic. [131] studied biochar modified with lauric acid, iron-oxide, and the combination of the two components, and compared them to biochar without treatment. They found that biochar treated with lauric acid had significantly higher uptake of oil as compared to the other biochar adsorbents. The mechanism was attributed to the carboxylic acid groups on lauric acid being attracted to oxygen containing groups on the biochar surface. This resulted in hydrocarbon chains attaching to the biochar and preventing water for penetrating the pores [131]. Lauric acid increased the hydrophobicity of the biochar by increasing the water contact angle [132]. The acid was also used in several studies as a coupling agent for enhanced filler-polymer interactions such as between fly ash and recycled polypropylene [133], between epoxidized natural rubber with PLA, and flax fiber and montmorillonite [134], among others. Other treatments to increase the hydrophobicity of biochar include H_2SO_4, HNO_3, KOH and magnetization treatments. Table 2.3 summarizes various chemical treatments and their effects on adsorption of oil due to biochar hydrophobicity.

Table 2.3 Summary of Chemical Modifications of Biochar to Enhance Hydrophobicity. Table adapted from [135]

Feedstock	Pyrolysis Temperature (°C) and heating rate (°C/min)	Modification/activation method	Application	Sorption Capacity (g adsorbate/g adsorbent) (attributed to hydrophobic effects)	Reference
Commercially available biochar	900, -	Modification with lauric acid and iron oxide	Removal of crude oil via hydrophobic interactions	3.31–9.40	[131]
Goat hair	300-500, -	Activation with H_2SO_4	Removal of petrochemical oils (crude, diesel, kerosene and petrol) via hydrophobic interactions	4.66 (diesel), 5.10 (crude oil), 3.67 (kerosene), 3.44 (petrol)	[136]
Coconut shell	1000, -	Acid activation with HNO_3 and H_2SO_4 (AC)	Removal of petrochemical oils (used and premium motor oils) via hydrophobic interactions	2.22 (premium oil) and 5.64 (used oil)	[137]
		Base activation with KOH impregnation (KC)		9.33 (premium oil) and 5.54 (used oil)	
		Activated carbon/iron oxide composite by in-situ co-precipitation technique (ACf = AC–iron oxide composite material and KCf =KC–iron oxide composite material)		3.01 ACf and 12.9 KCf (premium oil) and 7.59 ACf and 7.65 KCf (used oil)	
Date palm pits	800, 5	Modification with magnetic Fe_3O_4 nanocrystals (magnetic impregnation)	Removal of petrochemical oils (diesel and gasoline) via hydrophobic interactions	Diesel: 22.4 in deionized water, 21.9 in sea water Gasoline: 21.9 in deionized water, 21.0 in sea water	[138]
Water hyacinth	350-400, -	Chemical modification using NaOH and HCl, chemical activation with H_3PO_4 and $ZnCl_2$, immobilize magnetite	Removal of petrochemical oil via hydrophobic interactions	30.2	[139]

2.4. Current State and Performance Comparison

Several studies have aimed to ascertain the amount of biochar that can replace carbon black in rubber fillers without sacrificing performance. To date, the most promising result is the discovery that rubber composites filled with biochar derived from waste lignin could mechanically match and in some areas, outperform the carbon black control composites [21]. This has so far been the only study with a successful 100% substitution of carbon black with biochar without sacrificing mechanical performance.

Other studies have shown that partial substitution of traditional carbon black and silica fillers with biochar showed improvement over their control counterparts. In a progression of studies dating back to 2012 [6], the Peterson et al. research group have steadily experimented with feedstock selection [5, 7, 30], hydrophobizing treatments [31] and ball milling processes [73, 29, 30, 75] to optimize the biochar properties. Their recent breakthrough was using nanosilica as a co-milling agent in the biochar milling process, leading to replacement of 50% of carbon black with silver maple biochar in styrene butadiene composites [75].

Numerous studies on rice bran biochar in nitrile and SBR type rubber indicate that rice-based biochar is an effective filler, to an extent, as compared to unreinforced rubber controls [33, 122, 123]. However, the feedstock's high natural silica content caused excessive filler-filler interactions, which presented a challenge. As with traditional silica fillers, modifications with the appropriate organosilane coupling agents greatly enhanced the fillers' performance. Out of all the rice-based studies, the highest composite tensile strength recorded was 16.43 MPa in SBR filled with rice bran biochar functionalized with 4,4-methylene bis(phenyl isocyanate) (MDI) [122]. This was a 56.5% improvement over the control sample (unfilled SBR), which had a tensile strength of 10.5 MPa. Another rice-based biochar study [32] was able to replace 25% of carbon black filler with rice husk ash biochar in SBR rubber composites, improving the tensile strength compared to the 100% carbon black control (22.2 MPa for the biochar-carbon black blend vs 21.3 MPa for the control).

Several smaller independent studies indicate that when biochar replaces 100% of traditional fillers it has semi-low reinforcing characteristics while when it partially replaces traditional fillers it can have high reinforcing characteristics. This classification is based on comparing biochar as a filler against different grades of carbon black. Biochar with semi-low reinforcing characteristics mean that it performs similar to semi-reinforcing carbon black grades (like N990), as opposed to high reinforcing carbon black grades (like N330). These studies involved biochar fillers synthesized from coconut shell [34], dead leaves [112], dried distillers' grain [140] and bamboo [141]. On its own, coconut shell-based biochar behaved as a semi-to-low-reinforcing filler. The highest composite tensile strength reached 5.68 MPa as compared to carbon black control values of 20 MPa and 26 MPa for N772 and N330, respectively. Similarly, biochar from dried distillers grain resulted in a composite tensile strength of 15.6 MPa as compared to 29.5 MPa for the control composite filled with N762 carbon black. Dead-leaf based biochar performed better but was still in the semi-reinforcing range, indicated by a composite tensile strength of roughly 15 MPa as compared to 21 MPa for the N330 carbon black control [112]. Another study involved coupling bamboo-based biochar with silica formed in situ inside the rubber matrix from hydrolyzing tetraethoxysilane over a nitric acid catalyst. The composite performance was relatively poor when the biochar was used alone (2.76 MPa). However, in a 1/3 biochar 2/3 silica mixture, the composite performance improved by well over 300% (12 MPa). Even compared to a silica-only control (9.5 MPa) the mixture of biochar and silica yielded a 23.5% improvement in tensile strength. Table 2.4 presents a summary of the progress made incorporating biochar into rubber composites. The table includes results from the controls for performance comparison purposes.

Table 2.4 Summary of Current State Mechanical Performance of Biochar Fillers in Rubber Composites

Source	Feedstock, Rubber Type (BC = biochar, CB carbon black)	Process Conditions, Average Particle Size	Filler Concentration (phr)	Tensile Strength (MPa)	Elongation (%)	300% Modulus (MPa)	Hardness (Shore A)	Tear Strength (kN/m)
[32]	Rice Husk Ash (RHA), Emulsion SBR	-,6.97 ± 0.137 μm	22.5 RHA 67.5 CB	22.2	408	15.4	64	35
	Control (N234 CB)	-	90.0	21.3	454	13.7	71	37
[33]	Rice Bran Carbon (RBC), Nitrile Rubber	-,3.40 μm	100	7.65	492	6.36	72	45
	Control (no filler)	n/a	0	3.79	696	1.72	50	13
[122]	Rice Bran Carbon (RBC), SBR	Latex compounding method with 4,4-methylene bis(phenyl isocyanate) (MDI), 3.40 μm	-	16.4	306	16.3	77	51
	Control (no filler)	n/a	0	10.5	587	4.54	62	23
[123]	Rice Bran Carbon (RBC), SBR	Silane functionalized RBC (with 3-MPTMS) with 3phr silane agent, 3.40 μm	20.0	7.64	541	3.44	64	33
	Control (no filler)	n/a	0	2.11	640	1.30	55	11
[21]	Waste Lignin, SBR	-, 474 ± 81.9 nm (mean aggregate size)	40.0	9.86	507	6.11	-	-
	Control (N330 CB)	-, 807 ± 386 nm (mean aggregate size)	40.0	9.22	464	5.71	-	-
[75]	Silver Maple Biochar, SBR	Co-milled with 0.16% nanosilica (12.0 nm), mean particle size~1.30 μm	40.0 (40% BC, 60% CB)	23.5	419	-	-	-
	Control (CB N339)	-	40.0	24.7	318	-	-	-

[30]	Coppiced BC from Paulownia, Natural Rubber Biochar Only	Biochar co-milled with 1 wt% silica, -	50.0	7.40	275	7.60	-	-
	Mixture	Biochar co-milled with 1 wt% silica, -	50.0 (30% Paulownia BC, 70% CB)	20.1	443	4.30	-	-
	Control (CB N339)	-	50.0	21.0	388	6.00	-	-
[29]	Coppiced BC from Paulownia, Natural Rubber	Biochar co-milled with 1 wt% silica, -	42.8	19.3	519	2.20	-	-
	Mixture	50/50 mixture of biochar and carbon black	42.8 (50% BC, 50% CB)	24.3	527	2.80	-	-
	Control (CB N339)	-	42.8	25.7	476	3.90	-	-
[112]	Dead Leaf Biochar, NR	Pyrolyzed at 1000°C, 28.9 μm	15.0	~15.3	~675	~3.25	-	~51
	Control (CB N330)	-	15.0	~21.0	~550	~4.75	-	~51
[140]	Dried distillers' grain with solubles in NR Biochar Only	Pyrolyzed at 900 °C, ramp rate of 7.5 °C/min, ball milled in a FRITSCH Pulverisette Ball mill for 4 hrs Particle size distribution: 800 nm to 2.00 μm.	30.0	15.6	770	3.20	-	49
	Mixture	-	30.0 (50% BC, 50% CB)	21.4	750	4.00	-	51
	Control CB (N762)	-	30.0	29.5	675	5.00	-	71
[81]	Rice Husk Ash Biochar (57 wt% biochar and 43 wt% silica), NR	Dry milled in planetary ball mill for 720 minutes at 500 rpm, 5.81 μm	50.0	19.3	1487	2.88	-	39
		Ethanol milled in planetary ball mill for 720 minutes at 500 rpm, 5.28 μm	50.0	21.3	1268	3.53	-	39

		Wet milled in planetary ball mill for 720 minutes at 400 rpm, 3.72 µm	50.0	20.4	1248	3.66	-	37
	Control CB (N774)	-	50.0	18.3	1225	4.01	-	44
[34]	Pyrolytic coconut shell, SBR	600 °C temperature, 10 °C/min heating rate, 90 min holding time, wet Tema milled for 1.5 min, 40 µm	60.0	5.68	653	2.82	59	-
	Control CB (N330)	-	60.0	25.9	453	17.0	67	-
	Control CB (N772)	-	60.0	20.4	586	9.30	57	-
[141]	Bamboo charcoal, SBR	3-(methacryloxy) propyl trimethoxy silane modification, 10 µm	5.00 phr biochar, 40.0 phr of silica sol precursor (TEOS)-theoretical silica yield of 10.0 phr	11.7	1178	2.38	60	-
	Silica* and Bamboo charcoal mix	-	15.0 phr biochar	2.76	649	1.69	56	-
	Silica* control *silica derived from tetraethoxysilane (TEOS) hydrolysis over acid catalyst	-	50.0 phr of silica sol precursor (TEOS)-theoretical silica yield of 15.0 phr	9.48	1059	2.64	60	-
[6]	Biochar only (corn stover)	-, 0.890 mm (number average)	40.0	1.48	279	0.78	-	-
	Mixture 1:1 corn flour and biochar	-	40.0 (50% corn flour 50% biochar)	2.15	34.0	15.0	-	-
	CB only (N-339)	0.310 mm (number average)	40.0	5.10	156	12.0	-	-

[5]	Biochar Only (Low-Ash Woody Waste), SBR	-, 0.740 + 0.370 μm	30.0	2.76	257	2.57	-	-
	25% BC, 75% CB	-	30.0 (25% BC, 75% CB)	12.6	392	2.74	-	-
	CB only (N-339)	-	30.0	19.6	410	4.36	-	-
[7]	Biochar Only (birchwood)	-, ~80% of particles were 0.753 μm with 1.7% of particles 5.56 μm	30.0	8.01	538	-	-	-
	25% BC, 75% CB	-	30.0	19.7	548	-	-	-
	CB only (N-339)	-	30.0	15.9	618	-	-	-
[31]	Dry hardwood biochar, SBR	Biochar only (uncoated), -	40.0	7.15	459	5.84	-	-
	Dry hardwood biochar, SBR	coated with 5wt% heat treated maize starch, -	40.0	11.4	683	3.16	-	-

2.5. Conclusions

Reinforcing fillers are an essential component ensuring optimal safety and mechanical performance of rubber products. The rigidity of the fillers improves the stiffness, and the developed filler-rubber network leads to immobilized rubber, which serves as reinforcement when the composite is subjected to high strains. Carbon black and silica are the most common commercial fillers but there is ongoing effort to finding lower cost and more environmentally friendly fillers, such as biochar. Two attractive properties of biochar-based fillers are its comparatively higher carbon content over other bio-based fillers and its ability to be synthesized from renewable, low-cost biomass streams. However, studies conducted over the past decade indicate that biochar requires tailoring and is not a simple drop-in replacement for carbon black. The main issue with biochar is its tendency to have a larger primary particle size with a broader size distribution, which can lead to stress concentrations in the rubber matrix. Another issue is the hydrophilicity of the biochar which can reduce filler-polymer interactions. Biochar also tends to contain more ash and non-reinforcing material compared to carbon black and silica.

Though debate of the nature of reinforcement of rubber fillers is ongoing, the general consensus is that there are 3 main important physicochemical properties to optimize when creating a highly reinforcing filler: (1) small particle size, usually on the nanoscale with high surface area, (2) a highly disordered (turbostratic) structure leaving plenty of active sites for filler-polymer interactions and (3) a high level of surface activity, meaning strong interfacial bonding between filler particles and rubber polymers such that a well dispersed network is formed to allow effective stress transfer that reduces wear on the rubber matrix. Research indicates that biochar particle structure and surface activity can be optimized by controlling pyrolysis conditions such as the temperature, pressure, atmosphere, and pre-treatment of the biomass. The pre-treatment of biomass is a particularly promising route as not only can it remove exogenous ash, but it can also concentrate the char forming portions of biomass, namely lignin. To date, lignin-based biochar has had the most successful mechanical performance, achieving a 100% filler substitution on par with carbon black in SBR rubber. Future studies testing mechanical performance of lignin extracted from a variety of biomass streams could provide further confirmation of its potential. Though there are many environmentally harmful compounds in rubber composite manufacturing, reducing the environmental footprint of the filler component would represent a significant improvement. Biochar is a highly potential substitute, offering a multitude of research opportunities into its optimization for the rubber composite industry.

Connecting Statement

As indicated in Chapter 2, biochar can be effectively tailored for partial replacement of carbon black in rubber composites. The review identified the important considerations of reinforcing fillers to be their particle size, their structure, and their surface chemistry, all of which can be optimized during pyrolysis and through various pre and post treatment techniques. These optimization techniques were also reviewed and discussed in detail. The next chapter presents a study of the reinforcing performance of biochar fillers synthesized from 3 different corn feedstocks (corn cob, corn stover and corn starch). The physicochemical properties of these biochar types were examined in terms of size, structure, and surface chemistry, as these areas were deemed important from the literature review. Their reinforcing performance in SBR was then measured through testing the composite cure profiles, tensile properties and dynamic mechanical properties. The study effectively determined the current performance of corn starch, corn stover and corn cob-based biochar, identifying their advantages and limitations in terms of reinforcement potential, satisfying research objective 2.

Chapter 3.

Evaluating Corn Cob, Corn Stover and Corn Starch Based Biochar

Abstract

This study presents a characterization of corn-based biochar materials and examines their suitability as reinforcing fillers in styrene-butadiene rubber (SBR) composites. The specific objectives were to determine whether there were significant differences in performance, depending on (1) the part of the plant they are sourced from and (2) how refined the feedstock was prior to processing. Corn cob, corn stover and the more highly refined corn starch feedstocks were pyrolyzed at 700 °C for 1 h, at a heating rate of 50 °C min^{-1} under nitrogen gas. Fillers were evaluated in terms of size, structure, and surface chemistry, which are the 3 primary areas contributing to filler reinforcement mechanisms. The cure, tensile and dynamic mechanical properties of the biochar SBR composites were also evaluated and compared to SBR composites filled with N772 grade carbon black. The results indicate that corn stover biochar has the highest reinforcing index in SBR, only 17.5% lower than that of N772 in SBR. Biochar fillers from corn cob and corn stover had relatively similar characteristics, suggesting that they could be combined with minimal loss in performance. Starch biochar SBR composites were highly crosslinked but also significantly more brittle. Though all show promising reinforcing characteristics, corn-based biochar fillers are not yet on par with N772 carbon black, having poorer filler dispersion and lower reinforcement indexes. Further investigation and optimization of these alternative fillers is required before they can be considered for widespread use.

Keywords: rubber composites; biochar; carbon black; reinforcement; mechanical properties

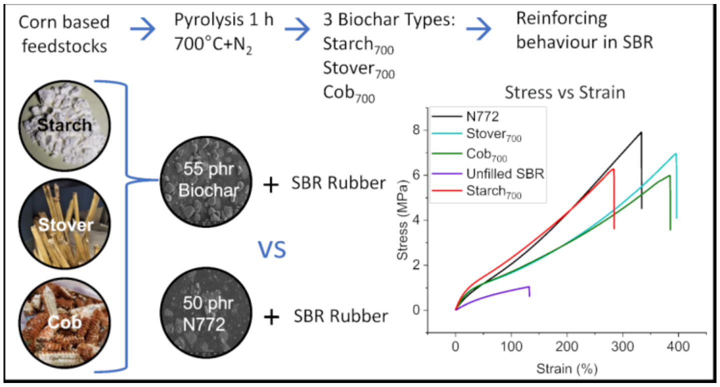

3.1 Introduction

Reinforcing fillers remain ever important for enhancing the performance and versatility of rubber materials. Though the nuances of rubber reinforcement mechanisms are still debated, the performance of fillers is thought to depend on their particle size, their structure, their surface chemistry and interaction with the elastomer matrix and vulcanizing system. Conventional fillers, such as carbon black and silica continue to dominate the market, but there is increasing pressure to shift to environmentally friendlier options. Numerous studies have evaluated the performance of fillers synthesized from clays [11, 13], carbon nanotubes [15] and natural fibers [16, 19, 22]. The alternative filler investigated in this study is biochar, a carbon rich material that can be synthesized from agricultural by-products via pyrolysis. The idea is that biochar could work on the same or similar principles as carbon black but use bio-based feedstocks as opposed to petrochemical feedstocks.

Biochar is a growing field of study, and the material has numerous applications, in soil amendment, filtration and carbon sequestration among others [23, 24, 84]. Its potential as a filler has also been explored in materials such as plastics, cement, etc. [142, 143]. Within the last decade, several studies have sought to characterize and test the rubber-reinforcing performance of biochar sourced from feedstocks such as corn stover [6], woody biomass [7, 29–31], rice husk ash [32], rice bran [33], dead leaves [112] and coconut shell [34, 35]. Most of these studies evaluated rubber composites made with biochar and carbon black blends, whereas this study shows the results from a full 100% replacement of carbon black with biochar. Evaluation of 100% biochar composites allows for a true apples-to-apples comparison with carbon black, since it is desirable that renewable fillers replace carbon black entirely without loss of performance.

This study focuses on biochar production from corn-based feedstocks, namely corn stover, corn cob and corn starch. Corn cob and corn stover feedstocks were selected for their widespread availability as agricultural by-products that are often unused. A comparison of their performance as biochar fillers could indicate whether there are significant differences in biochar produced from different parts of the same plant. Corn starch was then chosen to test the effect of pyrolysis on a purified form of polysaccharides, also taken from the same type of plant.

Worldwide, corn is considered the number one cereal crop, with an estimated 594 million tons of grain produced from 139 million ha [144]. After harvest, an estimated 8.6-8.9 Mg/ha of plant matter, including corn stover and corn cob is left on the field [8, 9]. Depending on the tillage method, 0.75-1.5 Mg/ha of residues should be left on the field for soil health, leaving 7.1-8.15 Mg/ha still available for other uses [9]. Thus, corn cob and stover are one of the most abundant sources of lignocellulosic material available to the bioeconomy, which aims to produce and convert renewable biological resources and waste streams into food, feed, bio-based products and energy [145].

Corn cob and corn stover are composed of hemicellulose, cellulose and lignin, in different ratios. From literature, corn cob contains between 28.7-41.3% cellulose, between 39.3-46.0% hemicellulose and 7.40-19.6% lignin [146, 147]. Compared to corn cob, corn stover contains more cellulose (34.2-46.5%), less hemicellulose (28.1-32.1%), and more lignin (21.4-24.8%) [147–149].

Corn starch, unlike corn cob and stover residues, is not a waste by-product. However, it is produced in abundance and has applications in the food and beverage, chemical, construction, mineral and metal processing industries [150] . It is composed of refined amylose and amylopectin, which are glucopyranose units joined by α(1-4) glycosidic bonds in the case of amylose, and α(1-6) glycosidic bonds in the case of amylopectin [151]. To the authors' knowledge, no studies exist where corn starch-based biochar is used as a filler in rubber composites.

This study first presents a physiochemical comparison between N772 carbon black and the three corn-based biochar fillers, in terms of filler size, structure and surface chemistry. Then the performance of the same fillers in SBR is evaluated in terms of cure kinetics, tensile properties, and dynamic properties.

3.2 Methodology

3.2.1 Biochar Preparation

Corn cob and corn stover feedstock were both collected from McGill's Macdonald campus farm, located in Sainte-Anne-de-Bellevue, Québec, Canada. Corn starch was provided by Sigma Aldrich (Oakville, Ontario, Canada). Husks and soil residues were removed from the corn stover through brushing. Each feedstock was dried at 105 ºC for 18-24 hours in a laboratory oven. The corn stalk and corn cob were ground using a Thomas® Wiley® steel mill (Thomas Scientific, n./a.). The ground feedstock was placed in a pre-weighed low-grade stainless steel cylindrical crucible measuring 15" in length and 1 ¼" in diameter. The full crucible was weighed before being placed in a horizontal, electrically heated pyrolysis unit, connected to a thermocouple device for temperature feedback. The unit's temperature was set to dwell at 700 ºC for 60 minutes, with a heating rate of approximately 50 ºC/min and under a constant flow of N_2 until the crucible cooled down to at least 150 ºC and was ready to be removed. The pyrolysis residence time of 60 minutes was chosen due to the high biochar yield, as demonstrated by [147]. The temperature of 700 ºC was justified by the fact that a higher temperature and heating rate favors a high biochar reactivity, as well as the carbonization of lignin, contributing to the overall carbon content and aromaticity of the biochar [152]. After cooling, the resulting biochar was weighed again to determine the yield, and then milled and filtered using a small kitchen blender and a 425 µm sieve. The biochar samples are referred to hereafter as $Cob_{700,}$ $Stover_{700}$ and $Starch_{700.}$

3.2.2 Preparation of Rubber Composites

Styrene-butadiene rubber (SBR), carbon black N772, N-(1,3-dimethylbutyl)-N'-phenyl-1,4-benzenediamine (6PPD), diphenyl guanidine (DPG), zinc oxide (ZnO), and stearic acid (SAD) were provided by Michelin Inc. (Greenville, South Carolina, USA). Biochar was pre-ground using a BlendTec commercial kitchen blender for 3 minutes, followed by sieving through a No. 120 mesh for 10 minutes. The sieved samples were then placed into a planetary ball mill (MTI Corporation, USA) and milled for 6 hours at 45 Hz. The ball mill set up consisted of two 500 cubic centimeter stainless steel jars, each filled with 15 grams of biochar, 750 grams of 1mm yitria-stabilized zirconia (YSZ)ball milling media and 60 g of ethanol (solvent). After milling, the contents were placed in a vacuum at 70 ºC overnight to dry and sieved for 90 minutes to remove the milling media. The biochar samples were then placed in a sealed container until their incorporation into the composite mix.

The rubber compounds were prepared according to the formulation shown in Table 3.1. The antiozonant 6PPD was used, along with diphenyl guanidine (DPG) as the accelerator, zinc oxide (ZnO) as an activator, and stearic acid (SAD) as a curing/release agent. From Table 3.1, the filler loading in the biochar-filled samples is slightly higher than the filler loading in the control N772-filled mix. This decision was made to attempt to balance the rigidity in each of the mixes, as bio-based fillers tend to have less structure than carbon black and are therefore less rigidifying in the rubber.

Table 3.1 Rubber Mix Ratios

Raw Material	Part per hundred rubber (phr)	
SBR 2300	100	100
Biochar	55	
Carbon Black (N772)		50
6PPD	2.0	2.0
DPG	2.0	2.0
ZnO	2.0	2.0
SAD	3.2	3.2

The mixing was done in a HAAKE PolyLab OS RheoDrive 16 (ThermoFisher Scientific, USA) rheometer, while the mixing parameters (rotor speed and mixing chamber plate temperature) were monitored by the Haake PolySoft OS software. An overview of the mixing process is shown in Table 3.2.

Table 3.2 Mixing Parameters

Time (minutes)	Rotor speed (rpm)	Step
0	90	Add elastomer
1	30	Add ½ biochar
2	30	Add ½ biochar
3	30, increase to 70 gradually	Add 6PPD, DPG, ZnO, SAD
4	70	Piston cleanse
5	70	Drop

The rubber mixture was subsequently milled using a two-roll mill (C.W. Brabender, USA) to incorporate the curatives, sulfur and the n-cyclohexyl-2-benzothiazole sulfenamide (CBS), at a temperature of 55 °C and a rotor speed of 9 rpm. The final thickness of the rubber composite was 3 mm.

3.2.3 Filler Particle Size Analysis (laser scattering method)

The agglomerate size of the biochar post ball-milling was analyzed by a Horiba laser scattering particle size analyzer (HORIBA, Ltd, Japan). The machine was calibrated using the refractive index of carbon black, 1.36 [153].

3.2.4 Filler Structure Analysis

3.2.4.1 BET/Surface Area

The surface area of the biochar samples was analyzed by a Quantichrome instruments analyzer (NOVA 4200e Quantachrome, United States). All samples were degassed at 120 ºC under vacuum overnight prior to BET analysis. The surface area was then calculated in terms of area per sample mass (m^2/g) based on the Brunauer, Emmett and Teller theory. The t-plot method was used to determine the micropore surface area and the average pore size was calculated using the Gurvitsch 4V/A BET method and the Barrett−Joyner−Halenda (BJH) method.

3.2.4.2 Structural Analysis (XRD)

X ray diffraction analysis was carried out on samples of the biochar agglomerates post ball milling, using a Bruker D8 Advance powder X-ray diffractometer (Bruker, USA, n.d). The operating voltage was 40 kV, and operating current was 40 mA. A Cu Kα X-ray tube was used to generate X-rays at a wavelength of 0.1541 nm. The measurements were performed at a scanning speed of 1.5°/min from 10° to 90°. Background subtraction and signal smoothing were done with HighScore Plus 3.0 software (PANalytical, Westboroough, MA).

3.2.5 Filler Surface Chemistry Analysis

3.2.5.1 Proximate Analysis

Proximate analysis was performed in triplicate for the corn cob, corn stover and corn starch feedstocks and their resulting biochar samples, Cob_{700}, $Stover_{700}$ and $Starch_{700}$. The quantities of moisture, volatile matter, ash and fixed carbon were determined according to procedures adapted from ASTM D1762-84 standards, as described in the book Biochar, a guide to Analytical Methods [154].

3.2.5.2 Elemental Analysis

Elemental composition was performed at the Université de Sherbrooke by the Laboratoire de Chimie Analytique, Laboratoire des Technologies de la Biomasse (LTB) (Sherbooke, Québec, Canada). The mass percentage of carbon, hydrogen, nitrogen, oxygen and sulfur (CHNOS) in the samples were determined using an adaptation of the ASTM D-5373-16 standard method. Analysis was conducted on samples in triplicate on a 2000 Organic Elemental Analyzer (Thermo Scientific, USA). The detection limit of N, S, O was 0.01%, 0.2%, and 0.01%, respectively, and the results are expressed in terms of mass fraction.

3.2.5.3 Surface Functional Group Analysis (FTIR)

Spectral components of the prepared biochar and feedstock samples were recorded in absorbance mode using a Thermo Scientific™ Nicolet™ iS5 FTIR Spectrometer (ThermoFisher Scientific, USA) with an iD5 ATR accessory. For each set, 32 scans were performed with a resolution of 4 cm^{-1} in the 4000-600 cm^{-1} range. The background spectrum was recorded on the disinfected laminated diamond crystal plate before recording the spectrum of each sample. The experiments were performed in triplicate and the resulting spectra were then corrected and analyzed using SpectraGryph 1.2 software. The absorption peaks were assigned to chemical functional groups based on data from literature.

3.2.5.4 pH

Biochar solutions were prepared with 1 g biochar in 10 mL of deionized water. The mixtures were mechanically agitated for one hour and the pH was subsequently measured using a pH meter with glass calomel electrodes. All biochar samples were measured in triplicate with the logarithmic mean calculated to report an average pH value. These average pH values were then compared with results from a carbon black sample that had been previously prepared under the same conditions.

3.2.6 Thermal Stability (TGA)

TGA analysis was performed using a TA Instruments Q50 Thermogravimetric Analyzer (TA Instruments, USA) under a 60.0 mL/min flowrate of nitrogen. The temperature was increased with a ramp rate of 10 °C/min from 25 °C to 700 °C. Experiments were conducted in triplicate on both feedstock and biochar. Data was analyzed using TA Universal Analysis Instrument software.

3.2.7 Composite Characterization

3.2.7.1 Cure Characteristics

The minimum time required to cure the composites was determined using an Alpha technologies 2000 rubber process analyzer (RPA) (Alpha Technologies, USA). Studies were carried out on mixed, unvulcanized samples for one hour at 150 °C. After, the unvulcanized samples were placed in a mold and cured in a Carver Press (Carver, Inc., USA) at 150 °C for 25 minutes under two platens imparting 12,000 lbs. of force onto the samples.

3.2.7.2 Morphology

The filler dispersion into the rubber was measured with a JSM-7100F thermal field emission electron microscope (JEOL, Belgium). A razor blade was used to cut the rubber to expose a fresh surface for the analysis. The samples were examined under magnification ranges between 50-10,000X under an accelerating voltage of 1.00 kV.

3.2.7.3 Tensile Properties

Dumbell shaped rubber composite samples were cut and tested using an Instron 5966 extensometer (Instron, USA). Tests were done according to ISO 37 type 2 at a constant rate of traverse of 500 mm/min until failure at break. Four samples were tested for each rubber mix.

3.2.7.4 Dynamic Mechanical Properties

Dynamic mechanical properties were examined with a Metavib dynamic mechanical analyzer (DMA) 450 Newton (Metavib, USA). Tests were performed at 10 Hz using a temperature sweep at a fixed shear strain of 0.7 MPa and a strain sweep at a 23 °C deformation temperature.

3.3 Results & Discussion

3.3.1 Filler Agglomerate Size Analysis

When discussing filler sizes, it is important to distinguish between 3 terms, agglomerates, aggregates, and primary particles. Primary particles can group together to form aggregates, which in turn can group together to form agglomerates. In this analysis, the sizes refer to the size of the agglomerates after they have been ball milled, and just before their incorporation into rubber. As observed in Figure 3.1, the agglomerate sizes for the biochar fillers taken post ball milling all appear to have 2 distinct modes: one centered at the 0.49-1.6-micron size and the other at the 50-60 microns range. The $Starch_{700}$ filler has slightly different sized distribution characteristics compared to $Stover_{700}$ and Cob_{700} fillers, having a broader distribution across the submicron range. N772 carbon black, on the other hand has several peaks, most of which fall below 60 microns. This distribution across several modes suggests that N772's agglomerates break apart more easily than the biochar, a property which could lead to superior dispersion when they are incorporated into SBR. Carbon blacks are also known to have a hierarchal structure, meaning that they form aggregates of smaller primary particles [48]. Though the agglomerates typically break down during the mixing process, the aggregates often stay intact, and their structure can affect their degree of dispersion in and reinforcement of the rubber matrix [155]. Biochar also forms agglomerates, but it is not fully clear whether these agglomerates are made of aggregates that also maintain their structure post mixing. In other terms, it is unclear whether the biochar could also have a high structure, like carbon black.

SEM images of the fillers can confirm the validity of the size distribution data from the laser scattering method give insight into the morphology of the agglomerates. SEM images of the fillers are shown in Figures 3.2 and 3.3.

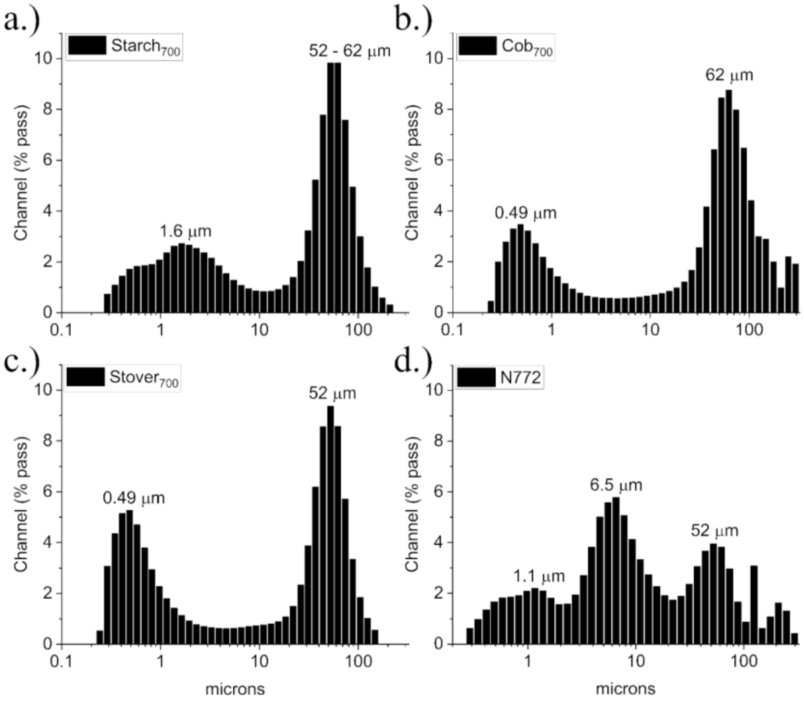

Figure 3.1 Particle Size Distribution for (a) Starch$_{700}$ (b) Cob$_{700}$ (c) Stover$_{700}$ and (d) N772

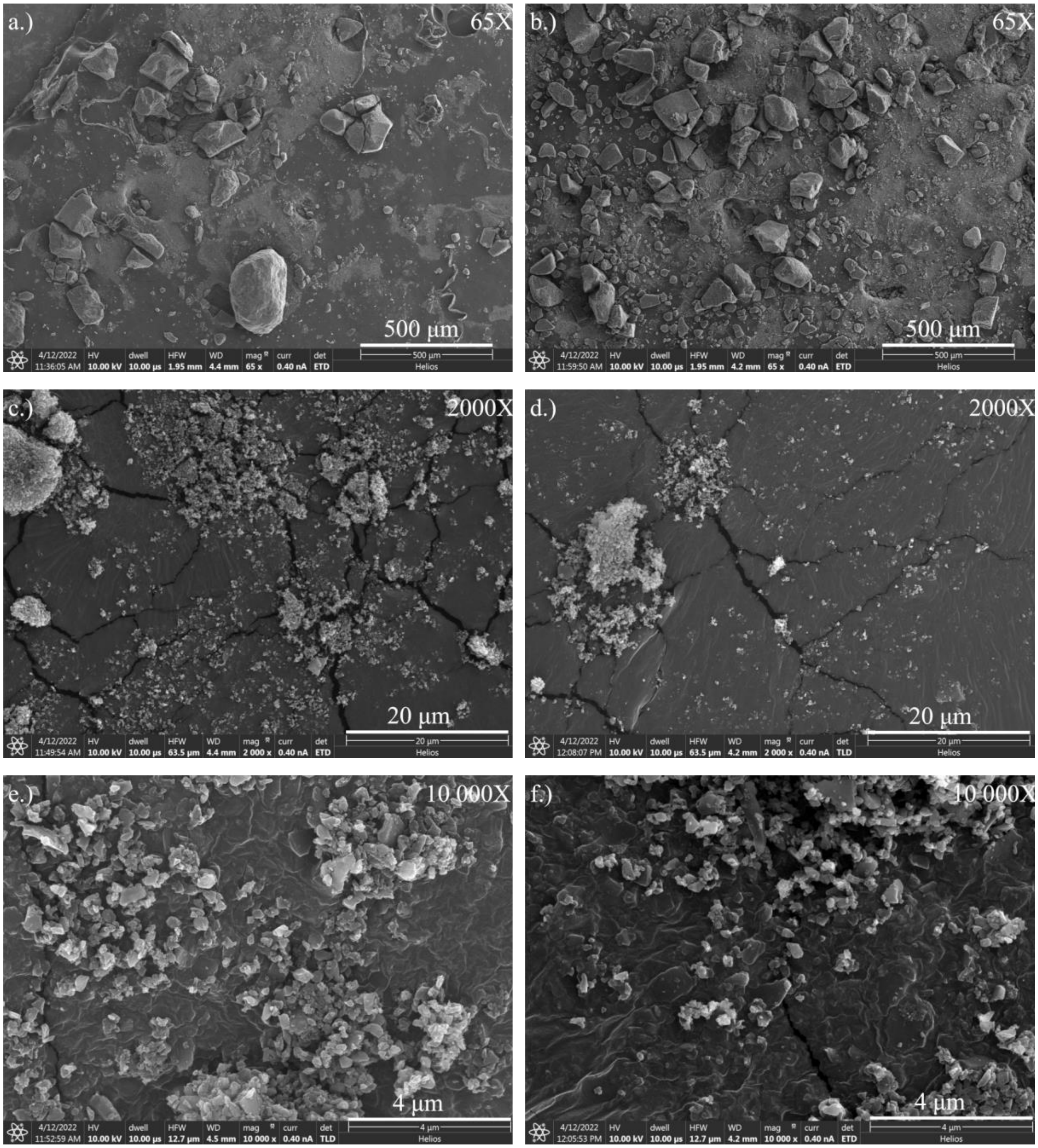

Figure 3.2 SEM images of (a, c &e) the Cob_{700} and (b, d, &f) Stover_{700} fillers at 65x, 2000x, and 10,000x

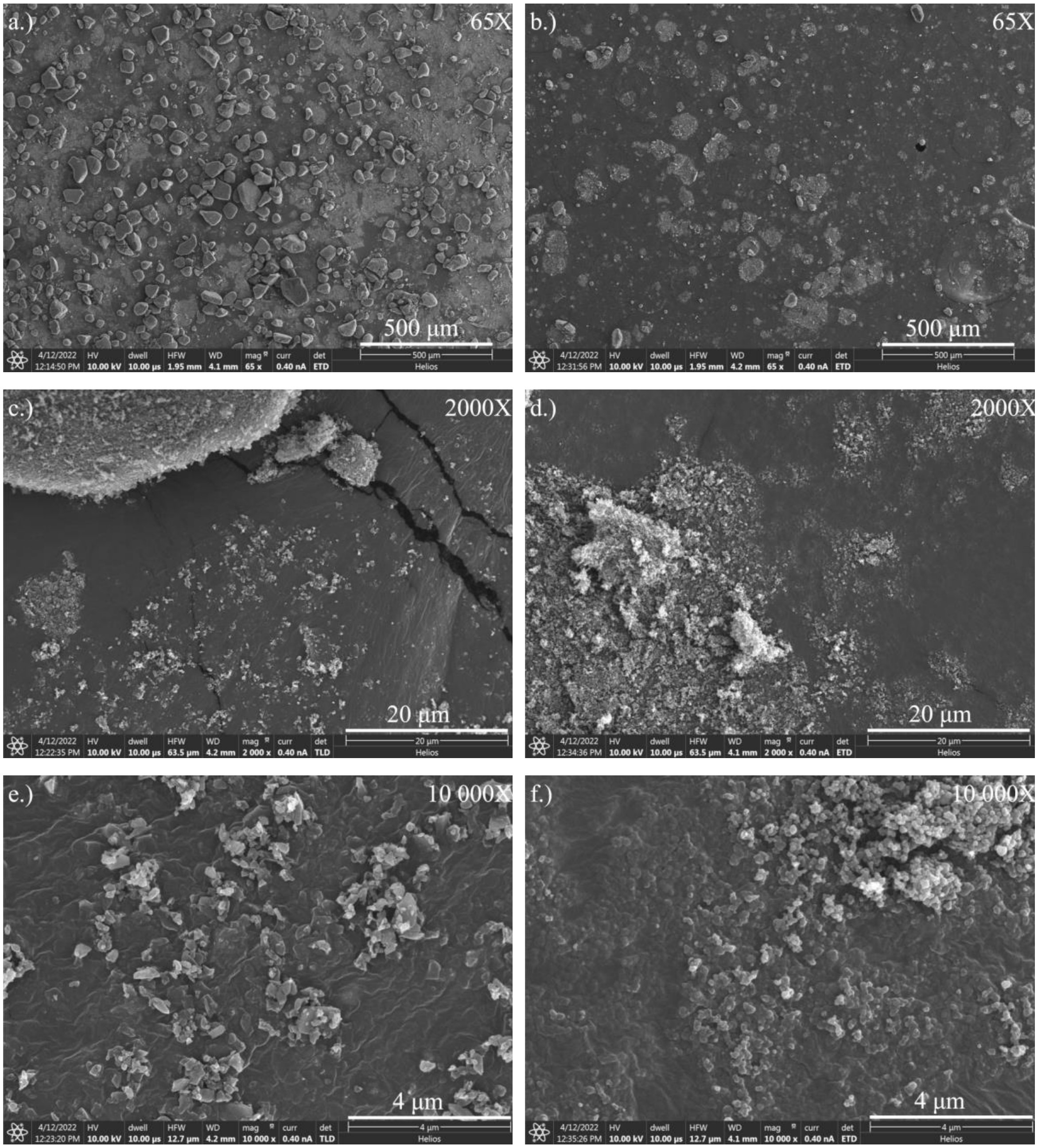

Figure 3.3 SEM images of (a, c &e) Starch$_{700}$ (b, d &f) N772 fillers at 65x, 2000x and 10,000x

Previous studies indicate the tendency of biochar to have a broader size distribution across primary particles, compared to carbon black, which is more homogeneous [5]. This presents a challenge when attempting to use biochar as a filler, as even small amounts of larger particles (> 3 μm) can be detrimental to the filler reinforcing effect. Having primary particles greater than 3 μm reduces the maximum packing fraction of the fillers, creating stress concentrations which can lead to early failure in the composite [7, 47]. The percentiles, or the D_{10}, D_{50} and D_{90} values of each of the fillers in this study are shown in Table 3.3.

Table 3.3 D_{10}, D_{50} and D_{90} values for biochar and CB N772 samples, on a volume percent basis

Sample	D_{10}	D_{50}	D_{90}
N772	0.802	7.37	78.35
Cob_{700}	0.440	43.09	124.4
$Stover_{700}$	0.369	24.69	66.50
$Starch_{700}$	0.776	33.47	77.79

Clearly, N772 has smaller agglomerates, with a D_{50} value of 7.36 compared with 43.1, 24.7 and 33.5 for cob, stover and starch biochar respectively. This means that 50% of the N772 agglomerates are smaller than 7.36 nm, while 50% of the corn cob biochar agglomerates are less than 43.1 nm, and so on. From the data, Cob_{700} has the broadest range across the D_{10} – D_{90} range and contains larger agglomerates sizes compared to $Starch_{700}$, $Stover_{700}$ and N772. Conversely, out of the 3 bio-based fillers, $Stover_{700}$ has the smallest D_{10} – D_{90} values, while $Starch_{700}$ has values between Cob_{700} and $Stover_{700}$.

The SEM images in Figures 3.2 and 3.3 give excellent insight into the morphology and particle size distribution of the fillers. In Figures 3.2a, 3.2d and 3.3a at 65x, all biochar samples appear to have larger, more irregularly shaped agglomerates compared to carbon black, shown in Figure 3.3d. Cob_{700} appears to have the largest agglomerates (>200 μm), with the larger agglomerates of $Stover_{700}$ and $Starch_{700}$ being slightly smaller (<200 μm). Additionally, $Starch_{700}$ appears to have a more uniform agglomerate size distribution compared to the other biochar samples. Overall, these results show good agreement with the data obtained from the laser scattering particle size analysis.

3.3.2 Filler Structure

3.3.2.1 BET Surface Area of Biochar Samples

For the purposes of fair comparison, BET values were compared to each other using the same method and degassing conditions rather than assessed based on values in literature. In terms of pore size determination, the results using the Gurvitsch 4V/A BET method are presented for comparison over the data from the Barrett−Joyner−Halenda (BJH) method, due to large variations between values estimated from the adsorption and desorption isotherms using the latter method [156]. Analysis of BET data shown in Table 3.4 confirms that the biochar sample surface areas are significantly larger than the surface area of N772, with Stover$_{700}$ having a surface area of 35.3±0.728m²/g, which is closest to that of the N772 carbon black sample (29.0±0.0620m²/g).

Table 3.4 Summary of BET, t-plot and pore size results

Sample	Total BET surface area (m²/g)	t-plot Micropore Area (m²/g)	Adsorption Average Pore Diameter (4V/A by BET) (nm)
N772	29.0±0.0620	3.10	42.5
Cob$_{700}$	47.8±1.97	59.6	1.11
Stover$_{700}$	35.3±0.728	33.4	1.99
Starch$_{700}$	125±5.18	121	Data unavailable

In biochar, it appears that most of the surface area is due to microporosity. Indeed, the micropore areas compose 94.6% and 96.8% of the total BET surface areas for the Stover$_{700}$ and Starch$_{700}$ samples, respectively. The micropore surface area of Cob$_{700}$ however, is larger than the total surface area, which is nonsensical. This could be explained by the fact that N_2 is used rather than CO_2, as well as by the equations used in the t-plot approximation [157]. Carbon black on the other hand is more mesoporous, with the micropore area representing just 10.7% of the total BET surface area. Comparing the average pore diameter, N772 has significantly larger pores falling in the mesoporous category (>2nm and <50nm). For where data is available, the biochar samples have average pore sizes falling in the microporous category (<2 nm). This could impact its reinforcing capability in two ways. The first way is that biochar's high surface area and microporous nature could cause adsorption of more vulcanizing agents which could slow the vulcanization rate, decreasing the cure rate index

[21]. The second effect is that micropores are generally too small to provide additional active sites with the rubber chains. Rubber chain sizes are in the mesoporous (2-50nm) to macroporous range (>50 nm), so mesoporous fillers would provide more opportunities for rubber-filler interactions, given that the rubber chains can access the interior of the pores [56, 57].

3.3.2.2 X-Ray Diffraction

The diffraction patterns of ball-milled biochar samples and N772 are presented in Figure 3.4. The 2 broad peaks, shown at 23° and 43° in all 4 samples correspond to the 002 and 100 planes of graphene sheets within turbostratic carbon, which is widely supported in literature [158–161]. The 002 plane is associated with turbostratic graphene sheets in the vertical orientation while the 100 crystalline plane related to the lateral growth of the sheets [162, 163]. The peak intensity of the 002 plane is noticeably sharper for the N772 sample than it is for the biochar samples, indicative of having a comparatively more ordered carbon structure [164, 165]. Turbostratic carbon is thought to be an effective filler in the free radical theory of bound rubber formation. This is because the disorder in the structure may provide a source of delocalized electrons at the crystallite edges, which can then combine with polymer free radicals to form bound rubber [52, 55].

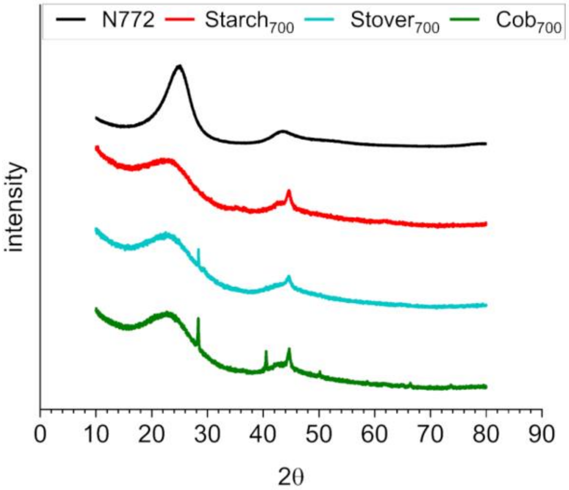

Figure 3.4 X ray Diffraction Patterns for ball-milled filler materials

Another noticeable series of peaks at 44° in all 3 biochar is attributed to chromium, which has been confirmed by an adapted ISO-16967 elemental analysis study performed on the corn stover biochar, both before and after ball milling. Analysis of samples taken post ball milling show elevated chromium, suggesting the process may have introduced additional minerals into the samples. Other minerals detected in the study include Mg, Al, Si, P, K, Ca, Cr, Fe and Cu. Overall, the 3 biochar samples have similar patterns, with slight variations seen in the smaller crystalline peaks, which are likely due to differences in ash composition.

3.3.3 Filler Surface Chemistry

3.3.3.1 Proximate Analysis, Elemental Analysis and pH Values

Carbon black is known to have oxygen containing functional groups, which are believed to enhance its rubber reinforcing potential [166]. Various techniques were thus used to verify biochar's chemical composition, to see if there were similarities with carbon black. The results for elemental and proximate analysis of both the feedstock and biochar samples are displayed in Table 3.5, along with the biochar pH values.

In terms of feedstock composition, Cob_{700} and $Stover_{700}$ appear to be similar with some slight variation that can be seen especially in the proximate analysis values. The larger trends tend towards $Stover_{700}$ having a higher quantity of ash (2.47±0.63% vs 0.49±0.53 wt.%) and a lower amount of fixed carbon (11.62±0.07 wt.% vs 13.56±1.57 wt.%) compared to Cob_{700}. $Starch_{700}$, on the other hand has an exceptionally low ash content (trace) and a low fixed carbon content (1.70±0.80), with 98.30±0.80 wt.% in volatile matter.

As can be seen in the elemental analysis portion of Table 3.5, pyrolysis increases the fixed carbon content of the biochar samples, as the volatile matter is consumed. The mass fraction occupied by the ash also appears to increase, again, likely due to the loss of the heavier volatile matter in the feedstock. The composition of the N772 carbon black reference sample is primarily carbon (96.1 ± 1.2 %), with small quantities of hydrogen, oxygen, and sulfur. This is consistent with the proximate analysis of carbon black, which indicates a high fixed carbon (FC) content (97.09 ± 0.44 %), as well as low levels of volatile matter (VM) (2.61±0.81 %) and ash (0.300±0.52 %). Though the fixed carbon content of the biochar samples is higher than the feedstocks, carbon levels are significantly lower compared to carbon black, a finding which is supported in studies on biochar based fillers [5, 6]. Along with lower carbon content, the biochar samples contain higher amounts of other elements, notably hydrogen, oxygen and nitrogen, as well as higher levels of volatile matter and ash, relative to carbon black. The biochar sample with the highest fixed carbon content is Cob_{700} (80.82 ± 1.27 %). This biochar also contains the lowest percentage of volatile matter (14.72 ± 0.94 %). On the other hand, $Starch_{700}$ has the lowest ash content (0.60 ± 0.34 %), a value that is the closest to carbon black's ash content. $Starch_{700}$ also contains the second to highest amount of carbon and fixed carbon, with levels of 78.9 ± 0,8 and 78.90 ± 1.46 %, respectively. $Stover_{700}$ shows the lowest amount of fixed carbon (77.93±0.54) and the highest ash content (6.90±0.62) of the 3 biochar types.

In biochar, a higher percentage of carbon implies an increase in aromaticity and lower amounts of elements that make up polar and hydrophilic functional groups [167, 168]. Therefore, biochar with a higher carbon content may be more hydrophobic and, possibly, more compatible with the non-polar and hydrophobic rubber matrix. On the other hand, studies on carbon black indicate that oxygen-containing functional groups may enhance bound rubber formation through providing a source of free radicals [34]. Studies indicate the functional groups on the surface of carbon black may generate free radicals which can help decompose polymer groups (such as SO_2Cl groups on Chlorosulphonated Polyethylene Rubber (CSM)), generating polymer free radicals which can then combine with the carbon black surface to form bound rubber. In this way, carbon black behaves both as a free radical donor and acceptor [166].

The surface pH of a filler can impact reinforcement in 2 ways. First, it can indicate presence of oxygen-containing functional groups, which may assist in the formation of bound rubber. Secondly, the pH can have an impact on the vulcanization rate by affecting the efficiency of the crosslinking agents [166]. Studies indicate that while alkali groups on fillers increase the cure rate, acidic groups tend to slow down the curing rate, which can have negative repercussions on the crosslinking density [60, 62]. The N772 carbon black has a pH of 8.55 in literature [34] and in this study, an experimentally measured value of 7.56 was found. All three biochar samples have basic pH levels with corn stover having the highest value (10.2), followed by corn cob (8.91) and corn starch (8.03). These findings suggest that, in terms of pH, the biochar samples could possess reasonable surface chemistry promoting the formation of bound rubber.

Table 3.5 Basic Physicochemical Properties of Feedstocks and Biochar Samples

Sample	Yield (wt. %)	pH (logarithmic mean)	Elemental analysis (wt.%)					Proximate analysis (wt.%)			
			C	H	N	O	S	Moisture content	Volatile matter (VM)	Ash content	Fixed carbon (FC)
N772	n/a	7.56	96.1±1.2	0.29±0.01	trace	0.34±0.02	1.28±0.04	0.56±0.97	2.61±0.81	0.30±0.52	97.1±0.44
Corn Cob (feedstock)	n/a	n/a	46.0±0.64	5.96±0.08	0.56±0.01	27.8±0.50	trace	4.53±2.7	86.0±1.5	0.49±0.53	13.6±1.6
Cob$_{700}$	22.6	8.91	81.3±0.60	2.30±0.13	0.79±0.02	8.49±0.67	trace	2.99±0.98	14.7±1.2	4.45±0.61	80.8±1.6
Corn Stover (feedstock)	n/a	n/a	45.1±0.57	5.94±0.18	0.41±0.02	29.2±0.60	trace	5.33±0.58	85.9±0.70	2.47±0.63	11.6±0.07
Stover$_{700}$	20.6	10.2	77.4±1.1	2.11±0.04	1.07±0.03	8.23±0.30	trace	3.65±0.57	15.2±0.51	6.90±0.62	77.9±0.54
Corn Starch (feedstock)	n/a	n/a	39.3±0.40	6.2±0.10	trace	51.6±0.60	trace	trace	98.3±0.80	trace	1.70±0.80
Starch$_{700}$	7.48	8.03	78.9±0.80	2.76±0.08	0.24±0.01	12.1±0.30	trace	3.67±0.58	20.8±0.93	0.60±0.34	78.9±1.5

3.3.3.2 FTIR

Feedstock

Data from FTIR is shown in Figure 3.5, with specific labels on major peaks. Beginning with the feedstock spectra for corn starch (Figure 3.5a), there is a prominent peak at 3319 cm^{-1} which is attributed to O-H stretching, and a peak at 2929 cm^{-1}, which is related to C-H stretching modes [169]. At 1643 cm^{-1} , there is another peak which, in the case of starches, is attributed to water adsorbed in amorphous regions of the molecule [169–172]. A series of peaks between 1338 and 1500 cm^{-1} is attributed to CH_2 bending [173], while a peak near 1094 cm^{-1} is attributed to C-O-H bending modes [173]. Peaks at 999 cm^{-1} and in the 705-850 cm^{-1} range are respectively attributed to C-O stretching and the C-O-C ring vibrations associated with carbohydrates [170]. Finally, a peak at 570 cm^{-1} could indicate the vibrations of the pyranose ring within the glucose units of starches [169].

The FTIR spectra corresponding to corn cob and corn stover are very similar to one another, showing peaks typical of lignocellulosic materials. The first identifiable peak, at around 3363 cm^{-1}, is indicative of alkene groups mono-substituted by hydroxyl and carboxyl groups with O-H stretching vibrations [174–176]. Then, a saturated aliphatic group with a C-H stretching vibration can be seen around 2908 cm^{-1} [175–177]. The group of bands ranging from 1740 to 1700 cm^{-1} are attributed to the presence of carboxyl and ketone C=O stretching vibrations [176, 178]. The band at around 1630 cm^{-1} is attributed to cis C=C stretching bonds [176, 178]. Entering the fingerprint region of the feedstocks, another C-H bending vibration can be identified by the two peaks situated at around 1430 and 1370 cm^{-1} [87, 176]. These are followed by some C-O-C stretching vibrations from cellulose and hemicellulose components, shown by the series of peaks from around 1320 to 1000 cm^{-1} [174, 176]. Finally, there are a few peaks which fall within the aromatic C-H deformation region of 900 to 700 cm^{-1} [174, 176, 179].

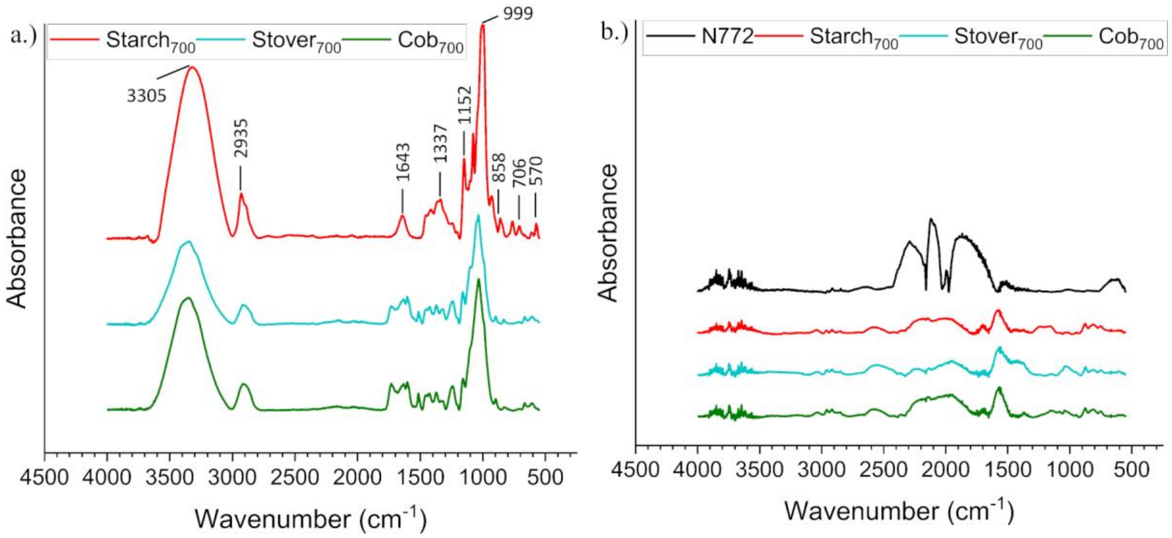

Figure 3.5 FTIR data of (a) feedstocks and (b) N772, Starch$_{700}$, Stover$_{700}$ and Cob$_{700}$ fillers

Biochar

Through pyrolysis, most functional groups initially present in the feedstock are reduced or removed completely, due to the dehydration and deoxygenation reactions that occur in the feedstock [87, 88, 180]. The removal of most functional groups is clearly observed, given the lower peak heights for the biochar spectra (Figure 3.5b), compared to the feedstock spectra (Figure 3.5a). In the biochar samples, the O-H peak is completely removed and the C-H peaks at 2916 cm^{-1} are vastly reduced. Additionally, the spectra for all 3 biochar samples show the presence of peaks associated with aromatic structures. For instance, a strong peak at 1570 cm^{-1} is associated with aromatic C=C stretching of carbonyl groups [85]. Weaker peaks observed in all biochar samples near 1427 cm^{-1} represent C-O stretching vibrations of phenolic groups present in the materials [181]. The series of peaks between 900 and 700 cm^{-1} revealed aromatic C-H deformations, which are often observed in spectra of biochar made of corn cob and other lignocellulosic feedstocks [174, 176, 177, 179]. Overall, the spectral data correlates to the increased fixed carbon content, indicated by the data from proximate and elemental analysis.

The relationship between the filler surface chemistry and reinforcement is somewhat conflicted in literature, yet most carbon black fillers have oxygen-containing functional groups such as carboxyls, lactones and quinones among others, while maintaining high affinity with rubber [48]. The quinonic and phenolic hydroxyl groups on carbon black have, in fact, been identified as potential primary free radical sites [166]. In lieu of sulfonate linkages, these radicals may combine with polymer free radicals formed during the mixing process, leading to the formation of covalently bound rubber. This is in contrast to other research which suggests that oxygen containing groups may negatively affect reinforcement, generally through slowing the curing rate and reducing the crosslinking density [60–62]. Other research indicates that carbon black with surface oxidation increases the thickness of the bound rubber layer [182].

Therefore, it is not clear whether there is an ideal limit to surface groups on biochar. Elemental analysis of the biochar and N772 samples indicates biochar has a significantly higher percentage of oxygen compared to N772. However, FTIR does not give conclusive results on whether the surface chemistry of biochar is similar to carbon black. There are little differences in peak intensities and peak locations present on the different biochar samples suggesting that there is little difference in terms of surface chemistry among the different biochar types. Due to the similarity in the surface functional groups from FTIR, any differences in performance between the biochar types would likely be due to other factors, such as porosity, ash content, etc.

3.3.4 TGA

Thermogravimetric analysis served two important purposes. It was first performed on the corn-based feedstocks to simulate their conversion into different biochar samples. The intention was to gain insight into the different conversion stages and confirm the complete transition of the biomass into a carbon-rich, bio-based filler. Thermogravimetric analysis was then performed on the biochar samples to evaluate the thermal stability of the fillers, as rubber composites must withstand higher temperatures during formation and during application [183] . The thermal behavior of the feedstocks as well as the biochar samples are presented in Figure 3.6 and Table 3.6.

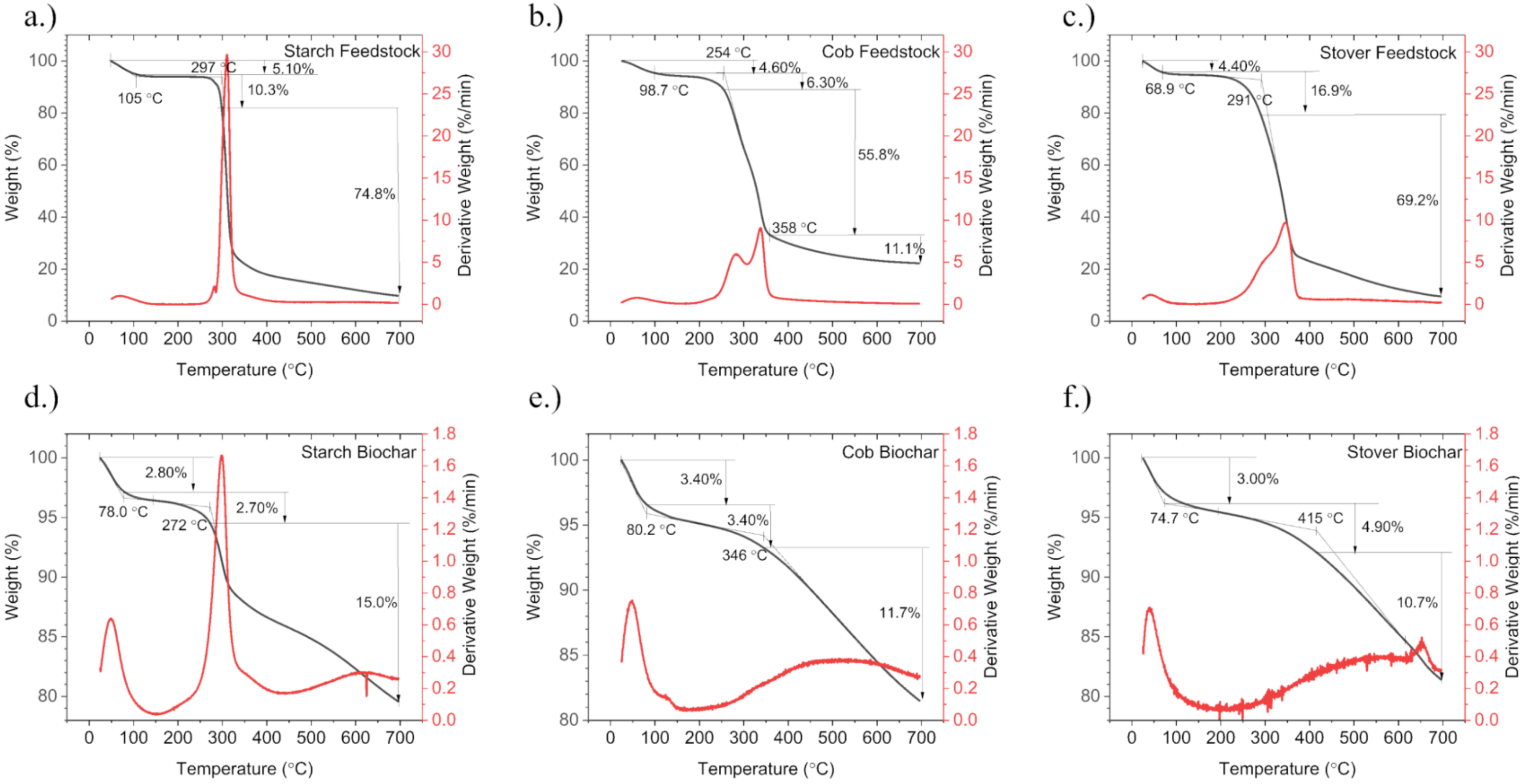

Figure 3.6 TGA graphs of corn starch, corn cob and corn stover feedstocks (a-c) and biochar (d-f)

Table 3.6 Percent Weight Remaining of Filler Samples with Increasing Temperature (FS = Feedstock)

	Percentage of weight remaining						
Sample	100 °C	200 °C	300 °C	400 °C	500 °C	600 °C	700 °C
Cob_{700}	96.1	95.1	94.1	91.8	88.2	84.5	81.5
$Stover_{700}$	96.4	95.4	94.5	92.5	89.2	85.3	81.4
$Starch_{700}$	96.8	96.1	91.1	86.6	84.8	82.3	79.6
Corn Cob FS	95.3	93.7	66.5	29.9	25.5	23.3	22.2
Corn Stover FS	94.8	94.1	74.3	23.0	17.2	12.3	9.49
Corn Starch FS	95.2	93.9	79.1	17.9	14.8	12.0	9.75

Feedstocks

Figures 3.6a-c show the thermal conversion of the corn-based feedstocks into biochar. The onset temperatures for each stage were determined based on ASTM E2550 methods, using the TA Universal Analysis Instrument software.

In the case of corn starch (Figure 3.6a), there are two distinct stages in the thermogravimetric curve, corresponding to results in literature [184–186]. In the first stage, called the preheating or drying stage, there is evaporation/dehydration until nearly 300 ºC, where the percentage of mass loss corresponds to the moisture present in the sample (approximately 15.4%). Then, beginning at 297 ºC and in agreement with literature, there is another large change in mass (74.8%), due to thermal decomposition reactions. This is called the devolatilization stage, where most of volatile matter (CO, CO_2, and hydrocarbon) is released.-As previously mentioned in section 1.0, corn starch is composed of glucopyranose units with two different configurations. Amylose has a linear structure, connected with α(1-4) glycosidic bonds, while amylopectin has a branched structure, connected with α(1-6) glycosidic bonds [151, 185]. The thermal decomposition of corn starch occurs at the glucose ring level, typically with hydrolysis of the α-1,4 glucosidic linkages prior to the α(1-6) glucosidic linkages [184, 185, 187]. From Figure 3.4a, the cornstarch appears to degrade almost entirely by 700 ºC, with just 9.75% mass (ash) remaining at the final temperature.

With corn cob and corn stover feedstocks (figures 3.6b and 3.6c), the thermogravimetric curves have 3 distinct stages. In the preheating/drying stage, moisture is lost, accounting for an 4.60% mass loss in corn cob and a 4.40% mass loss in corn stover. In the second stage, devolatilization occurs, with onset temperatures of 254 ºC and 291 ºC for the cob and the stover respectively. This is consistent with literature as both corn cob and stover are primarily composed of cellulose, hemicellulose, and lignin, which have different onset temperatures for their decomposition.

Hemicellulose is the least thermally stable, due to its simple linear structure, and typically starts to degrade above 200 ºC into CO, CO_2 and hydrocarbons [188]. More precisely, [189] suggests that the pyrolytic degradation of hemicellulose occurs between 225-325 ºC, while cellulose begins to degrade later, between 326-375 ºC [189]. Lignin is the least thermally reactive constituent, as it has a more complex, heterogeneous structure [188, 190]. As a result, it also has a broader decomposition range, with the largest reported range being from 150 ºC up to 900 ºC [188]. Primary reactions are said to take place between 200-400 ºC , with a peak in DTG curve near 350 ºC, while secondary reactions take place above 450 ºC [190]. The decomposition of these primary constituents can be seen in Figures 3.6b and 3.6c, with the overlap of peaks in the 300-350 ºC region, along with the flatter curve at the tail end. The first shoulder can be ascribed to the degradation of hemicellulose, while the second can be ascribed to the degradation of cellulose [146]. The slightly curved end tail, beyond 400 ºC is associated with lignin, which decomposes more gradually [149, 191].

As corn stover contains less hemicellulose (28.1-32.1%) compared to corn cob (39.3-46.0%), this results in a barely noticeable initial shoulder in Figure 3.4c. In contrast, the curve of the corn cob feedstock in Figure 3.6b has a distinct first shoulder, with the DTG curve peaking just prior to 300 ºC. Corn stover feedstock also contains more lignin (21.7-24.8%) than corn cob (7.40-19.6%), which may explain the higher weight loss in the carbonation stage for corn stover. In both thermogravimetric curves, the materials are nearly completely degraded by 700 ºC, with just 22.2% mass of corn cob and 9.49% mass of corn stover remaining.

Biochar

Of the biochar samples, Cob_{700} appears to be the most thermally stable, losing 18.5% mass during heating to 700 ºC, followed by $Stover_{700}$ and $Starch_{700}$, which lose 18.6% and 20.4% mass, respectively. The derivative weight loss (DTG) curves also reflect the improved thermal stability of biochar compared to the raw biomass. The maximum weight loss for the biomass varies between 9 to 30 wt% min^{-1}, whereas the maximum weight loss for the biochar samples is significantly lower, varying between 0.6 and 0.8 wt% min^{-1}.

The initial sharp weight loss in all samples is due to moisture loss and water evaporation, as samples were not dried before being analyzed. The second, broader weight loss stage is attributed to the removal of residual volatile matter and organic materials from around 200 ºC to 600 ºC [192–194]. Studies indicate that hemicellulose and cellulose components are thermally degraded by 400 ºC [146, 189], hence biochar produced above these temperatures would likely no longer have these constituents. Therefore, we can assume that all weight loss related to organic material is due to further lignin decomposition in the biochar samples [195]. Proximate analysis results in Table 3.5 indicate that the biochar samples retain 14.7-20.8% of their mass in volatile matter, which provides the source for the devolatilization seen in the thermogravimetric curves.

While biochar is inherently more thermally stable than biomass, it is significantly more thermally volatile compared to N772. In the same heating process, carbon black (TGA curve not shown) lost an average of 2.3% mass, while the biochar samples lost nearly 10 times that amount. This could be an area of weakness for biochar fillers, as rubber composites in high friction applications will build up heat, and it is vital for the embedded filler to withstand higher temperatures to ensure the rubber composite structure remains intact. In contrast, considering that rubber applications need to be maintained below the melting temperature of the rubber, the thermal stability of biochar may be sufficient. In this study, biochar loses 4-5% of the initial mass by 200 ºC, some of which is likely moisture. However, compared to N772 which only lost 1% at 200 ºC, there is still a difference in thermal stability which could prove significant. It is possible that biochar could be made more thermally stable by manipulating the thermal treatment conditions, such as the temperature and residence time, as literature shows that the higher the temperature during pyrolysis, the less volatile matter the biochar will contain and thus, the thermal stability will be greater [196].

3.3.5 Composite Performance

3.3.5.1 Cure Characteristics

The rheographs in Figure 3.7 presents the cure behavior of rubber reinforced with the different biochar samples along with the N772-reinforced rubber control sample. The cure rate indices shown in Table 3.7 were calculated based on the ASTM D-2084 and ASTM D5289 methods. The ASTM D5289 method of finding the scorch time (T_{C10}) was used over the ASTM D-2084 method, (T_{s2}), because T_{C10} can be measured independently of the torque units used, and it is the better parameter for comparison among composite samples with large variances in maximum torque, M_H, values [197].

The cure rate index was calculated using the formula

$$CRI = \frac{100}{(t_{90} - t_{C10})} \tag{1}$$

where

T_{C10} is the incipient scorch time and is equal to the time to reach a 10% state of cure, and T_{90} is the optimum cure time and is equal to the time required to reach 90% of the maximum torque, M_H.

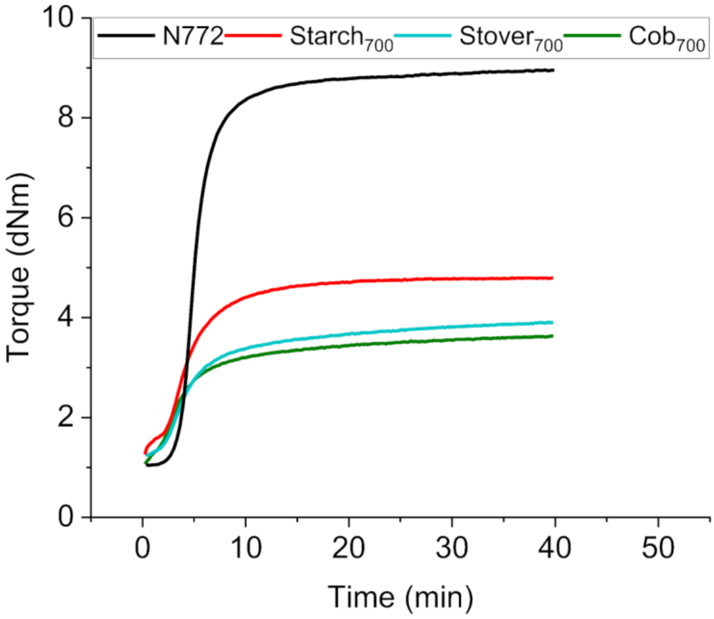

Figure 3.7 Cure curves for biochar filled composites and N772 filled composite

Table 3.7 Cure Rate Indices for corn cob, corn stover and corn starch biochar samples

Sample	Optimum cure time, t_{C90} (min)	Incipient scorch time, t_{C10} (min)	Maximum Torque, M_H (dNm)	CRI
$Starch_{700}$	9.06	2.54	4.80	15.3
Cob_{700}	11.9	2.05	3.63	10.2
$Stover_{700}$	13.4	2.83	3.90	9.48
N772	8.53	3.79	9.01	21.1

Examining the initial section in Figure 3.7, all biochar samples have lower scorch times than the N772-filled rubber, showing rapidly increasing torque values in the initial mixing process. It is known that carbon black and fillers with hydroxylic and carboxylic functional groups can adsorb the accelerator, which has been associated with shorter scorch times [198, 199]. In these cases, the shorter scorch time has been attributed to alteration of the cure system from a semi-efficient system to a conventional system, due to a change in the sulfur to accelerator ratio [199]. It is possible that the high specific surface area and extra oxygen content within biochar also allows it to adsorb more accelerator, leading to the lower scorch times.

On the other hand, too high of a sulfur to accelerator ratio would have the opposite effect, slowing the overall curing process [200]. It is possible that biochar adsorbs even more accelerator than other filler types, leading to an eventual decrease in the curing rate, despite a rapid start [21]. This could explain why the biochar-based composites have lower cure rate index values than N772, despite their rapid start. Additionally, fillers with higher thermal conductivity have been shown to have accelerated curing profiles, due to an increase in heat transfer and molecular movement of the polymer network [201]. Biochar, however is highly microporous, which reduces its thermal conductivity [202]. This may be another reason why its cure profile is slower overall compared to carbon black. More thorough studies are required to explore to what extent biochar reacts with the vulcanizing system and whether the filler porosity influences the cure rate index.

Within the overcuring region, it is thought that efficient vulcanization is characterized by a plateau in the curve [203]. This signifies that the filler and rubber matrix has reached a network equilibrium, and that the stiffness of the reinforced rubber is stable. In Figure 3.7, the Starch_{700} sample appears close to equilibrium, like the N772 control, while Cob_{700} and Stover_{700} show a slight upwards slope, signifying marching modulus behavior [204]. These results, combined with the cure rate index results in Table 3.8 suggest that Starch_{700} is the more stable biochar composite of the 3.

3.3.5.2 Filler and Composite Morphology (SEM)

SEM images were taken for all biochar composites along with the control N772 composite to compare the structure of the fillers embedded in the rubber, with respective filler concentrations of 55 and 50 phr. Figure 3.8 shows the results of the SEM.

The biochar fillers in Figures 3.8a-c all clearly show agglomerates which did not break up during mixing, indicated in the appearance of larger crater like forms in contrast to areas with more even filler coverage. Conversely, N772 shows smooth, even dispersion throughout the entire section with no apparent remaining agglomerates showing up in Figure 3.8d.

Poor filler dispersion often indicates excessive filler-filler interactions [205]. This can be due to the surface chemistry of the filler or due to the mixing parameters. For instance, silica-based fillers are notoriously prone to aggregation, due their polar silanol groups [62]. Meanwhile, low rotor speeds during mixing on insufficient mixing time can lead to large aggregates being left in the mix [206]. In the case of surface chemistry, the FTIR results do not indicate any special surface chemistry in the biochar filler that could otherwise cause aggregation. It is possible that the rotor speed or mixing temperature used may not be ideal for the biochar filler system and that optimization could improve the dispersion.

Uniform dispersion is not always indicative of performance, but usually the more well dispersed and homogenous the composites are, the better they are able to distribute the applied loads and dissipate energy [207, 208].

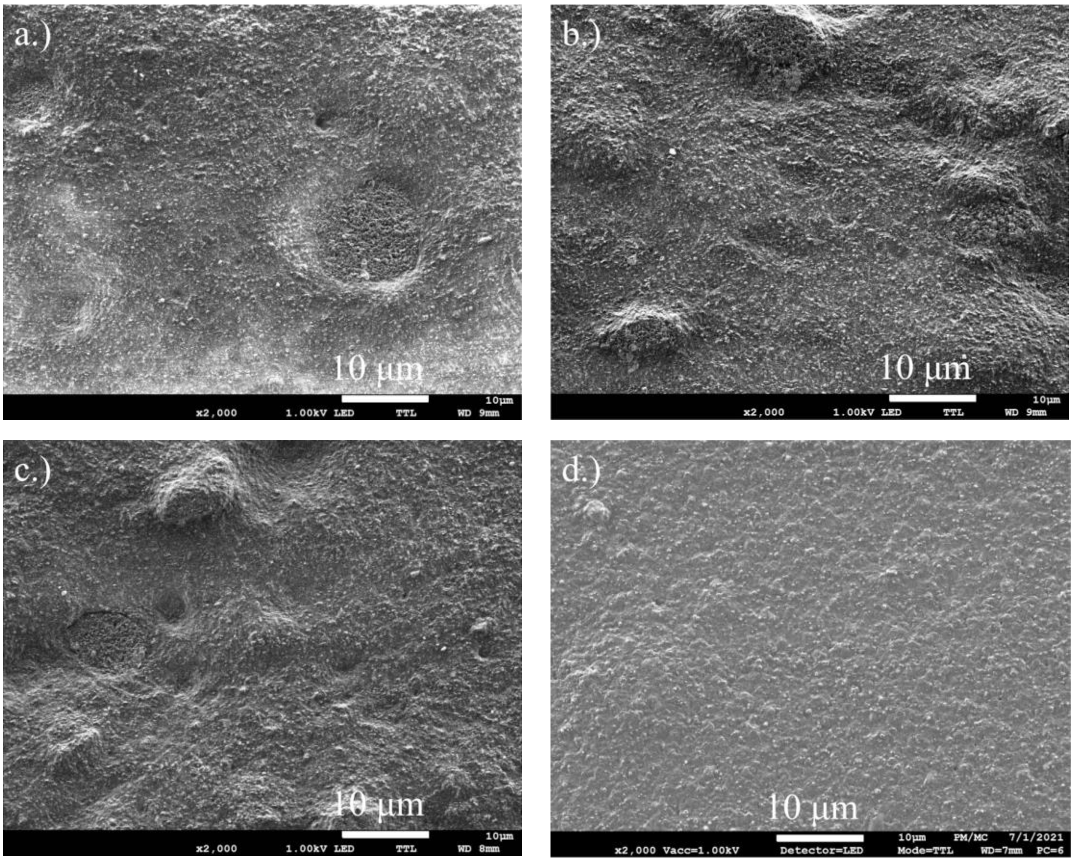

Figure 3.8 SEM images of the microstructure and dispersion of (a) Cob$_{700}$, (b) Stover$_{700}$, (c) Starch$_{700}$ and (d) N772 in SBR rubber

3.3.5.3 Tensile Properties

Presented in Figures 3.9 and 3.10, the stress strain curves of rubber composites typically exhibit 5 regions of different behavior, based on the slope, (modulus E) which are shown in Figure 3.9 [48]. Region 1 is between 0.1 and 10% strain and typically shows strain-softening, known as the Payne effect [209, 210]. The Payne effect is due to breakdown of filler-filler bonds, which can be observed in both tensile and dynamic oscillatory tests [211]. In Figure 3.9, all samples show a pronounced drop in the modulus in low-strain regions, indicating that this effect is taking place. The subsequent region, region 2, is the transition zone between the strain softening and strain stiffening sections. The modulus of elasticity, E, reaches its minimum value here. We can see the representative Starch_{700} composite hits its minimum value at 42% strain with Cob_{700} and Stover_{700} following at 52.4% and 58.5% strain respectively. The N772 filled composite has a similar performance to the corn starch composite, hitting its minimum modulus value at 45.1% strain. Region 3 is known as the stress upturn section, which shows the opposite effect of region 1. Instead of strain softening, there is now strain hardening, due to the limited extensibility of the polymer chain network, which becomes more stressed when coupled with the fillers [212, 213]. As expected, this effect is not seen at all in the unfilled SBR as it has no filler-polymer interactions. The strain range where stress upturn begins depends on both crosslink density and filler loading [48]. The level of crosslinking is affected by the interplay between the filler surface activity and the vulcanizing agents, making it difficult to attribute the performance to one factor [201]. Regions 3 and 4 are where the behavior of the biochar composites deviates the most from the N772 control composite. While the N772-filled composite shows a characteristic curve of a single stress upturn area followed by a relatively smooth plateau region, the biochar composites do not show the same behavior. In their case, the initial stress upturn region occurs, but rather than levelling out to a plateau region, the strain hardening continues and fluctuates in intensity until reaching the breaking point. Region 5 is the final region where ultimate softening and fracture occurs in the composite. The fracture occurs due to the strain-induced development and propagation of material defects, such as cracks and vacuole formations and polymer-particle slippage. In this experiment, the Starch_{700} composite breaks earlier than Cob_{700} and Stover_{700}, suggesting a higher crosslink density or a potentially higher filler volume fraction [48]. From Figure 3.10 this composite also follows the profile of

N772 more closely over the others, suggesting higher rigidity in its rubber-filler network compared to that of Cob_{700} and $Stover_{700}$ composites.

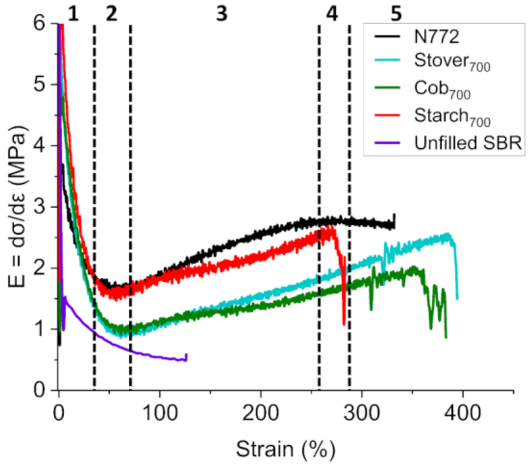

Figure 3.9 Change in tangent modulus, E, for Cob_{700}, $Stover_{700}$, $Starch_{700}$, and N772 composites. Regions are labelled with respect to the N772 curve.

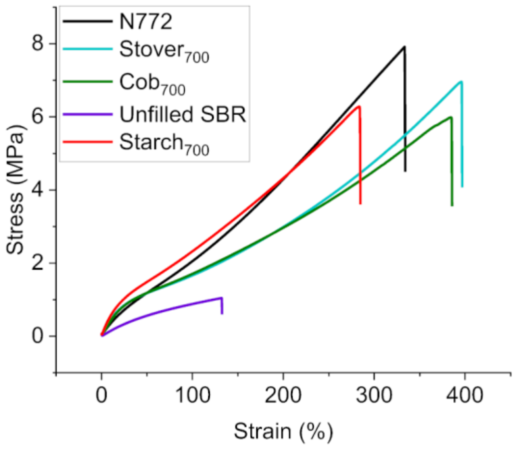

Figure 3.10 Stress vs Strain curves for Cob_{700}, $Stover_{700}$, $Starch_{700}$, and N772 composites and unfilled SBR.

Table 3.8 shows the averaged reinforcement indices for each composite type, calculated based on the ratio of the stress at 300% strain to the stress at 100% strain [48]. All replicate composites filled with $Starch_{700}$ yielded prior to reaching 300% strain, thus there is no reinforcement index calculated for this composite type.

Table 3.8 Reinforcement indices for biochar and N772 filled rubber composites

Sample	Stress @ 300% (M300)	Stress @ 100% (M100)	Reinforcement Index (M300/M100)	Max Stress (MPa)	Max Strain (%)
Cob_{700}	4.65±0.25	1.76±0.067	2.65±0.045	5.99±0.20	377±20
$Stover_{700}$	4.89±0.17	1.67±0.033	2.92±0.051	6.62±0.72	378±37
$Starch_{700}$	-	2.37±0.046	-	5.70±0.85	255±37
N772	7.01±0.068	2.05±0.0040	3.43±0.035	8.17±0.328	347±23
Unfilled SBR	-	0.88±0.01	-	1.13±0.12	166±55

Clearly, from the data in Figures 3.9, 3.10 and Table 3.8, the performance of the biochar composites is lower than that of the N772 filled control. This could be due to the uneven dispersion of the different biochar fillers, caused by the heterogeneous mixture of larger unbroken agglomerates and smaller agglomerates remaining after the mixing period. However, with only a 17.5% difference between the reinforcement indexes of the

Stover_{700} composites versus the N772 composites, there is clear potential for these biobased fillers. Based on the curing data, the level of crosslinking in the Starch_{700} composites is superior to Cob_{700} and Stover_{700}, which could explain why the representative Starch_{700} tensile curve in Figure 3.10 behaves more like the curve of the N772 filled control sample. However, the Starch_{700} composites are considerably more brittle and reach yield at a lower stress and strain. Considering the feedstock source, this finding is prevalent across studies where cornstarch has been used as a filler in other composites [6, 214, 215]. From the results of this study, despite being fully carbonized, the starch-based biochar still forms an incompatible network in the rubber, possibly a combination of poor dispersion and areas of excessive restriction of chain mobility. Meanwhile, though Stover_{700} outperforms Cob_{700}, the similarity in their performance indicates that they could potentially be blended without compromising performance. This would be logistically beneficial as it would eliminate the complexity of having to separate materials from the same plant. Furthermore, even the more brittle Starch_{700} composites have a 400% higher maximum stress compared to unfilled SBR rubber, indicating that all three biobased fillers are effective at reinforcing SBR rubber. Though their tensile strength in SBR is not yet on par with N772 filled SBR, their reinforcing properties may already be sufficient for lower stress applications.

3.3.5.4 Dynamic Mechanical Properties

The viscoelastic behaviors of the filled composites were assessed under varying strains (at 23 °C) and at varying temperatures (under a constant shear stress of 0.7 MPa). The measured properties were the shear storage modulus, G’, the shear loss modulus, G”, and tan δ. Variations in these parameters, with respect to changes in strain and temperature are displayed in Figure 3.11.

Variation in G’

In Figure 3.11a, all 3 biochar filled composites have higher starting G’ values compared with the N772 control composite, indicating increased rigidity. This is attributed to strong interactions between filler particles that remain unbroken at small strains [45]. These stronger filler-filler interactions could be due to interactions of polar surface groups of the filler, given the higher oxygen content of the biochar [216]. In effectively reinforced composites, the G’ should decrease with increasing strain, as the filler agglomerates break up and there are smaller mobile aggregates in the composite. A lower variation of G’ with increasing strain, or a lower level of nonlinearity indicates superior dispersion of the filler in the matrix [216]. Of the biochar samples, Starch$_{700}$ shows the greatest drop in G’ (79%), followed closely by Cob$_{700}$ and Stover$_{700}$ (69% and 68% respectively). In contrast, N772 shows a drop of 54%, thus indicating superior dispersion. These results complement the SEM images in Figure 3.8, which show the more uniform dispersion of N772 across the SBR matrix, while the Starch$_{700}$ and other biochar samples shows areas of non-uniform dispersion and filler aggregation.

Lower reinforcing fillers with larger particle sizes tend to have a more rapid decrease in G’ across temperatures, while higher values of G’ at the glassy state are associated with a smaller filler particle size [45]. In Figure 3.11b, the onset of the drop in G’ is relatively close among the fillers. As expected, the N772 filler has a higher value of G’ at low temperatures, given its smaller particle size and increased surface area compared to the biochar fillers [45].

Variation in G”

In Figure 3.11c, the shear loss modulus was highest for the Starch$_{700}$ composite, followed by Cob$_{700}$, Stover$_{700}$ and N772. The maximum G” value appears at around 4% strain in N772 and Cob$_{700}$, while it appears at 2% for the Starch$_{700}$ and Stover$_{700}$. The N772 has the most pronounced peak while the Starch$_{700}$ and Stover$_{700}$ filled composites have more pronounced peaks compared to the Cob$_{700}$ composite. This finding is in agreement with other studies, which find that the loss modulus increases with fillers which have smaller particle size or otherwise superior reinforcing characteristics [45]. As discussed in Section 3.1, Stover$_{700}$ and Starch$_{700}$ fillers both have smaller particle sizes than the Cob$_{700}$ filler.

From Figure 3.11d, all three biochar samples showed identical glass transition temperatures, estimated by the peak of the G” values be -38.9 °C for all 3 samples, while the N772 reinforced composite was slightly higher at -37.9 °C. The peak of the G” curve was used in lieu of the peak of the tan δ curve as it is known to provide a more accurate estimate of the glass transition temperature [217].

Variation in tan δ

Strong interfacial interactions between the filler particles and rubber matrix restrict movement of the polymer chain segments, and tend to lower or shift the tan δ peak to the right, towards higher temperatures [218, 219]. This is due to the reduced internal friction generated by the mobile chain segments, which reduces the G” modulus. This peak transformation can also be due to a high concentration of nano or micro filler particles, which can also increase interfacial interactions [218, 220].

In Figure 3.11e, there is a significant discrepancy between the behavior of the biochar samples and the N772 sample. The N772 sample has a distinct tan δ peak, while the curves of the biochar filled composites are relatively undefined and continue an upward trend rather than reaching a true peak. This is due to biochar fillers having greater non-linearity, as indicated in their larger drop in G’ in Figure 3.11a.

In Figure 3.11f, the N772 composite shows the highest tan δ peak compared to the others, but it is shifted to the right compared to the biochar fillers, indicating its stronger rubber-filler interactions [218, 219]. The tan δ peaks in the biochar samples are all in the same location but in terms of magnitude, Stover$_{700.}$ has the highest peak, followed by Cob$_{700}$ and Starch$_{700}$. These results, along with the curing data suggest that the extensive rubber filler interactions in the Starch$_{700}$ composites may be restricting the motion of the polymer chains in more places compared to the Cob$_{700}$ and Stover$_{700}$ composites. This in turn, would reduce the friction between these immobile polymer chains, thereby lowering the G” modulus and the tan δ peak [221]. These results and that Starch$_{700}$ composites have the lowest tensile strength illustrates the delicate balance between having sufficient polymer filler interactions for rigidity yet retaining sufficient mobility of the polymer chains for flexibility.

In the tire industry in particular, the tan δ values at 0 °C and 60 °C are used as rubber performance indicators for wet traction and rolling resistance respectively [222]. A higher tan δ value at 0 °C predicts better traction control on wet surfaces, while a lower tan δ value at 60 °C predicts a lower rolling resistance and greater efficiency. From Figure 3.11f, the N772 sample has both a higher tan δ value at 0 °C and a lower tan δ value at 60 °C, indicating a superior performance compared to the biochar filled composites. Among the biochar filled composites, the only difference is that the Starch$_{700}$ sample has a slightly higher tan δ value at 0 °C compared to the others. In terms of performance at 60 °C, the difference in tan δ values among the biochar composites is negligible.

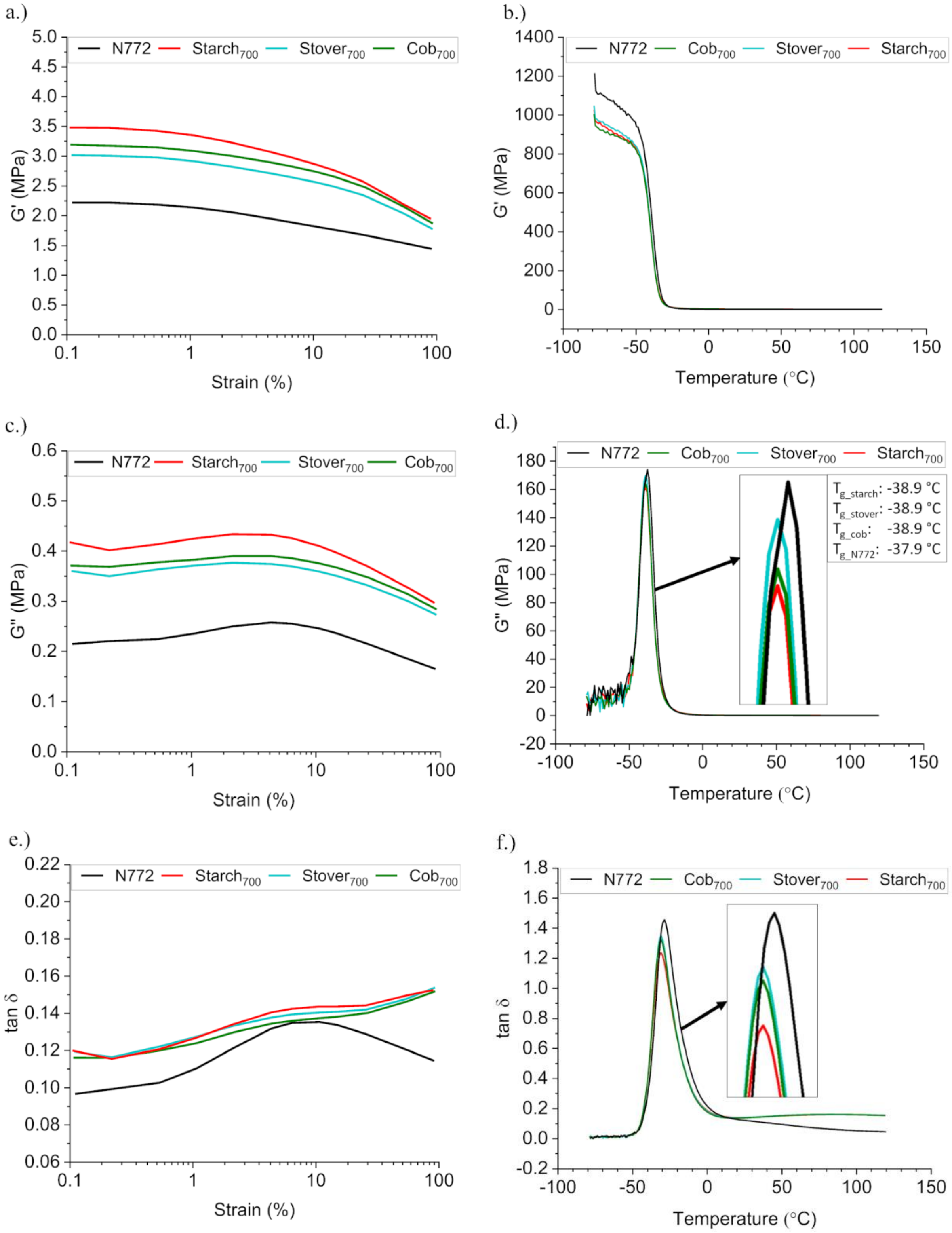

Figure 3.11 Plots of (a) G’ vs strain, (b) G’ vs temperature, (c) G” vs strain, (d) G” vs temperature, (e) tan δ vs strain and (f) tan δ vs temperature

3.4 Conclusions

It has been shown that biochar produced from corn-based feedstocks have some physicochemical similarities to N772 carbon black and exhibit semi-reinforcing behavior when applied as fillers in SBR rubber composites. The major physicochemical differences between corn-based biochar and N772 are in terms of particle size and filler structure. The corn-based biochar samples were found to have a wider size distribution, with larger aggregates compared to N772. Additionally, the structure of the primary particles and aggregates was irregular, whereas the N772 carbon black had round, homogenous primary particles forming secondary aggregates. Furthermore, the biochar samples had a more polar chemistry, with a lower carbon content and higher oxygen and hydrogen content, compared with N772. This may have caused a level of flocculation and aggregation in the biochar composites, affecting their mechanical performance. Out of the three biochar-based composites tested, $Starch_{700}$ had the most crosslinking and formed the stiffest composite with properties most comparable to N772. It experienced earlier failure however, than the other two biochar composites. Cob_{700} and $Stover_{700}$ had similar performances in SBR, suggesting that despite some variation in the lignocellulosic composition of their feedstock counterparts, as biochar fillers they could be blended without a significant loss in performance. While the $Starch_{700}$ composites were more brittle, they followed the performance curve of N772 more closely at lower strains. The strong performance at lower strains could be the result of using refined materials with more homogeneity prior to upgrading via pyrolysis. It is therefore possible that depolymerizing lignocellulosic feedstocks into more homogeneous streams prior to pyrolysis could be key to tailoring effective biochar-based fillers with the desired reinforcing characteristics. It was also found that the biochar, with its high microporosity, may be interacting with the vulcanizing agents in a way that affects the crosslinking and dispersion. Further studies would be useful to determine to what extent the biochar interacts with the vulcanizing agents and whether its reinforcing potential could be improved though the optimization of the pore size, the use of covering agents and or the adjustment of mixing parameters.

Connecting Statement

From Chapter 3, it was shown that despite having a lower performance than N772, biochar from corn cob, stover and starch are all effective at reinforcing SBR rubber. The results indicate that biochar from corn stover has the highest reinforcing performance in SBR, though it has similar physicochemical properties to corn cob. This suggests that there is not a large difference in the performance of biochar from different lignocellulosic portions of the plant, despite having different ratios of cellulose, hemicellulose, and lignin. Additionally, corn starch had a strong reinforcing performance in SBR but experienced brittle failure at higher strains. In Chapter 4, biochar from corn starch was examined in more detail to determine whether the starch structure (linear amylose and branched amylopectin) had any bearing on the physicochemical properties of the resulting biochar. The effect of 4 different pyrolysis activations were also studied to determine whether the properties of starch biochar could be improved through physical activation processes. The activations were (1) pyrolysis under N_2, considered the control condition, (2) pyrolysis under CO_2, (3) pyrolysis with steam and N_2 and (4) pyrolysis of a biochar-water slurry under N_2. The outcome of the study satisfied the remaining research objectives 3 and 4.

Chapter 4.

Assessing Starch-Based Biochar as a Renewable Filler in Styrene-Butadiene Rubber Composites

Abstract

In this study, biochar synthesized from corn starch with three different amylose/amylopectin ratios were characterized and their reinforcing performance in styrene-butadiene rubber (SBR) rubber was compared to that of N772. Biochar samples from each feedstock were produced via slow pyrolysis at 700 °C for 1 h, at a heating rate of 50 °C min−1 under N_2 gas. Additionally, for each feedstock type, 3 different activated biochar samples were created, notably (1) activation under CO_2 in lieu of N_2, (2) activation with steam and N_2 (Steam), and (3) steam activation via pyrolysis of a biochar-water slurry (SteamT2). The physicochemical properties of the fillers were examined, and all biochar samples were blended with SBR to form composites, which were tested to evaluate their cure profiles and tensile properties. The results indicate that the amylose and amylopectin ratios of the feedstock had little effect on the reinforcing performance of the composites, but composites with biochar from high amylose corn starch, (HA-CS), had longer scorch periods during curing. Physical activation treatments, however, had a significant impact on the physicochemical properties of the biochar, specifically on the porosity, carbon, oxygen, and ash content. In terms of performance in SBR, composites with biochar pyrolyzed under normal N_2 conditions and biochar activated with Steam had the most consistent tensile performance with the least brittle characteristics. Conversely, composites made with biochar activated with SteamT2 were exceptionally brittle, with limited reinforcement capabilities, despite having a comparatively higher carbon content. Thus, though physical activation can increase the carbon concentration of biochar, this does not necessarily correlate to improvements in its mechanical performance in SBR. As such, other optimization techniques may be more useful to tailor biochar for application in the rubber filler industry.

Keywords: rubber composites; biochar; carbon black; reinforcement; starch

4.1 Introduction

Industries are developing strategies towards a circular economy and the rubber manufacturing industry is no exception. Several of the existing materials used in rubber manufacturing are toxic and nonbiodegradable, including carbon black, which has been identified as a probable carcinogen [2]. For over a century, carbon black has been the lead reinforcing filler in rubber, increasing the durability and longevity of rubber products. Now, the rubber industry is focusing on development of more sustainable alternative materials that could substitute carbon black. Biochar is one of these materials, with the potential to green the filler industry. Its attractive properties are that it can be made from low-cost renewable feedstocks, which are often by-products of other industries, such as agriculture, forestry and pulp and paper milling. Converting these feedstocks into biochar involves heating the feedstocks in a low oxygen environment to reduce the combustion reactions and to elevate the level of fixed carbon in the material, while reducing the volatile matter [28]. This process can be tailored extensively, from the feedstock selection and pre-treatment process to the pyrolysis temperature, heating rate and residence time, among other factors. Further finetuning of biochar properties can be done through activation methods. Activations of biochar can be done through physical activation via steam or CO_2 [126, 223–226] or by using chemical agents such as zinc chloride, potassium hydroxide and phosphoric acid [227–229]. These activations can greatly modify biochar's physicochemical properties, which may improve its performance, depending on the application.

In this study, biochar was first synthesized using 3 different mixtures of starch as precursor materials. Starch is primarily composed of amylose and amylopectin, which are glucopyranose units with different structural arrangements. Amylose is composed of a linear structure of glucopyranose units joined by 1,4 glucosidic linkages while amylopectin has a more complex branched structure of glucopyranose units joined by 1,6 glucosidic linkages [151, 185]. Starch has been known to have a brittle effect on composites, from thin films to plastics, etc [6, 214, 215]. However, it is not clear whether the brittle properties of starch are impacted by the proportions of amylose and amylopectin or how they may change through carbonization. Therefore, in this study, three different starch mixtures were used to determine whether different ratios of amylose and amylopectin affect the physicochemical properties of starch once converted into biochar.

The second part of this study focused on the impact of physical activation methods on starch-based biochar. Three different physical activation processes involving steam, a steam slurry and CO_2 were applied to each type of biochar to determine the impact of the activations on the physicochemical properties of the biochar and their performance as a filler in SBR composites. To the authors knowledge, this is the only existing study on (1) the impact of starch structure on the physicochemical properties of the resulting biochar and (2) the influence of different physical activations on starch-based biochar.

4.2 Methodology

4.2.1 Biochar Preparation

Three varieties of cornstarch (high amylose, high amylopectin and regular) were provided by Sigma Aldrich (Oakville, Ontario, Canada). Regular cornstarch has an amylose/amylopectin ratio of 27%/73% while high amylose is nearly pure amylose starch and high amylopectin is nearly pure amylopectin starch. Feedstocks were weighed and then pyrolyzed in a bench scale pyrolysis unit under different activation conditions described in Table 4.1. The flow rate of both N_2 and CO_2 was approximately 400 mL/min while the flowrate of steam was approximately 517 mL/min.

Table 4.1 Activation Methods for Biochar Samples

Activation Name	Description
Regular Pyrolysis with N_2	Pyrolysis at 700 ºC/ 1 h with N_2 and cool down with N_2
Pyrolysis with CO_2 activation	Pyrolysis at 700 ºC/ 1 h with CO_2 and cool down with CO_2
Pyrolysis with Steam activation	Pyrolysis at 700 ºC/ 1 h with steam and N_2 and cool down with steam and N_2
Pyrolysis with SteamT2 activation	1. Pyrolysis at 700 ºC/ 1 h with N_2 and cool down with N_2 2. Biochar soaked in cold tap water to form slurry 3. Activation of slurry at 700 ºC/ 1 h with N_2 and cool down with N_2

Feedstock was placed in a pre-weighed low-grade stainless steel cylindrical crucible measuring 15” in length and 1 ¼” in diameter. The full crucible was weighed before being placed in a horizontal, electrically heated pyrolysis unit, connected to a thermocouple device for temperature feedback. The unit’s temperature was set to dwell at 700 ºC for 60 min, with a heating rate of approximately 50 ºC/min and under a constant flow of N_2 until the crucible cooled down to at least 150 ºC and was ready to be removed. The pyrolysis residence time of 60 min was chosen due to the high biochar yield, as demonstrated by [147]. The temperature of 700 ºC was justified by the fact that a higher temperature and heating rate favors a high biochar reactivity, as well as the carbonization of lignin, contributing to the overall carbon content and aromaticity of the biochar [152]. After cooling, the resulting biochar was weighed again to determine the yield, and then milled and filtered using a small kitchen blender and a 425 µm sieve. Regular cornstarch, high amylose corn starch and high amylopectin corn starch are hereby referred to as R-CS, HA-CS and HAP-CS respectively. The activation types are subsequently referred to as Steam, SteamT2 and CO_2. The different biochar samples and their activations are hereby referred to using the abbreviations described in Table 4.2.

Table 4.2 Abbreviations of All Biochar Samples

Abbreviaton	Definition
CB N772	N772 carbon black
R-CS $_{700}$	Biochar from regular cornstarch, normal pyrolysis under N_2
R-CS $_{700+CO2}$	Biochar from regular cornstarch, pyrolysis under CO_2
R-CS $_{700+steam}$	Biochar from regular cornstarch, pyrolysis under Steam
R-CS $_{700+steamT2}$	Biochar from regular cornstarch, pyrolysis under Steam (Type 2)
HA -CS $_{700}$	Biochar from high amylose cornstarch, normal pyrolysis under N_2
HA-CS $_{700+CO2}$	Biochar from high amylose cornstarch, pyrolysis under CO_2
HA-CS $_{700+steam}$	Biochar from high amylose cornstarch, pyrolysis under Steam
HA-CS $_{700+steamT2}$	Biochar from high amylose cornstarch, pyrolysis under Steam (Type 2)
HAP-CS $_{700}$	Biochar from high amylopectin cornstarch, normal pyrolysis under N_2
HAP-CS $_{700+CO2}$	Biochar from high amylopectin cornstarch, pyrolysis under CO_2
HAP-CS $_{700+steam}$	Biochar from high amylopectin cornstarch, pyrolysis under Steam
HAP-CS $_{700+steamT2}$	Biochar from high amylopectin cornstarch, pyrolysis under Steam (Type 2)

4.2.2 Preparation of Rubber Composites

Styrene-butadiene rubber (SBR), carbon black N772, N-(1,3-dimethylbutyl)-N’-phenyl-1,4-benzenediamine (6PPD), diphenyl guanidine (DPG), zinc oxide (ZnO), and stearic acid (SAD) were provided by Michelin Inc. (Greenville, South Carolina, USA). Biochar was pre-ground using a BlendTec commercial kitchen blender for 3 min, followed by sieving through a No. 120 mesh for 10 min. The sieved samples were then placed in a planetary ball mill (MTI Corporation, USA) and milled for 6 h at 45 Hz. The ball mill set up consisted of two 500 cubic centimeter stainless steel jars, each filled with 15 grams of biochar, 750 grams of 1mm yttria-stabilized zirconia (YSZ) oxide ball milling media and 60 g of ethanol (solvent). After milling, the contents were placed in a vacuum at 70 ºC overnight and sieved for 90 min to remove the milling media. The biochar samples were then placed in a sealed container until their incorporation into the composite mix.

The rubber compounds were prepared according to the formulation shown in Table 4.3. The antiozonant 6PPD was used, along with diphenyl guanidine (DPG) as the accelerator, zinc oxide (ZnO) as an activator, and stearic acid (SAD) as a release agent. From Table 4.1, the filler loading in the biochar-filled samples is slightly higher than the filler loading in the control N772-filled mix. This decision was made to attempt to balance the rigidity in each of the mixes as bio-based fillers tend to have less structure than carbon black and are therefore less rigidifying in the rubber.

Table 4.3 Rubber Mix Ratios

Raw Material	Part per hundred rubber (phr)	
SBR 2300	100	100
Biochar	55	
Carbon Black (N772)		50
6PPD	2.0	2.0
DPG	2.0	2.0
ZnO	2.0	2.0
SAD	3.2	3.2

The mixing was done in a HAAKE PolyLab OS RheoDrive 16 (ThermoFisher Scientific, USA) rheometer, while the mixing parameters (rotor speed and mixing chamber plate temperature) were monitored by the Haake PolySoft OS software. An overview of the mixing process is shown in Table 4.4.

Table 4.4 Mixing Parameters

Time (min)	Rotor speed (rpm)	Step
0	90	Add elastomer
1	30	Add ½ biochar
2	30	Add ½ biochar
3	30, increase to 70 gradually	Add 6PPD, DPG, ZnO, SAD
4	70	Piston cleanse
5	70	Drop

The rubber mixture was subsequently milled using a C.W. Brabender two-roll mill (C.W. Brabender, USA) to incorporate the curatives sulfur and the n-cyclohexyl-2-benzothiazole sulfenamide (CBS) at a temperature of 55 °C and a rotor speed of 9 rpm. The desired thickness of the rubber mixture was 3 mm.

4.2.3 Filler Characterization

4.2.3.1 BET/Surface Area Analysis

The surface area of the biochar samples was analyzed by a Quantichrome instruments analyzer (NOVA 4200e Quantachrome, United States). All samples were degassed at 120 ºC under vacuum overnight prior to BET analysis. The surface area was then calculated in terms of area per sample mass (m^2/g) based on the Brunauer, Emmett and Teller theory. The t-plot method was used to determine the micropore surface area and the average pore size was calculated using the Gurvitsch 4V/A BET method and the Barrett−Joyner−Halenda (BJH) method.

4.2.3.2 Proximate Analysis

Proximate analysis was performed in triplicate for the corn cob, corn stover and corn starch feedstocks and their resulting biochar samples, Cob_{700}, Stover_{700} and Starch_{700}. The quantities of moisture, volatile matter, ash and fixed carbon were determined according to procedures adapted from ASTM D1762-84 standards [154].

4.2.3.3 Elemental Analysis

Elemental composition was performed at the Université de Sherbrooke by the Laboratoire de Chimie Analytique, Laboratoire des Technologies de la Biomasse (LTB) (Sherbooke, Québec, Canada). The mass percentage of carbon, hydrogen, nitrogen, oxygen and sulfur (CHNOS) in the samples were determined using an adaptation of the ASTM D-5373-16 standard method. Analysis was conducted on samples in triplicate on a 2000 Organic Elemental Analyzer (Thermo Scientific, USA). The detection limit of N, S, O was 0.01%, 0.2%, and 0.01%, respectively, and the results are expressed in terms of mass fraction.

4.2.3.4 pH

Biochar solutions were prepared with 1 g biochar in 10 mL of deionized water. The mixtures were mechanically agitated for 1 h and the pH was subsequently measured using a pH meter with glass calomel electrodes. All biochar samples were measured in triplicate and compared with results from a carbon black sample that had been previously prepared under the same conditions.

4.2.3.5 FTIR

Spectral components of the prepared biochar and feedstock samples were recorded in absorbance mode using a Thermo Scientific™ Nicolet™ iS5 FTIR Spectrometer

(ThermoFisher Scientific, USA) with an iD5 ATR accessory. For each set, 32 scans were performed with a resolution of 4 cm^{-1} in the 4000-600 cm^{-1} range. The background spectrum was recorded on the disinfected laminated diamond crystal plate before recording the spectrum of each sample. The experiments were performed in triplicate and the resulting spectra were then corrected and analyzed using SpectraGryph 1.2 software. The absorption peaks were assigned to chemical functional groups based on data from literature.

4.2.4 Composite Characterization

4.2.4.1 Cure Characteristics

The minimum time required to cure the composites was determined using an Alpha technologies 2000 rubber process analyzer (RPA) (Alpha Technologies, USA). Studies were carried out on mixed, unvulcanized samples for 1 h at 150 °C. After, the unvulcanized samples were placed in a mold and cured in a Carver Press ICarver, Inc., USA) at 150 °C for 25 min under two platens imparting 12,000 lbs. of force onto the samples.

4.2.4.2 Morphology

The filler dispersion into the rubber was measured with a JSM-7100F thermal field emission electron microscope (JEOL, Belgium). A razor blade was used to cut the rubber to expose a fresh surface for the analysis. The samples were examined under magnification ranges between 50-10,000X under an accelerating voltage of 1.00 kV.

4.2.4.3 Tensile Testing

Dumbell shaped rubber composite samples were cut and tested using an Instron 5966 extensometer (Instron, USA). Tests were done according to ISO 37 type 2 at a constant rate of traverse of 500 mm/min until failure at break. Four samples per mix were tested and their values averaged.

4.3 Results & Discussion

4.3.1 Filler Characterization

4.3.1.1 BET/Surface Area Analysis

The BET analysis shown in Table 4.5 indicates several trends in terms of BET surface area, pore size and relative share of microporosity. In general, all biochar samples have significantly higher surface areas as compared to N772 carbon black, except for HA -CS $_{700}$ for reasons which are unclear. The BET surface area appears to generally increase based on activation type in the order of SteamT2>Steam>CO_2 > N_2, though samples made from R-CS prove an exception to this order. Examining the average pore size diameter, pore size appears to increase based on activation in the order of SteamT2>Steam>CO_2 > N_2. This is in agreement with literature on steam and CO_2 activated biochar, suggesting that steam activations decrease the microporosity while increasing the mesoporosity through pore widening [225]. Pores are considered potential rubber-filler interaction sites, but only if their size permits the access of rubber polymer chains. Mesopores, ranging from 2 to 50 nm, have an ideal size range to provide access to rubber chains [56, 57]. The Steam and SteamT2 activated samples have mean pore sizes that fall within the lower end of the mesoporous range, and they generally have the lowest percentage of microporosity, especially seen in the SteamT2 treated samples. These two properties could give them a reinforcing advantage over the other biochar samples in that it would potentially allow for more rubber-filler interactions to occur during the mixing process [57]. However, the Steam and SteamT2 activated samples also have the highest overall BET surface areas. Higher surface areas have been thought to present a risk for the adsorption of vulcanization agents during the curing process, which can negatively impact the cure rate index by reducing the rate of vulcanization [21]. Therefore, while Steam and SteamT2 activated samples may have the advantage of a larger mean pore size, they may have a disadvantage in being more porous overall compared to the N_2 activated samples.

Similarly, CO_2 activated samples generally have a higher percentage of microporosity among other samples, even nonsensically high in the case of HA-CS $_{700+CO2}$. This is in agreement with literature which found that barley straw biochar activated with CO_2 had a significantly higher microporosity compared to the same biochar activated with steam [225].

Table 4.5 Summary of BET, t-plot and pore size results

Sample	Total BET surface area (m^2/g)	t-plot Micropore Area (m^2/g)	% microporosity[1]	Adsorption Average Pore Diameter (nm)	BJH adsorption
CB N772	29.0±0.06	3.10	10.7	42.5	47.8
R-CS $_{700}$	125±5.18	121	96.8	Data unavailable	Data unavailable
R-CS $_{700+CO2}$	79.8±1.65	73.0	91.5	1.74	104.7
R-CS $_{700+steam}$	97.1±1.91	94.4	97.2	1.66	125.8
R-CS $_{700+steamT2}$	130±5.54	113	86.9	2.02	40.4
HA -CS $_{700}$	27.8±0.676	32.7	117.6	1.56	156.6
HA-CS $_{700+CO2}$	151±4.76	158	104.6	1.51	Data unavailable
HA-CS $_{700+steam}$	259±4.33	218	84.2	2.10	6.28
HA-CS $_{700+steamT2}$	333±12.6	279	83.8	2.14	2.91
HAP-CS $_{700}$	73.0±3.88	Data unavailable	Data unavailable	Data unavailable	Data unavailable
HAP-CS $_{700+CO2}$	163±4.63	158	96.9	1.68	110.7
HAP-CS $_{700+steam}$	215±3.68	181	84.2	2.12	7.46
HAP-CS $_{700+steamT2}$	226±8.96	186	82.3	2.19	7.77

4.3.1.2 Proximate Analysis, Elemental Analysis and pH Values

Elemental, and proximate composition is shown in Table 4.6, along with measured pH values. Analysis of trends indicates no significant feedstock-based variances in biochar chemical composition. However, the type of activation applied appears to have a significant effect on the carbon, oxygen and ash content of the biochar.

With carbon composition, there is a noticeable difference in biochar activated with Steam as opposed to SteamT2, as well as between biochar synthesized under N_2 compared to biochar activated with SteamT2. Steam activated samples have lower carbon contents compared to both SteamT2 and regular N_2 pyrolysis, while biochar activated under SteamT2 conditions show the highest carbon content among all samples. This can be attributed to the differences in the activation procedures. With the SteamT2 treatment, biochar is first synthesized under N_2 at 700 °C for 1 h, made into a slurry with tap water and then pyrolyzed under N_2 at 700 °C for another hour. Conversely, with the Steam activation, the feedstock is heated to 700 °C and then held at 1 h under a steady flow of steam and N_2. In the case of SteamT2, it could be that the additional residence time in the pyrolysis unit allows for further tar reformation reactions in the biochar, releasing more volatile matter and thus increasing the carbon concentration [230]. Indeed, this appears plausible, given that the SteamT2 samples all contain the lowest amount of volatile matter

---

[1] Calculated by the t-plot micropore area (m^2/g) over the total BET surface area (m^2/g)

compared to the other samples. Meanwhile, the Steam activation occurs as the feedstock is being converted into biochar. Previous studies indicate that steam dissociates to form H/OH radicals which influences the tar reformation process in the biomass, leading to more oxygen containing functional groups on the biochar surface compared to treatment with CO_2 [126]. The results from this study appear to support this finding, as the Steam activated biochar samples all have higher oxygen contents compared to biochar treated with CO_2 or with other activations.

In terms of ash content, the differences between activations are less pronounced, but biochar activated with CO_2 and with N_2 have the greatest difference, with CO_2 activated samples tending to have a higher ash content compared to the others, while biochar produced from regular N_2 pyrolysis have the lowest ash content. This is in agreement with another study which found that biochar activated with CO_2 had a 30-50% higher concentration of inorganic elements as compared to the same biochar sample activated with steam [225]. In this study, samples activated with SteamT2 had the second highest levels of ash after samples activated with CO_2. This could be due in part to the minerals in the tap water, which was used in the slurry process. Unlike the Steam activation, where the steam was passed through the biochar and the minerals left behind in the steam unit, the slurry allowed for the minerals in the tap water to adhere to the biochar and be left behind as the water evaporated.

Previous studies indicate that high carbon-low ash biochar fillers (>89% carbon, >2% ash) have superior performance over biochar fillers with lower carbon and higher ash levels [5–7]. In this case, all biochar fillers have ash content comparable to that of N772, though their carbon content is 4-17% lower, depending on the activation applied. Considering both carbon and ash content, SteamT2 samples would appear to have an advantage over the other biochar samples, having the highest carbon content (>90%) and a relatively low ash content (<2%).

Table 4.6 Basic Physicochemical Properties of Feedstocks and Biochar Samples

Sample	Yield (wt%)	Elemental Analysis (wt%)					Proximate Analysis (wt%)				pH
		C	H	N	O	S	Moisture Content	Volatile Matter	Ash Content	Fixed Carbon	
CB N772	not applicable	96.1±1.2	0.29±0.01	trace	0.34±0.02	1.28± 0.04	0.56±0.97	2.61±0.81	0.30±0.52	97.1±0.44	7.56±0.18
R-CS	not applicable	39.3±0.4	6.20±0.1	trace	51.6 ± 0.60	trace	12.0±0.00	98.30±0.80	trace	1.70±0.80	not applicable
R-CS$_{700}$	11.4±1.7	78.9±0.8	2.76±0.08	0.24±0.01	12.1±0.30	trace	3.67±0.58	20.76±0.93	0.34±0.60	78.90±1.46	8.07±0.21
R-CS$_{700+CO2}$	8.1±0.5	86.6±1.1	2.36±0.21	0.14±0.01	6.52± 0.34	trace	0.97±0.61	15.07±0.35	2.57±0.46	82.37±0.67	6.37±0.10
R-CS$_{700+steam}$	10.8±2.8	82.8±0.8	1.76±0.01	0.25±0.03	8.0±0.90	trace	0.66±3.38	15.10±3.42	0.39±0.18	84.51±3.60	5.54±0.05
R-CS$_{700+steamT2}$	8.2±0.9	91.1±3.1	2.05±0.56	0.21± 0.05	3.09± 0.10	trace	0.06±0.05	10.78±0.65	0.96±0.01	88.26±0.66	6.32±0.15
HA-CS	not applicable	38.6±0.5	6.30±0.1	trace	52.1±0.50	trace	0.00±0.0	98.49±0.66	Trace	1.51±0.66	not applicable
HA -CS$_{700}$	10.4±1.3	84.9±0.6	2.14±0.08	0.31±0.03	6.40±0.29	trace	3.00±1.00	12.72±0.72	0.68±0.59	86.60±0.14	6.22±0.67
HA-CS$_{700+CO2}$	11.7±0.6	86.6±1.4	2.29±0.13	0.33± 0.02	5.79± 0.10	trace	0.70±0.62	13.15±0.18	2.01±0.20	84.84±0.21	6.58±0.17
HA-CS$_{700+steam}$	9.1±3.0	82.6±0.2	1.93±0.02	0.41±0.05	10.4±0.10	trace	0.60±0.53	17.18±1.18	2.22±0.85	80.60±2.03	7.06±0.06
HA-CS$_{700+steamT2}$	9.8±2.9	91.0 ± 2.2	1.72 ± 0.11	0.30 ± 0.05	3.89 ± 0.11	trace	0.00±0.0	11.56±0.11	1.21±0.08	87.23±0.16	6.96±0.13
HAP-CS	not applicable	38.9±0.4	6.30±0.3	trace	52.0±2.0	trace	0.00±0.0	95.56±0.05	trace	4.44±0.05	not applicable
HAP-CS$_{700}$	10.1±0.6	86.7±0.5	2.13±0.01	trace	6.10±0.02	trace	3.32±0.55	12.37±1.03	1.03±1.03	86.60±1.79	7.24±0.05
HAP-CS$_{700+CO2}$	8.4±0.7	86.3±2.6	2.37±0.21	trace	6.14±0.40	trace	1.26±0.12	15.36±0.61	1.95±0.49	82.69±0.46	8.17±0.16
HAP-CS$_{700+steam}$	10.8±2.4	80.2±0.6	2.3±0.10	trace	11.7±0.50	trace	0.37±0.32	26.19±0.52	0.87±0.81	72.94±0.95	7.97±0.04
HAP-CS$_{700+steamT2}$	11.1±0.7	92.4 ± 2.6	1.37 ± 0.08	trace	2.55 ± 0.06	trace	0.29±0.25	9.37±0.41	1.53±0.16	89.10±0.57	7.61±0.25

4.3.1.3 FTIR

Feedstock

Shown in Figure 4.1, the spectra for all 3 starch feedstocks are virtually identical, except for the relative peak heights. The prominent peak at 3319 cm^{-1} is attributed to O-H stretching, while the peak at 2929 cm^{-1} is related to C-H stretching modes [169] . According to several sources [169–172], the peak at 1643 cm^{-1} is related to water adsorbed in the amorphous region of the starch molecule.

The peaks between 1338 and 1500 cm^{-1} are attributed to CH_2 bending and the peak near 1094 cm^{-1} is attributed to C-O-H bending modes [173]. C-O stretching is observed based on the peak at 999 cm^{-1} and C-O-C ring stretching is indicated given the peaks in the range of 705-850 cm^{-1} [170]. The last peak observed at 570 cm^{-1} could indicate pyranose ring vibrations within the starch glucose units [169].

Biochar Activations

There are little to no differences between biochar spectra among different feedstock groups, however there are a few observable spectral differences between the different activation groups. For instance, all starch biochar samples activated by Steam appear to retain some O-H groups, given the small broad peak near 3319 cm^{-1}, as reflected in the elemental analysis data shown in Table 4.6. The detectable presence of O-H groups may be an advantage for the Steam samples, as oxygen containing surface functional groups in fillers are believed to play a role in enhancing bound rubber formation, based on free radical theory [34, 166]. Conversely, the samples treated with the SteamT2 activation do not have peaks in that area, indicating that biochar with SteamT2 treatment do not retain the surface OH groups. Additionally, the biochar activated with Steam appear to retain some C-O-H bending modes and C-O stretching modes, given the weak peaks in the same areas as the feedstock. In both the regular samples pyrolyzed under N_2 and the samples pyrolyzed with CO_2, the end peaks in the 890 cm^{-1} to 750 cm^{-1} range are slightly more prominent, possibly indicating aromatic C-H deformations [174, 176, 177, 179]. Finally, all samples appear to have peaks at 1570 cm^{-1}, which is indicative of aromatic C=C stretching of carbonyl groups [85].

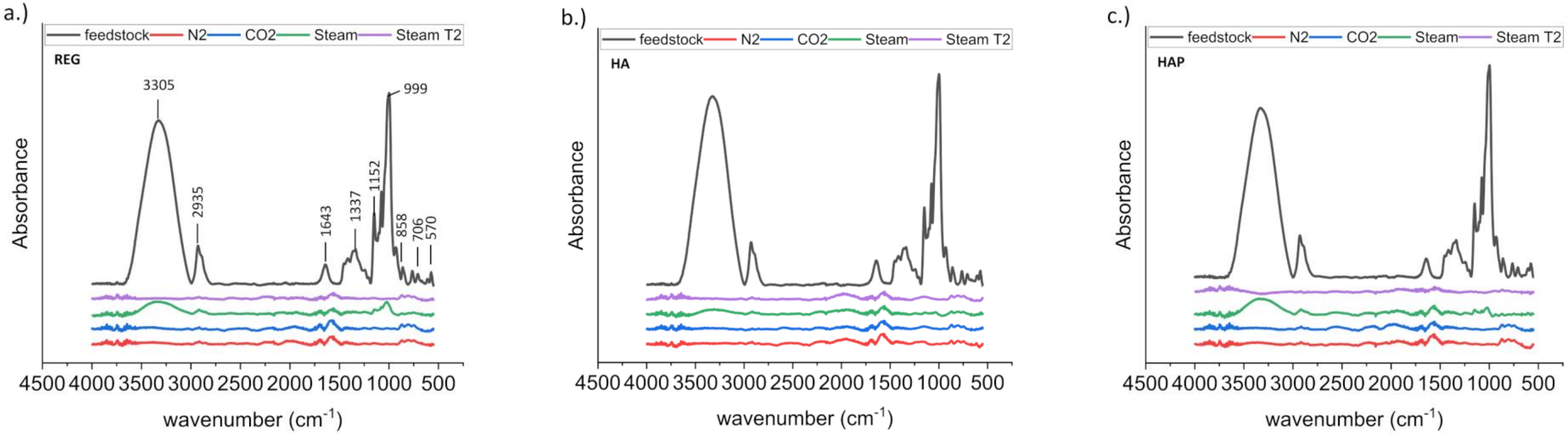

Figure 4.1 FTIR Spectra of Feedstocks and Biochar for a.) R-CS b.) HA-CS and c.) HAP-CS based samples, including activations

4.3.2 Composite Performance

4.3.2.1 Cure Characteristics

The rheographs in Figure 4.2 show the cure behaviour of the different activated fillers in SBR rubber, grouped by filler feedstock type. For comparison, each graph also shows the cure behaviour of a typical N772 SBR composite and an unfilled SBR rubber composite. The cure rate indices, shown in Table 4.7, were calculated based on the ASTM D-2084 and ASTM D5289 methods.

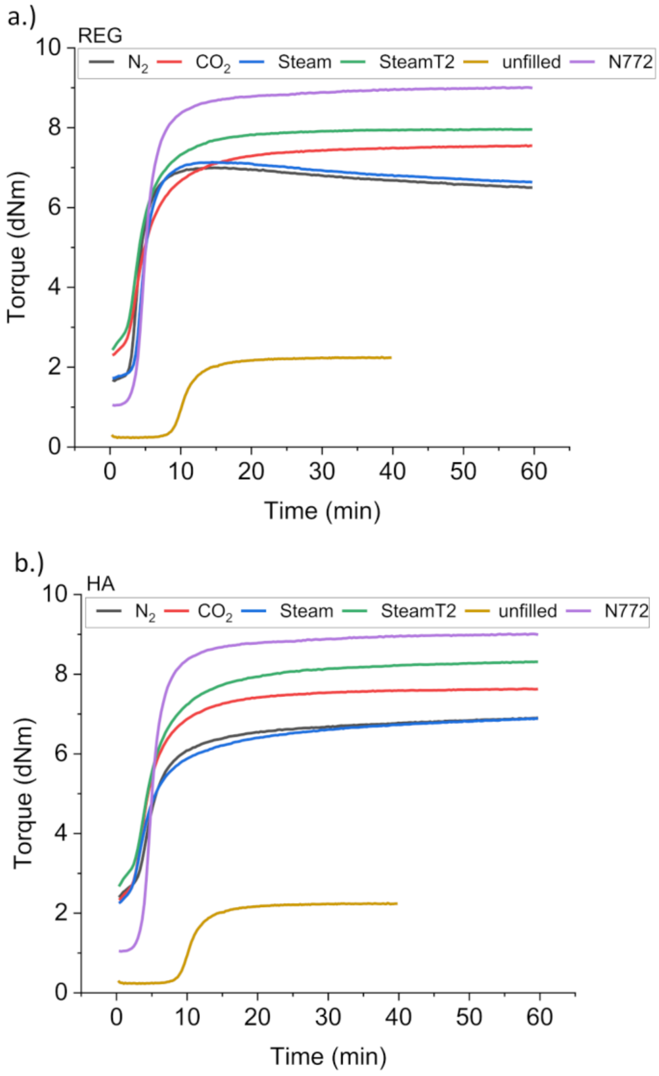

c.)

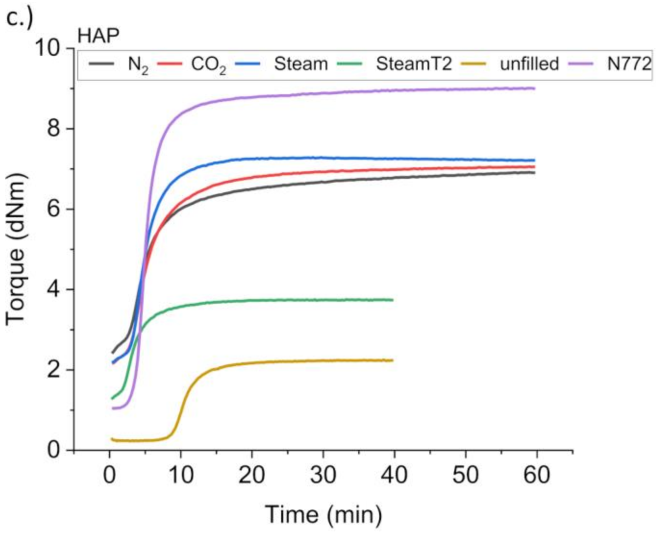

Figure 4.2 Cure curves for a.) R-CS, b.) HA-CS and c.) HAP-CS biochar filled composites, including N772 filled composites and unfilled SBR rubber for reference

Table 4.7 Cure Rate Indices for Unfilled SBR, Biochar and N772 Composites

Sample	Optimum cure time, t_{C90} (min)	Incipient scorch time, t_{C10} (min)	Minimum Torque, M_L (dNm)	Maximum Torque, M_H (dNm)	CRI
CB N772	3.79	8.53	1.04	9.01	21.1
Unfilled SBR	15.2	8.98	0.23	2.25	16.0
R-CS $_{700}$	3.17	6.17	1.66	7.00	33.3
R-CS $_{700+CO2}$	3.15	11.1	2.30	7.56	12.7
R-CS $_{700+steam}$	3.81	6.84	1.72	7.14	33.0
R-CS $_{700+steamT2}$	2.97	8.95	2.43	7.96	16.7
HA -CS $_{700}$	3.64	11.7	2.40	6.91	12.4
HA-CS $_{700+CO2}$	3.03	9.98	2.34	7.63	14.4
HA-CS $_{700+steam}$	2.92	14.6	2.25	6.89	8.54
HA-CS $_{700+steamT2}$	3.18	11.9	2.67	8.31	11.5
HAP-CS $_{700}$	3.42	12.6	2.41	6.92	10.9
HAP-CS $_{700+CO2}$	3.58	11.7	2.17	7.06	12.3
HAP-CS $_{700+steam}$	3.61	8.29	2.18	7.29	21.4
HAP-CS $_{700+steamT2}$	2.34	6.59	1.28	3.76	23.6

Similar to the previous study, several biochar samples have lower scorch times than the N772 filler rubber. This could be due to a change in the cure system from a semi-efficient system to a conventional system, which often takes place if the filler adsorbs the accelerator [198, 199]. Indeed, it is possible that the higher porosity and oxygen levels of biochar allow it to adsorb more of the accelerator agents as compared to N772. This would lead to lower scorch periods for the biochar-based samples, which are seen several, though not all cases. Following this trend, composites with the lowest scorch times also have fillers with comparatively higher oxygen contents and higher specific surface areas, such as R-CS $_{700}$, R-CS $_{700+steam}$, and HAP-CS $_{700+steam}$, which have respective oxygen contents of 12.1±0.3, 8.0±0.9 and 11.7±0.5 and respective composite t_{C10} scorch times of 6.17, 6.84 and 8.29 min. Both R-CS $_{700+steamT2}$ and HAP-CS $_{700+steamT2}$ have higher surface areas of 130±5.54 and 226±8.96 respectively and produce composites with respective scorch times of 8.95 and 6.59 min. Interestingly, HA-CS type samples do not appear to follow this trend, since HA-CS $_{700+steam}$ and HA-CS $_{700+steamT2}$ both have high surface area and/or high oxygen content, yet their composites have significantly longer incipient scorch times compared to their HAP-CS and R-CS based counterparts. In fact, all mixes made with HA-CS type fillers have longer scorch times than the N772 CB mix. This could indicate a difference in biochar performance based on feedstock, as both the R-CS and HAP-CS have high amylopectin content while HA-CS is primarily amylose. Additionally, the 4 composites which have cure rate indexes above that of N772, (R-CS $_{700}$, R-CS $_{700+steam}$, HAP-CS $_{700+steamT2}$, and HAP-CS $_{700+steam}$), all contain higher amounts of amylopectin starch. Though some of the cure rate indexes are higher than carbon black, closer inspection of the curves reveals less than ideal cure characteristics. For instance, despite having respective cure rate indexes of 33.3 and 33.0, composites with R-CS $_{700}$, and R-CS $_{700+steam}$, both show reversion in their cure profiles, indicating crosslink breakage and poorer cure characteristics overall [231].

Another interesting trend is that CO_2 activated biochar all appear to have similar scorch times and cure curves, regardless of precursor feedstock. This could be due to the similarities in their physicochemical properties, as all biochar activated with CO_2 have little variation in their composition, as indicated by the elemental analysis.

Finally, out of the biochar activation with SteamT2, the HAP-CS $_{700+steamT2}$ composite appears to have a low cure rate index and the lowest maximum torque of all biochar samples, while HA-CS $_{700+steamT2}$ and R-CS $_{700+steamT2}$ have relatively stable curves and high maximum torque values. The reasons for this poor performance are unclear but may be attributed to a degree of experimental error, as the HAP-CS $_{700+steamT2}$ sample was processed separately from all other samples.

The pH of the fillers were also compared with the scorch time, as carbon black with alkaline pH has been shown to increase the vulcanization and reduce the scorch period, while fillers with acidic or neutral pH can increase the scorch period [62, 232] . In this study however, comparing the pH of the fillers to the scorch times produced no such trend.

Overall, all samples have cure characteristics which are superior to unfilled SBR rubber but still inferior compared to N772 filled rubber. Though there are a few interesting trends noted, there do not appear to be definitive correlations between the cure rate index and the activations or the type of starch feedstock.

4.3.2.2 Morphology

In terms of composite morphology, the effect of the amylose-amylopectin ratio is minimal, however there appear to be some differences among activations. Figure 4.3 shows SEM images for HA-CS under each activation condition.

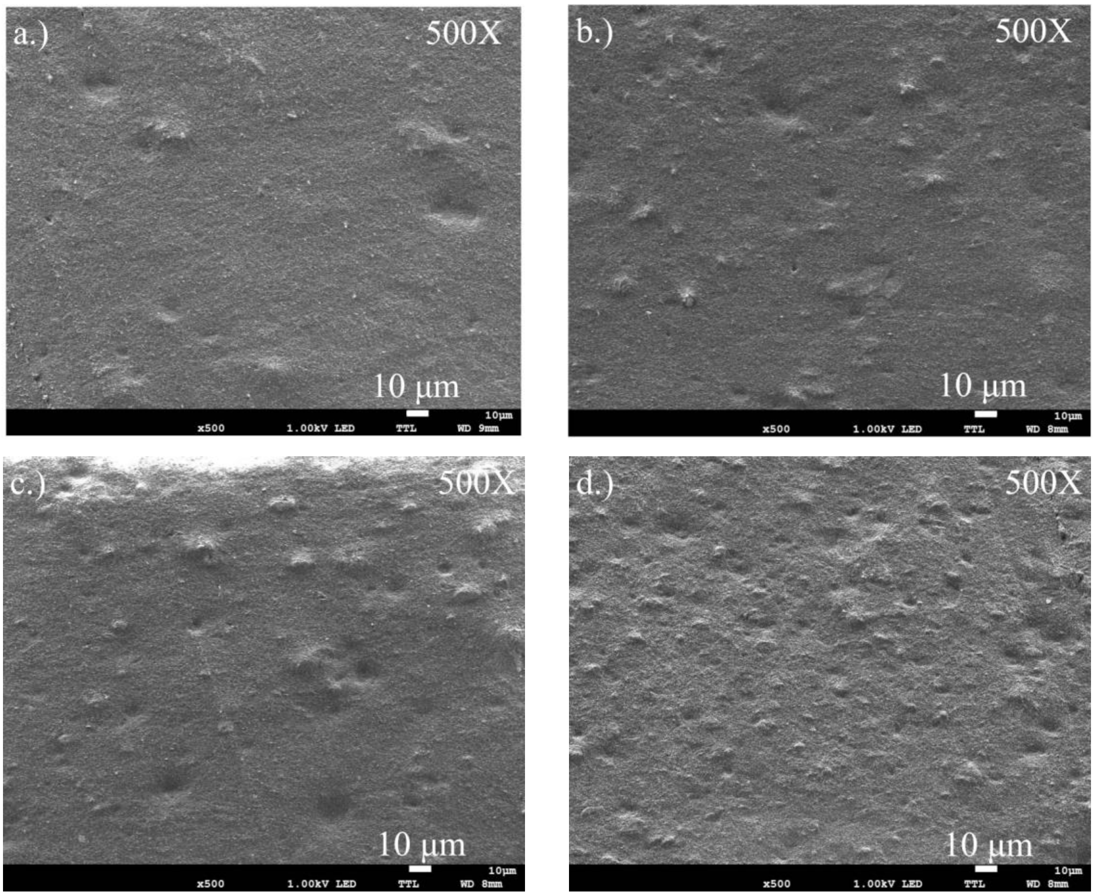

Figure 4.3 SEM images of the microstructure and dispersion of (a) HA -CS 700, (b) HA-CS 700+CO2 (c) HA-CS 700+steam and (d) HA-CS 700+steamT2 in SBR rubber

Undispersed aggregates are observable in all samples. While the images look similar from Figures 4.3a-c, showing biochar samples pyrolyzed with N_2, CO_2 and Steam respectively, the SteamT2 activated samples appear to have a greater number of undispersed aggregates. While most of the aggregates in this sample appear smaller than those shown in Figures 4.3a-c, there are more of them, which could cause more areas of stress concentration leading to a higher chance of early failure when subjected to dynamic loads.

4.3.2.3 Tensile Properties

Table 4.8 shows the average reinforcement indices for each composite mix, calculated based on the ratio of the stress at 300% strain vs the stress at 100% strain. Figure 4.4 shows the graphical minimum and maximum stress, strain and reinforcement index values, and Figure 4.5 shows the representative stress-strain curves compared to a typical N772 SBR mix and an unfilled SBR mix. In terms of trends among the activations, it appears that composites with SteamT2 activated fillers are especially brittle, with most samples breaking before 300% strain. This seems to agree with the morphology results, which showed a larger number of undispersed aggregates in the SteamT2 activated samples compared to the other activations. It is interesting that most of these samples broke, given that fillers with this type of activation had the highest carbon content and a larger average pore size, both properties which have been shown to be advantageous to reinforcement.

Table 4.8 Reinforcement indices for Unfilled SBR, Biochar and N772 Composites

Sample	Stress @ 300% (M300)	Stress @ 100% (M100)	Reinforcement Index (M300/M100)	Max Stress (MPa)	Max Strain (%)
CB N772	7.01±0.07	2.05±0.00	3.43±0.03	8.25±0.34	351.19±
Unfilled SBR rubber	-----	0.88±0.01	-----	1.13±0.12	166.15±
R-CS $_{700}$	5.96±0.04	1.85±0.01	3.22±0.02	7.40±0.69	353.54±
R-CS $_{700+CO2}$	7.15±0.07	2.09±0.02	3.42±0.02	8.16±0.68	331.73±
R-CS $_{700+steam}$	5.04±0.04	1.65±0.02	3.05±0.02	6.14±0.73	347.22±
R-CS $_{700+steamT2}$	8.45±	2.24±0.04	-----	6.48±1.38	254.03±
HA -CS $_{700}$	5.67±0.13	1.74±0.02	3.25±0.03	6.58±0.79	334.27±
HA-CS $_{700+CO2}$	-----	2.14±0.02	-----	6.20±0.75	260.29±
HA-CS $_{700+steam}$	5.91±0.04	1.81±0.02	3.26±0.01	7.45±1.27	352.56±
HA-CS $_{700+steamT2}$	-----	0.37±0.19	-----	7.74±0.45	280.56±
HAP-CS $_{700}$	5.65±0.09	1.77±0.02	1.14±0.01	7.44±1.49	361.72±
HAP-CS $_{700+CO2}$	6.81±0.10	1.97±0.03	3.46±0.01	7.38±1.34	316.58±
HAP-CS $_{700+steam}$	5.74±0.21	1.83±0.06	3.15±0.05	5.62±0.70	297.97±
HAP-CS $_{700+steamT2}$	-----	2.18±0.06	-----	5.60±1.10	241.82±

Trends among feedstock types indicate that samples filled with HAP-CS type filler have lower maximum stress compared to composites filled with HA-CS. Composites filled with R-CS type filler have maximum stresses between the 2, suggesting that there may be a link between amylopectin-based feedstock and increased sample brittleness. However, R-CS type biochar have more composites exceeding the 300% strain mark, compared to HA-CS and HAP-CS type biochar composites, making it difficult to state any definite conclusions.

Trends among activation type indicate that composites made with regular N_2 pyrolysis and Steam activation have a more consistent mechanical performance, as none of these composites broke early, regardless of feedstock type. Additionally, samples activated with CO_2 had a strong reinforcing performance in SBR, with the R-CS $_{700+CO2}$ composites and HAP-CS $_{700+CO2}$ composites having respective reinforcement indexes of 3.42±0.02 and 3.46±0.01, effectively on par or exceeding that of the N772 composites (3.43±0.03). Meanwhile, composites filled with biochar activated with SteamT2 appear to have the worst performance, despite the promising physicochemical properties of the SteamT2 activated fillers. Though their performance is not consistently on par with that of the N772 composites, all biochar-based composites show significant reinforcing effects compared to the unfilled SBR mix.

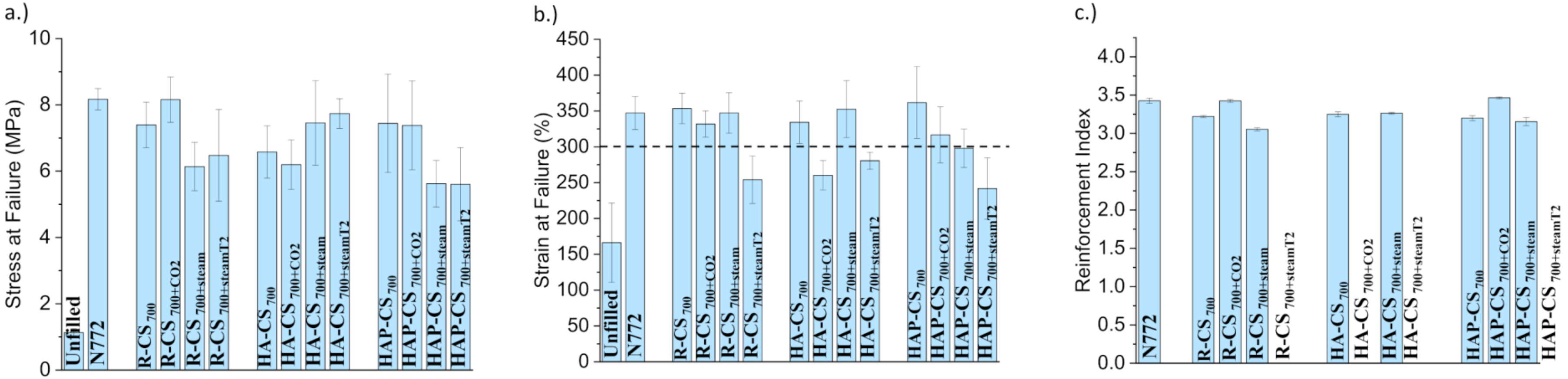

Figure 4.4 (a) Average maximum stress, (b) maximum strain, and (c) reinforcement index for all biochar composites, including N772 filled composites and unfilled SBR rubber for reference

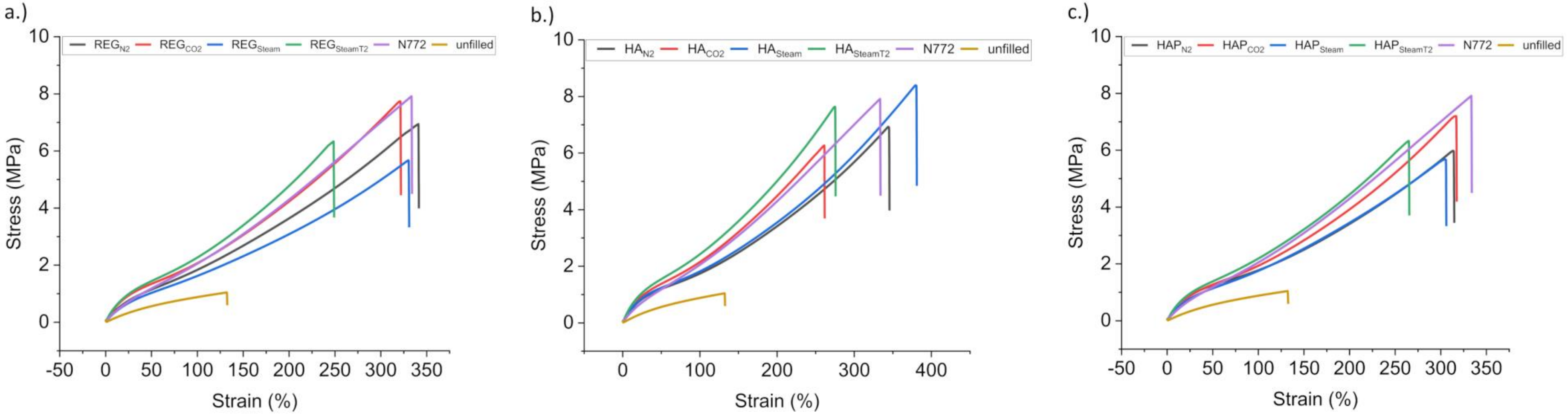

Figure 4.5 Stress vs Strain representative curves for (a) R-CS, (b) HA-CS and (c) HAP-CS biochar filled composites, including N772 filled composites and unfilled SBR rubber for reference

4.4 Conclusions

From the results of the experiments, it appears that both the amylose/amylopectin ratio of the starch feedstock and physical activation type do have some impact on the physicochemical properties of the resulting biochar and their reinforcing performance in SBR composites.

In terms of trends among activation type, biochar activated with SteamT2 has promising physicochemical properties, with a carbon content >90%, an ash content<2% and the largest average pore size among other fillers. However, in terms of reinforcement, it has the worst performance, producing brittle composites with almost all samples breaking before reaching 300% strain. Meanwhile, biochar activated with CO_2 has consistent physicochemical properties, regardless of feedstock, and as a filler, it produced composites with stable cure characteristics and reinforcement indexes near and above that of the N772 mix. Biochar activated with Steam had the lowest carbon content and highest oxygen content of all fillers yet still produced composites with strong reinforcement characteristics. Finally, biochar with regular N_2 pyrolysis also produced composites with strong reinforcement indexes, suggesting that activation of biochar does not necessarily outperform non-activated biochar in terms of reinforcement.

Though most trends in physicochemical properties and performance appeared related to the activation type, one feedstock related observation was that the scorch times of HA-CS based biochar were delayed relative to the N772 CB filled composites, while R-CS and HAP-CS based biochar composites had faster scorch times, despite having similar compound densities and no other obvious physicochemical differences. Overall, though activation of biochar can improve its tensile performance in SBR, optimization of other aspects such as particle size reduction may prove more beneficial to creating renewable, highly reinforcing biochar-based fillers for the rubber industry.

Chapter 5.

Summary, General Conclusions and Recommendations for Further Research

5.1 Summary and General Conclusions

The primary objectives of this research were to characterize and compare the reinforcing performance of biochar fillers from different corn-based feedstocks (corn cob, corn stover and corn starch) in SBR rubber. The first study in Chapter III explored how biochar fillers compare when they are derived from feedstock materials from the same plant (corn), but are (1) differing in lignocellulosic composition (corn cob vs corn stover) and (2) differing in terms of feedstock purity (corn starch vs corn cob or corn stover). Chapter IV then focused exclusively on the corn starch feedstock, examining the impact of amylose/amylopectin content and physical activation methods on the resulting biochar. The conclusions relating to the specific research objectives 1-4 are listed below:

From the study in Chapter 3, it was found that though the highly refined feedstock (starch) showed high levels of crosslinking and a superior cure profile compared to starch and stover, the crosslinking caused excessive polymer chain restriction resulting in earlier failure. Meanwhile, the lesser refined feedstocks showed greater elongation prior to breaking. The biochar from corn stover appeared to have the greatest reinforcing effect in rubber, possibly in part due to its smaller aggregate size compared to the corn cob biochar. However, the overall performance of biochar from corn cob and corn stover was similar, even though their feedstocks differed in lignocellulosic composition. This suggests that the 2 feedstocks could be blended prior to pyrolysis without sacrificing filler performance, which would be a processing advantage. Though all biochar fillers had lower dispersion in rubber compared to N772 carbon black, they had a reinforcing effect over 400% greater than that of unfilled rubber.

In Chapter 4, three varieties of corn starch (high amylose, high amylopectin and regular corn starch) were pyrolyzed under 4 different conditions (regular N_2, CO_2, Steam and SteamT2). There was little to no correlation between the amylose and amylopectin content of the feedstock and the physicochemical properties and performance of the biochar. However, composites filled with biochar produced from HA-CS all had delayed scorch times relative to N772 filled composites. This contrasted with composites filled with biochar from R-CS and HAP-CS, which had accelerated scorch times.

The activations, however, significantly influenced the physicochemical properties of the biochar. Biochar activated with Steam had the most oxygen functional groups while biochar activated with SteamT2 had the highest carbon content (>90%) of all activations. The reinforcement results were promising, with some CO_2 activated biochar composites having reinforcement indexes higher than the N772 control composite. Variations in performance between the Steam, N_2 and CO_2 samples were smaller but surprisingly, the SteamT2 samples were significantly more brittle despite having the highest carbon content. Overall, though the activations affected the physicochemical properties of the biochar, the effect of activations on the fillers' reinforcing performance in SBR was not as significant.

5.2 Recommendations for future research

While biochar fillers derived from corn cob, stover and starch have promising reinforcing effects in SBR, their performance is not yet on par with N772. As such, more research is needed to fully determine their potential in filler applications. The studies in Chapters 3 and 4 indicated that most biochar filled SBR samples had shorter scorch periods compared to the N772 control sample. It would be useful to run more tests to examine whether the biochar is adsorbing the vulcanization agents and whether this correlates with a faster scorch period. Another area of focus could be comparing the structure of different biochar fillers after different size reduction technologies. Where carbon black's structure is created during its synthesis, the structure of biochar fillers is largely dependent on post pyrolysis techniques. As such, it would be helpful to have more studies examining the effects of different size reduction processes, such as ball milling, ultrasonication etc. on the final structure of biochar fillers. Finally, there are several additional performance aspects for fillers aside from their reinforcing effect. To have biochar become a commercial filler, there would need to be studies examining the behaviour of biochar fillers subjected to ozone, sunlight, and aging, as well as testing their compatibility with other vulcanization systems and other rubber compounds. The scale up feasibility would also need to be considered, particularly in the size reduction post pyrolysis, as several methods are expensive and designed to process small quantities at a time. Overall, though more development is needed, the outlook of biochar fillers is favourable. As the processing technology matures, there may be opportunities to begin using it to partially replace traditional fillers, moving closer to the end goal of complete substitution with more sustainable fillers.

References

[1] Wang, M.-J.; Gray, C. A.; Reznek, S. R.; Mahmud, K.; Kutsovsky, Y. Carbon Black. In *Encyclopedia of Polymer Science and Technology*; John Wiley & Sons, Ltd, 2003. https://doi.org/10.1002/0471440264.pst477.

[2] IARC. *IARC Monographs on the Evaluation of Carcinogenic Risks to Humans Volume 93: Carbon Black, Titanium Dioxide, and Talc*; International Agency for Research on Cancer: Lyon, France, 2010; Vol. 93.

[3] Michelin - 100% Sustainable https://www.michelin.com/en/innovation/vision-concept/sustainable/ (accessed May 18, 2022).

[4] Green Tires Market by Vehicle Type, Sales Channel, Application, Region, Global Industry Analysis, Market Size, Share, Growth, Trends, and Forecast 2020 to 2027 - Fior Markets https://www.fiormarkets.com/report/green-tires-market-by-vehicle-type-commercial-vehicles-418272.html (accessed Jul 18, 2022).

[5] Peterson, S. C. Utilization of Low-Ash Biochar to Partially Replace Carbon Black in Styrene–Butadiene Rubber Composites. *Journal of Elastomers & Plastics*, **2013**, *45* (5), 487–497. https://doi.org/10.1177/0095244312459181.

[6] Peterson, S. C. Evaluating Corn Starch and Corn Stover Biochar as Renewable Filler in Carboxylated Styrene–Butadiene Rubber Composites. *Journal of Elastomers & Plastics*, **2012**, *44* (1), 43–54. https://doi.org/10.1177/0095244311414011.

[7] Peterson, S. C.; Chandrasekaran, S. R.; Sharma, B. K. Birchwood Biochar as Partial Carbon Black Replacement in Styrene–Butadiene Rubber Composites. *Journal of Elastomers & Plastics*, **2016**, *48* (4), 305–316. https://doi.org/10.1177/0095244315576241.

[8] García-Condado, S.; López-Lozano, R.; Panarello, L.; Cerrani, I.; Nisini, L.; Zucchini, A.; Van der Velde, M.; Baruth, B. Assessing Lignocellulosic Biomass Production from Crop Residues in the European Union: Modelling, Analysis of the Current Scenario and Drivers of Interannual Variability. *GCB Bioenergy*, **2019**, *11* (6), 809–831. https://doi.org/10.1111/gcbb.12604.

[9] Li, X.; Mupondwa, E.; Panigrahi, S.; Tabil, L.; Sokhansanj, S.; Stumborg, M. A Review of Agricultural Crop Residue Supply in Canada for Cellulosic Ethanol Production. *Renewable and Sustainable Energy Reviews*, **2012**, *16* (5), 2954–2965. https://doi.org/10.1016/j.rser.2012.02.013.

[10] Xing, W.; Tang, M.; Wu, J.; Huang, G.; Li, H.; Lei, Z.; Fu, X.; Li, H. Multifunctional Properties of Graphene/Rubber Nanocomposites Fabricated by a Modified Latex Compounding Method. *Composites Science and Technology*, **2014**, *99*, 67–74. https://doi.org/10.1016/j.compscitech.2014.05.011.

[11] Arroyo, M.; López-Manchado, M. A.; Herrero, B. Organo-Montmorillonite as Substitute of Carbon Black in Natural Rubber Compounds. *Polymer*, **2003**, *44* (8), 2447–2453. https://doi.org/10.1016/S0032-3861(03)00090-9.

[12] Liu, Q.; Zhang, Y.; Xu, H. Properties of Vulcanized Rubber Nanocomposites Filled with Nanokaolin and Precipitated Silica. *Applied Clay Science*, **2008**, *42* (1), 232–237. https://doi.org/10.1016/j.clay.2007.12.005.

[13] Sadek, E. M.; El-Nashar, D. E.; Ahmed, S. M. Effect of Organoclay Reinforcement on the Curing Characteristics and Technological Properties of Styrene–Butadiene Rubber. *Polymer Composites*, **2015**, *36* (7), 1293–1302. https://doi.org/10.1002/pc.23034.

[14] Sheikh, S. H.; Yin, X.; Ansarifar, A.; Yendall, K. The Potential of Kaolin as a Reinforcing Filler for Rubber Composites with New Sulfur Cure Systems. *Journal of Reinforced Plastics and Composites*, **2017**, *36* (16), 1132–1145. https://doi.org/10.1177/0731684417712070.

[15] Das, A.; Stöckelhuber, K. W.; Jurk, R.; Saphiannikova, M.; Fritzsche, J.; Lorenz, H.; Klüppel, M.; Heinrich, G. Modified and Unmodified Multiwalled Carbon Nanotubes in High Performance Solution-Styrene–Butadiene and Butadiene Rubber Blends. *Polymer*, **2008**, *49* (24), 5276–5283. https://doi.org/10.1016/j.polymer.2008.09.031.

[16] Ismail, H.; Shaari, S. M.; Othman, N. The Effect of Chitosan Loading on the Curing Characteristics, Mechanical and Morphological Properties of Chitosan-Filled Natural Rubber (NR), Epoxidised Natural Rubber (ENR) and Styrene-Butadiene Rubber (SBR) Compounds. *Polymer Testing*, **2011**, *30* (7), 784–790. https://doi.org/10.1016/j.polymertesting.2011.07.003.

[17] Xu, S. H.; Gu, J.; Luo, Y. F.; Jia, D. M. Effects of Partial Replacement of Silica with Surface Modified Nanocrystalline Cellulose on Properties of Natural Rubber Nanocomposites. *Express Polym. Lett.*, **2012**, *6* (1), 14–25. https://doi.org/10.3144/expresspolymlett.2012.3.

[18] Jiang, C.; He, H.; Jiang, H.; Ma, L.; Jia, D. Nano-Lignin Filled Natural Rubber Composites: Preparation and Characterization. **2013**. https://doi.org/10.3144/EXPRESSPOLYMLETT.2013.44.

[19] Jiang, C.; He, H.; Yao, X.; Yu, P.; Zhou, L.; Jia, D. In Situ Dispersion and Compatibilization of Lignin/Epoxidized Natural Rubber Composites: Reactivity, Morphology and Property. *Journal of Applied Polymer Science*, **2015**, *132* (23). https://doi.org/10.1002/app.42044.

[20] Jiang, C.; He, H.; Yao, X.; Yu, P.; Zhou, L.; Jia, D. The Aggregation Structure Regulation of Lignin by Chemical Modification and Its Effect on the Property of Lignin/Styrene–Butadiene Rubber Composites. *Journal of Applied Polymer Science*, **2018**, *135* (5), 45759. https://doi.org/10.1002/app.45759.

[21] Jiang, C.; Bo, J.; Xiao, X.; Zhang, S.; Wang, Z.; Yan, G.; Wu, Y.; Wong, C.; He, H. Converting Waste Lignin into Nano-Biochar as a Renewable Substitute of Carbon Black for Reinforcing Styrene-Butadiene Rubber. *Waste Management*, **2020**, *102*, 732–742. https://doi.org/10.1016/j.wasman.2019.11.019.

[22] Jong, L. Influence of Protein Hydrolysis on the Mechanical Properties of Natural Rubber Composites Reinforced with Soy Protein Particles. *Industrial Crops and Products*, **2015**, *65*, 102–109. https://doi.org/10.1016/j.indcrop.2014.12.004.

[23] Akhil, D.; Lakshmi, D.; Kartik, A.; Vo, D.-V. N.; Arun, J.; Gopinath, K. P. Production, Characterization, Activation and Environmental Applications of Engineered Biochar: A Review. *Environ Chem Lett*, **2021**, *19* (3), 2261–2297. https://doi.org/10.1007/s10311-020-01167-7.

[24] Batista, E. M. C. C.; Shultz, J.; Matos, T. T. S.; Fornari, M. R.; Ferreira, T. M.; Szpoganicz, B.; de Freitas, R. A.; Mangrich, A. S. Effect of Surface and Porosity of Biochar on Water Holding Capacity Aiming Indirectly at Preservation of the Amazon Biome. *Sci Rep*, **2018**, *8* (1), 10677. https://doi.org/10.1038/s41598-018-28794-z.

[25] Li, H.; Dong, X.; da Silva, E. B.; de Oliveira, L. M.; Chen, Y.; Ma, L. Q. Mechanisms of Metal Sorption by Biochars: Biochar Characteristics and Modifications. *Chemosphere*, **2017**, *178*, 466–478. https://doi.org/10.1016/j.chemosphere.2017.03.072.

[26] Li, H.; Hu, J.; Meng, Y.; Su, J.; Wang, X. An Investigation into the Rapid Removal of Tetracycline Using Multilayered Graphene-Phase Biochar Derived from Waste Chicken Feather. *Science of The Total Environment*, **2017**, *603–604*, 39–48. https://doi.org/10.1016/j.scitotenv.2017.06.006.

[27] Sajjadi, B.; Chen, W.-Y.; Mattern, D. L.; Hammer, N.; Dorris, A. Low-Temperature Acoustic-Based Activation of Biochar for Enhanced Removal of Heavy Metals.

Journal of Water Process Engineering, **2020**, *34*, 101166. https://doi.org/10.1016/j.jwpe.2020.101166.

[28] Butt, F. I.; Yaqub, G.; Khurshid, F. Role of Biochar Products towards Environmental Management and Technologies: A Brief Review. *ChemBioEng Reviews*, **2018**, *5* (2), 104–110. https://doi.org/10.1002/cben.201700006.

[29] Peterson, S. C. Silica-Milled Paulownia Biochar as Partial Replacement of Carbon Black Filler in Natural Rubber. *Journal of Composites Science*, **2019**, *3* (4), 107. https://doi.org/10.3390/jcs3040107.

[30] Peterson, S. C. Coppiced Biochars as Partial Replacement of Carbon Black Filler in Polybutadiene/Natural Rubber Composites. *Journal of Composites Science*, **2020**, *4* (4), 147. https://doi.org/10.3390/jcs4040147.

[31] Peterson, S. C.; Kim, S. Using Heat-Treated Starch to Modify the Surface of Biochar and Improve the Tensile Properties of Biochar-Filled Styrene–Butadiene Rubber Composites. *Journal of Elastomers & Plastics*, **2019**, *51* (1), 26–35. https://doi.org/10.1177/0095244318768636.

[32] Fernandes, M. R. S.; Sousa, A. M. F. de; Furtado, C. R. G. Rice Husk Ash as Filler in Tread Compounds to Improve Rolling Resistance. *Polímeros*, **2017**, *27*, 55–61. https://doi.org/10.1590/0104-1428.2385.

[33] Li, M.-C.; Zhang, Y.; Cho, U. R. Mechanical, Thermal and Friction Properties of Rice Bran Carbon/Nitrile Rubber Composites: Influence of Particle Size and Loading. *Materials & Design*, **2014**, *63*, 565–574. https://doi.org/10.1016/j.matdes.2014.06.032.

[34] Fan, Y.; Fowler, G. D.; Norris, C. Potential of a Pyrolytic Coconut Shell as a Sustainable Biofiller for Styrene–Butadiene Rubber. *Ind. Eng. Chem. Res.*, **2017**, *56* (16), 4779–4791. https://doi.org/10.1021/acs.iecr.7b00405.

[35] Jong, L.; Peterson, S. C.; Jackson, M. A. Utilization of Porous Carbons Derived from Coconut Shell and Wood in Natural Rubber. *J Polym Environ*, **2014**, *22* (3), 289–297. https://doi.org/10.1007/s10924-013-0637-4.

[36] Greenough, S.; Dumont, M.-J.; Prasher, S. The Physicochemical Properties of Biochar and Its Applicability as a Filler in Rubber Composites: A Review. *Materials Today Communications*, **2021**, *29*, 102912. https://doi.org/10.1016/j.mtcomm.2021.102912.

[37] Dannenberg, E. M. Carbon Black Dispersion and Reinforcement. **1952**, *44* (4), 6.

[38] Barrera, C. S.; Cornish, K. Processing and Mechanical Properties of Natural Rubber/Waste-Derived Nano Filler Composites Compared to Macro and Micro Filler Composites. *Industrial Crops and Products*, **2017**, *107*, 217–231. https://doi.org/10.1016/j.indcrop.2017.05.045.

[39] Bokobza, L. Natural Rubber Nanocomposites: A Review. *Nanomaterials*, **2019**, *9* (1), 12. https://doi.org/10.3390/nano9010012.

[40] Chausali, N.; Saxena, J.; Prasad, R. Nanobiochar and Biochar Based Nanocomposites: Advances and Applications. *Journal of Agriculture and Food Research*, **2021**, *5*, 100191. https://doi.org/10.1016/j.jafr.2021.100191.

[41] Ozbas, B.; O'Neill, C. D.; Register, R. A.; Aksay, I. A.; Prud'homme, R. K.; Adamson, D. H. Multifunctional Elastomer Nanocomposites with Functionalized Graphene Single Sheets. *Journal of Polymer Science Part B: Polymer Physics*, **2012**, *50* (13), 910–916. https://doi.org/10.1002/polb.23080.

[42] Niedermeier, W.; Freund, B. Nano-Structure Blacks - A New Carbon Black Family Designed to Meet Truck Tire Performance Demands. *Kautsch. Gummi Kunstst.*, **1999**, *52* (10), 670–676.

[43] ASTM D1765 - 2016 Standard Classification System for Carbon Blacks Used in Rubber Products, 2016.

[44] Fröhlich, J.; Niedermeier, W.; Luginsland, H.-D. The Effect of Filler–Filler and Filler–Elastomer Interaction on Rubber Reinforcement. *Composites Part A: Applied Science and Manufacturing*, **2005**, *36* (4), 449–460. https://doi.org/10.1016/j.compositesa.2004.10.004.

[45] Pöschl, M.; Vašina, M.; Zadrapa, P.; Měřínská, D.; Žaludek, M. Study of Carbon Black Types in SBR Rubber: Mechanical and Vibration Damping Properties. *Materials*, **2020**, *13*, 2394. https://doi.org/10.3390/ma13102394.

[46] PentaCarbon GmbH. Our Wiki: Everything about Carbon Black https://pentacarbon.de/en/wiki/ (accessed Oct 4, 2021).

[47] Gent, A. N.; Pulford, C. T. R. Micromechanics of Fracture in Elastomers. *J Mater Sci*, **1984**, *19* (11), 3612–3619. https://doi.org/10.1007/BF00552273.

[48] Robertson, C. G.; Hardman, N. J. Nature of Carbon Black Reinforcement of Rubber: Perspective on the Original Polymer Nanocomposite. *Polymers*, **2021**, *13* (4), 538. https://doi.org/10.3390/polym13040538.

[49] Khodabakhshi, S.; Fulvio, P. F.; Andreoli, E. Carbon Black Reborn: Structure and Chemistry for Renewable Energy Harnessing. *Carbon*, **2020**, *162,* 604–649. https://doi.org/10.1016/j.carbon.2020.02.058.

[50] Herd, C. R.; McDonald, G. C.; Smith, R. E.; Hess, W. M. The Use of Skeletonization for the Shape Classification of Carbon-Black Aggregates. *Rubber Chemistry and Technology*, **1993**, *66* (4), 491–509. https://doi.org/10.5254/1.3538323.

[51] Bunce, N. J. Introduction to the Interpretation of Electron Spin Resonance Spectra of Organic Radicals. *J. Chem. Educ.*, **1987**, *64* (11), 907. https://doi.org/10.1021/ed064p907.

[52] Kawakubo, M.; Tsunoda, K.; Yajima, H.; Ishii, T.; Kaidou, H.; Ahagon, A. Reactions of Radicals in Filled Rubber Compounds: I. Detection of Free Radicals in Rubbers by ESR. *Rubber Chemistry and Technology*, **2005**, *78* (4), 644–658. https://doi.org/10.5254/1.3547903.

[53] Collins, R. L.; Bell, M. D.; Kraus, G. Unpaired Electrons in Carbon Blacks. *Rubber Chemistry and Technology*, **1960**, *33* (4), 993–1004. https://doi.org/10.5254/1.3542243.

[54] Kraus, G.; Collins, R. L. Odd Electrons in Rubber Reinforcing Carbon Blacks. *Rubber Chemistry and Technology*, **1959**, *32* (1), 107–117. https://doi.org/10.5254/1.3542366.

[55] Wang, M.-J.; Wolff, S.; Donnet, J.-B. Filler—Elastomer Interactions. Part III. Carbon-Black-Surface Energies and Interactions with Elastomer Analogs. *Rubber Chemistry and Technology*, **1991**, *64* (5), 714–736. https://doi.org/10.5254/1.3538585.

[56] Fan, Y.; Fowler, G. D.; Zhao, M. The Past, Present and Future of Carbon Black as a Rubber Reinforcing Filler – A Review. *Journal of Cleaner Production*, **2020**, *247*, 119115. https://doi.org/10.1016/j.jclepro.2019.119115.

[57] López, B. L.; Pérez, L. D.; Mesa, M.; Sierra, L.; Devaux, E.; Camargo, M.; Campagne, C.; Giraud, S. Use of Mesoporous Silica as a Reinforcing Agent in Rubber Compounds. *e-Polymers*, **2005**, *5* (1). https://doi.org/10.1515/epoly.2005.5.1.182.

[58] Hair, M. L.; Hertl, W. Acidity of Surface Hydroxyl Groups. *J. Phys. Chem.*, **1970**, *74* (1), 91–94. https://doi.org/10.1021/j100696a016.

[59] Hockeaynd, J. A.; Pethica, B. A. Surface Hydration of Silicas. **1961**, *57*, 2247–2262.

[60] Lewis, C.; Buanpa, R.; Kiatkamjornwong, S. Effect of Rubber Ratio, Carbon Black Level, and Accelerator Level on Natural Rubber/Bromobutyl Rubber Blend Properties. *Journal of Applied Polymer Science*, **2003**, *90* (11), 3059–3068. https://doi.org/10.1002/app.13036.

[61] Li, S.-M. Utilization of Pyrolyzed Soybean Hulls as an Alternative Reinforcement Filler in Natural Rubber Compounds. M.Sc. Thesis, The University of Akron: Akron, Ohio, 2021.

[62] Wolff, S. Chemical Aspects of Rubber Reinforcement by Fillers. *Rubber Chemistry and Technology*, **1996**, *69* (3), 325–346. https://doi.org/10.5254/1.3538376.

[63] Kato, A.; Ikeda, Y.; Kohjiya, S. Reinforcement Mechanism of Carbon Black (CB) in Natural Rubber Vulcanizates: Relationship Between CB Aggregate and Network Structure and Viscoelastic Properties. *Polymer-Plastics Technology and Engineering*, **2018**, *57* (14), 1418–1429. https://doi.org/10.1080/03602559.2017.1381257.

[64] Lee, S. Y.; Kim, J. S.; Lim, S. H.; Jang, S. H.; Kim, D. H.; Park, N.-H.; Jung, J. W.; Choi, J. The Investigation of the Silica-Reinforced Rubber Polymers with the Methoxy Type Silane Coupling Agents. *Polymers*, **2020**, *12* (12), 3058. https://doi.org/10.3390/polym12123058.

[65] Luginsland, H.-D.; Fröhlich, J.; Wehmeier, A. Influence of Different Silanes on the Reinforcement of Silica-Filled Rubber Compounds. *Rubber Chemistry and Technology*, **2002**, *75* (4), 563–579. https://doi.org/10.5254/1.3544984.

[66] Raghunath, R.; Juhre, D.; Klueppel, M. A Physically Motivated Model for Filled Elastomers Including Strain Rate and Amplitude Dependency in Finite Viscoelasticity. *International Journal of Plasticity*, **2016**, *78*, 223–241. https://doi.org/10.1016/j.ijplas.2015.11.005.

[67] Payne, A. R. The Dynamic Properties of Carbon Black-Loaded Natural Rubber Vulcanizates. Part I. *Journal of Applied Polymer Science*, **1962**, *6* (19), 57–63. https://doi.org/10.1002/app.1962.070061906.

[68] Mullins, L. Effect of Stretching on the Properties of Rubber. *Rubber Chemistry and Technology*, **1948**, *21* (2), 281–300. https://doi.org/10.5254/1.3546914.

[69] Huang, L.; Yang, X.; Gao, J. Pseudo-Elastic Analysis with Permanent Set in Carbon-Filled Rubber. *Advances in Polymer Technology*, **2019**, *2019*, e2369329. https://doi.org/10.1155/2019/2369329.

[70] Toth, P.; Vikström, T.; Molinder, R.; Wiinikka, H. Structure of Carbon Black Continuously Produced from Biomass Pyrolysis Oil. *Green Chemistry*, **2018**, *20*. https://doi.org/10.1039/C8GC01539B.

[71] Kumar, M.; Xiong, X.; Wan, Z.; Sun, Y.; Tsang, D. C. W.; Gupta, J.; Gao, B.; Cao, X.; Tang, J.; Ok, Y. S. Ball Milling as a Mechanochemical Technology for Fabrication of Novel Biochar Nanomaterials. *Bioresource Technology*, **2020**, *312*, 123613. https://doi.org/10.1016/j.biortech.2020.123613.

[72] Dash, P.; Dash, T.; Kumar Rout, T.; Kumar Sahu, A.; Kumar Biswal, S.; Kanta Mishra, B. Preparation of Graphene Oxide by Dry Planetary Ball Milling Process from Natural Graphite. *RSC Advances*, **2016**, *6* (15), 12657–12668. https://doi.org/10.1039/C5RA26491J.

[73] Peterson, S. C.; Jackson, M. A.; Kim, S.; Palmquist, D. E. Increasing Biochar Surface Area: Optimization of Ball Milling Parameters. *Powder Technology*, **2012**, *228*, 115–120. https://doi.org/10.1016/j.powtec.2012.05.005.

[74] Pentecost, A.; Gour, S.; Mochalin, V.; Knoke, I.; Gogotsi, Y. Deaggregation of Nanodiamond Powders Using Salt- and Sugar-Assisted Milling. *ACS Appl. Mater. Interfaces*, **2010**, *2* (11), 3289–3294. https://doi.org/10.1021/am100720n.

[75] Peterson, S. C.; Kim, S. Reducing Biochar Particle Size with Nanosilica and Its Effect on Rubber Composite Reinforcement. *J Polym Environ*, **2020**, *28* (1), 317–322. https://doi.org/10.1007/s10924-019-01604-x.

[76] Xu, X.; Xu, Z.; Huang, J.; Gao, B.; Zhao, L.; Qiu, H.; Cao, X. Sorption of Reactive Red by Biochars Ball Milled in Different Atmospheres: Co-Effect of Surface

Morphology and Functional Groups. *Chemical Engineering Journal*, **2021**, *413*, 127468. https://doi.org/10.1016/j.cej.2020.127468.

[77] Naghdi, M.; Taheran, M.; Brar, S. K.; Rouissi, T.; Verma, M.; Surampalli, R. Y.; Valero, J. R. A Green Method for Production of Nanobiochar by Ball Milling-Optimization and Characterization. *Journal of Cleaner Production*, **2017**, *164*, 1394–1405. https://doi.org/10.1016/j.jclepro.2017.07.084.

[78] Zhang, P.; Wang, X.; Xue, B.; Huang, P.; Hao, Y.; Tang, J.; Maletić, S. P.; Rončević, S. D.; Sun, H. Preparation of Graphite-like Biochars Derived from Straw and Newspaper Based on Ball-Milling and TEMPO-Mediated Oxidation and Their Supersorption Performances to Imidacloprid and Sulfadiazine. *Chemical Engineering Journal*, **2021**, *411*, 128502. https://doi.org/10.1016/j.cej.2021.128502.

[79] Lopez-Tenllado, F. J.; Motta, I. L.; Hill, J. M. Modification of Biochar with High-Energy Ball Milling: Development of Porosity and Surface Acid Functional Groups. *Bioresource Technology Reports*, **2021**, *15*, 100704. https://doi.org/10.1016/j.biteb.2021.100704.

[80] Wang, B.; Gao, B.; Wan, Y. Entrapment of Ball-Milled Biochar in Ca-Alginate Beads for the Removal of Aqueous Cd(II). *Journal of Industrial and Engineering Chemistry*, **2018**, *61*, 161–168. https://doi.org/10.1016/j.jiec.2017.12.013.

[81] Xue, B.; Wang, X.; Sui, J.; Xu, D.; Zhu, Y.; Liu, X. A Facile Ball Milling Method to Produce Sustainable Pyrolytic Rice Husk Bio-Filler for Reinforcement of Rubber Mechanical Property. *Industrial Crops and Products*, **2019**, *141*, 111791. https://doi.org/10.1016/j.indcrop.2019.111791.

[82] Egbosiuba, T. C.; Abdulkareem, A. S.; Kovo, A. S.; Afolabi, E. A.; Tijani, J. O.; Auta, M.; Roos, W. D. Ultrasonic Enhanced Adsorption of Methylene Blue onto the Optimized Surface Area of Activated Carbon: Adsorption Isotherm, Kinetics and Thermodynamics. *Chemical Engineering Research and Design*, **2020**, *153*, 315–336. https://doi.org/10.1016/j.cherd.2019.10.016.

[83] Oleszczuk, P.; Ćwikła-Bundyra, W.; Bogusz, A.; Skwarek, E.; Ok, Y. S. Characterization of Nanoparticles of Biochars from Different Biomass. *Journal of Analytical and Applied Pyrolysis*, **2016**, *121*, 165–172. https://doi.org/10.1016/j.jaap.2016.07.017.

[84] Sajjadi, B.; Chen, W.-Y.; Egiebor, N. O. A Comprehensive Review on Physical Activation of Biochar for Energy and Environmental Applications. *Reviews in Chemical Engineering*, **2019**, *35* (6), 735–776. https://doi.org/10.1515/revce-2017-0113.

[85] Genovese, M.; Jiang, J.; Lian, K.; Holm, N. High Capacitive Performance of Exfoliated Biochar Nanosheets from Biomass Waste Corn Cob. *J. Mater. Chem. A*, **2015**, *3* (6), 2903–2913. https://doi.org/10.1039/C4TA06110A.

[86] Guo, F.; Bao, L.; Wang, H.; Larson, S. L.; Ballard, J. H.; Knotek-Smith, H. M.; Zhang, Q.; Su, Y.; Wang, X.; Han, F. A Simple Method for the Synthesis of Biochar Nanodots Using Hydrothermal Reactor. *MethodsX*, **2020**, *7*, 101022. https://doi.org/10.1016/j.mex.2020.101022.

[87] Zhao, L.; Cao, X.; Mašek, O.; Zimmerman, A. Heterogeneity of Biochar Properties as a Function of Feedstock Sources and Production Temperatures. *Journal of Hazardous Materials*, **2013**, *256–257*, 1–9. https://doi.org/10.1016/j.jhazmat.2013.04.015.

[88] Tomczyk, A.; Sokołowska, Z.; Boguta, P. Biochar Physicochemical Properties: Pyrolysis Temperature and Feedstock Kind Effects. *Rev Environ Sci Biotechnol*, **2020**, *19* (1), 191–215. https://doi.org/10.1007/s11157-020-09523-3.

[89] Zhang, H.; Chen, C.; Gray, E. M.; Boyd, S. E. Effect of Feedstock and Pyrolysis Temperature on Properties of Biochar Governing End Use Efficacy. *Biomass and Bioenergy*, **2017**, *105*, 136–146. https://doi.org/10.1016/j.biombioe.2017.06.024.

[90] Liu, Z.; Niu, W.; Chu, H.; Zhou, T.; Niu, Z. Effect of the Carbonization Temperature on the Properties of Biochar Produced from the Pyrolysis of Crop Residues. *BioResources*, **2018**, *13* (2), 3429–3446.

[91] Collard, F.-X.; Blin, J. A Review on Pyrolysis of Biomass Constituents: Mechanisms and Composition of the Products Obtained from the Conversion of Cellulose, Hemicelluloses and Lignin. *Renewable and Sustainable Energy Reviews*, **2014**, *38*, 594–608. https://doi.org/10.1016/j.rser.2014.06.013.

[92] Wang, L.; Skreiberg, Ø.; Gronli, M.; Specht, G. P.; Antal, M. J. Is Elevated Pressure Required to Achieve a High Fixed-Carbon Yield of Charcoal from Biomass? Part 2: The Importance of Particle Size. *Energy Fuels*, **2013**, *27* (4), 2146–2156. https://doi.org/10.1021/ef400041h.

[93] Tripathi, M.; Sahu, J. N.; Ganesan, P. Effect of Process Parameters on Production of Biochar from Biomass Waste through Pyrolysis: A Review. *Renewable and Sustainable Energy Reviews*, **2016**, *55*, 467–481. https://doi.org/10.1016/j.rser.2015.10.122.

[94] Rutherford, D. W.; Wershaw, R. L.; Rostad, C. E.; Kelly, C. N. Effect of Formation Conditions on Biochars: Compositional and Structural Properties of Cellulose, Lignin, and Pine Biochars. *Biomass and Bioenergy*, **2012**, *46*, 693–701. https://doi.org/10.1016/j.biombioe.2012.06.026.

[95] Apaydın-Varol, E.; Pütün, A. E. Preparation and Characterization of Pyrolytic Chars from Different Biomass Samples. *Journal of Analytical and Applied Pyrolysis*, **2012**, *98*, 29–36. https://doi.org/10.1016/j.jaap.2012.07.001.

[96] Jiang, C.; He, H.; Yu, P.; Wang, D. K.; Zhou, L.; Jia, D. M. Plane-Interface-Induced Lignin-Based Nanosheets and Its Reinforcing Effect on Styrene-Butadiene Rubber. *Express Polym. Lett.*, **2014**, *8* (9), 619–634. https://doi.org/10.3144/expresspolymlett.2014.66.

[97] Jiang, C.; He, H.; Yao, X.; Yu, P.; Zhou, L.; Jia, D. Self-Crosslinkable Lignin/Epoxidized Natural Rubber Composites. *Journal of Applied Polymer Science*, **2014**, *131* (23). https://doi.org/10.1002/app.41166.

[98] Garlapati, V. K.; Chandel, A. K.; Kumar, S. P. J.; Sharma, S.; Sevda, S.; Ingle, A. P.; Pant, D. Circular Economy Aspects of Lignin: Towards a Lignocellulose Biorefinery. *Renewable and Sustainable Energy Reviews*, **2020**, *130*, 109977. https://doi.org/10.1016/j.rser.2020.109977.

[99] Hu, J.; Zhang, Q.; Lee, D.-J. Kraft Lignin Biorefinery: A Perspective. *Bioresource Technology*, **2018**, *247*, 1181–1183. https://doi.org/10.1016/j.biortech.2017.08.169.

[100] M. Abu-Omar, M.; Barta, K.; T. Beckham, G.; S. Luterbacher, J.; Ralph, J.; Rinaldi, R.; Román-Leshkov, Y.; M. Samec, J. S.; F. Sels, B.; Wang, F. Guidelines for Performing Lignin-First Biorefining. *Energy & Environmental Science*, **2021**, *14* (1), 262–292. https://doi.org/10.1039/D0EE02870C.

[101] Paone, E.; Tabanelli, T.; Mauriello, F. The Rise of Lignin Biorefinery. *Current Opinion in Green and Sustainable Chemistry*, **2020**, *24*, 1–6. https://doi.org/10.1016/j.cogsc.2019.11.004.

[102] Liu, T.; Yang, L.; Liu, B.; Tan, L. Hydroxycinnamic Acids Release during Bioconversion of Corn Stover and Their Effects on Lignocellulolytic Enzymes. *Bioresource Technology*, **2019**, *294*, 122116. https://doi.org/10.1016/j.biortech.2019.122116.

[103] Ho Seo, J.; Jeong, H.; Lee, H. W.; Choi, C. S.; Bae, J. H.; Lee, S. M.; Kim, Y. S. Characterization of Solvent-Fractionated Lignins from Woody Biomass Treated via Supercritical Water Oxidation. *Bioresource Technology*, **2019**, *275*, 368–374. https://doi.org/10.1016/j.biortech.2018.12.076.

[104] Knežević, A.; Milovanović, I.; Stajić, M.; Lončar, N.; Brčeski, I.; Vukojević, J.; Ćilerdžić, J. Lignin Degradation by Selected Fungal Species. *Bioresource Technology*, **2013**, *138*, 117–123. https://doi.org/10.1016/j.biortech.2013.03.182.

[105] Lora, J. H.; Glasser, W. G. Recent Industrial Applications of Lignin: A Sustainable Alternative to Nonrenewable Materials. *Journal of Polymers and the Environment*, **2002**, *10* (1), 39–48. https://doi.org/10.1023/A:1021070006895.

[106] Wang, W.; Lee, D.-J. Lignocellulosic Biomass Pretreatment by Deep Eutectic Solvents on Lignin Extraction and Saccharification Enhancement: A Review. *Bioresource Technology*, **2021**, *339*, 125587. https://doi.org/10.1016/j.biortech.2021.125587.

[107] Blasi, C. D.; Branca, C.; D’Errico, G. Degradation Characteristics of Straw and Washed Straw. *Thermochimica Acta*, **2000**, *364* (1), 133–142. https://doi.org/10.1016/S0040-6031(00)00634-1.

[108] Raveendran, K.; Ganesh, A. Adsorption Characteristics and Pore-Development of Biomass-Pyrolysis Char. *Fuel*, **1998**, *77* (7), 769–781. https://doi.org/10.1016/S0016-2361(97)00246-9.

[109] Yang, H.; Yan, R.; Chen, H.; Zheng, C.; Lee, D. H.; Liang, D. T. Influence of Mineral Matter on Pyrolysis of Palm Oil Wastes. *Combustion and Flame*, **2006**, *146* (4), 605–611. https://doi.org/10.1016/j.combustflame.2006.07.006.

[110] Deng, L.; Zhang, T.; Che, D. Effect of Water Washing on Fuel Properties, Pyrolysis and Combustion Characteristics, and Ash Fusibility of Biomass. *Fuel Processing Technology*, **2013**, *106*, 712–720. https://doi.org/10.1016/j.fuproc.2012.10.006.

[111] Aston, J. E.; Thompson, D. N.; Westover, T. L. Performance Assessment of Dilute-Acid Leaching to Improve Corn Stover Quality for Thermochemical Conversion. *Fuel*, **2016**, *186*, 311–319. https://doi.org/10.1016/j.fuel.2016.08.056.

[112] Lay, M.; Rusli, A.; Abdullah, M. K.; Abdul Hamid, Z. A.; Shuib, R. K. Converting Dead Leaf Biomass into Activated Carbon as a Potential Replacement for Carbon Black Filler in Rubber Composites. *Composites Part B: Engineering*, **2020**, *201*, 108366. https://doi.org/10.1016/j.compositesb.2020.108366.

[113] Liliedahl, T.; Sjöström, K. Heat Transfer Controlled Pyrolysis Kinetics of a Biomass Slab, Rod or Sphere. *Biomass and Bioenergy*, **1998**, *15* (6), 503–509. https://doi.org/10.1016/S0961-9534(98)00053-1.

[114] Manyà, J. J.; Velo, E.; Puigjaner, L. Kinetics of Biomass Pyrolysis: A Reformulated Three-Parallel-Reactions Model. *Ind. Eng. Chem. Res.*, **2003**, *42* (3), 434–441. https://doi.org/10.1021/ie020218p.

[115] Radlein, D.; Quignard, A. A Short Historical Review of Fast Pyrolysis of Biomass. *Oil Gas Sci. Technol. – Rev. IFP Energies nouvelles*, **2013**, *68* (4), 765–783. https://doi.org/10.2516/ogst/2013162.

[116] Haykiri-Acma, H. The Role of Particle Size in the Non-Isothermal Pyrolysis of Hazelnut Shell. *Journal of Analytical and Applied Pyrolysis*, **2006**, *75* (2), 211–216. https://doi.org/10.1016/j.jaap.2005.06.002.

[117] Manyà, J. J.; Ortigosa, M. A.; Laguarta, S.; Manso, J. A. Experimental Study on the Effect of Pyrolysis Pressure, Peak Temperature, and Particle Size on the Potential Stability of Vine Shoots-Derived Biochar. *Fuel*, **2014**, *133*, 163–172. https://doi.org/10.1016/j.fuel.2014.05.019.

[118] Shen, J.; Wang, X.-S.; Garcia-Perez, M.; Mourant, D.; Rhodes, M. J.; Li, C.-Z. Effects of Particle Size on the Fast Pyrolysis of Oil Mallee Woody Biomass. *Fuel*, **2009**, *88* (10), 1810–1817. https://doi.org/10.1016/j.fuel.2009.05.001.

[119] Melligan, F.; Auccaise, R.; Novotny, E. H.; Leahy, J. J.; Hayes, M. H. B.; Kwapinski, W. Pressurised Pyrolysis of Miscanthus Using a Fixed Bed Reactor. *Bioresource Technology*, **2011**, *102* (3), 3466–3470. https://doi.org/10.1016/j.biortech.2010.10.129.

[120] Richard, J.-R.; Antal, M. J. Thermogravimetric Studies of Charcoal Formation from Cellulose at Elevated Pressures. In *Bridgwater, A.V. (eds) Advances in Thermochemical Biomass Conversion*; Springer, Dordrecht, 1993; pp 784–792.

[121] Qian, M.; Huang, W.; Wang, J.; Wang, X.; Liu, W.; Zhu, Y. Surface Treatment Effects on the Mechanical Properties of Silica Carbon Black Reinforced Natural Rubber/Butadiene Rubber Composites. *Polymers*, **2019**, *11* (11), 1763. https://doi.org/10.3390/polym11111763.

[122] Zhang, Y.; Li, X.; Ge, X.; Deng, F.; Cho, U. R. Effect of Coupling Agents and Ionic Liquid on the Properties of Rice Bran Carbon/Carboxylated Styrene Butadiene Rubber Composites. *Macromol. Res.*, **2015**, *23* (10), 952–959. https://doi.org/10.1007/s13233-015-3127-9.

[123] Zhang, Y.; Fei, D.; Xin, G.; Cho, U.-R. Surface Modification of Novel Rice Bran Carbon Functionalized with (3-Mercaptopropyl) Trimethoxysilane and Its Influence on the Properties of Styrene-Butadiene Rubber Composites. *Journal of Composite Materials*, **2016**, *50* (21), 2987–2999. https://doi.org/10.1177/0021998315615202.

[124] Janu, R.; Mrlik, V.; Ribitsch, D.; Hofman, J.; Sedláček, P.; Bielská, L.; Soja, G. Biochar Surface Functional Groups as Affected by Biomass Feedstock, Biochar Composition and Pyrolysis Temperature. *Carbon Resources Conversion*, **2021**, *4*, 36–46. https://doi.org/10.1016/j.crcon.2021.01.003.

[125] Banik, C.; Lawrinenko, M.; Bakshi, S.; Laird, D. A. Impact of Pyrolysis Temperature and Feedstock on Surface Charge and Functional Group Chemistry of Biochars. *Journal of Environmental Quality*, **2018**, *47* (3), 452–461. https://doi.org/10.2134/jeq2017.11.0432.

[126] Feng, D.; Zhao, Y.; Zhang, Y.; Gao, J.; Sun, S. Changes of Biochar Physiochemical Structures during Tar H2O and CO2 Heterogeneous Reforming with Biochar. *Fuel Processing Technology*, **2017**, *165*, 72–79. https://doi.org/10.1016/j.fuproc.2017.05.011.

[127] Fan, Q.; Sun, J.; Chu, L.; Cui, L.; Quan, G.; Yan, J.; Hussain, Q.; Iqbal, M. Effects of Chemical Oxidation on Surface Oxygen-Containing Functional Groups and Adsorption Behavior of Biochar. *Chemosphere*, **2018**, *207*, 33–40. https://doi.org/10.1016/j.chemosphere.2018.05.044.

[128] Kinney, T. J.; Masiello, C. A.; Dugan, B.; Hockaday, W. C.; Dean, M. R.; Zygourakis, K.; Barnes, R. T. Hydrologic Properties of Biochars Produced at Different Temperatures. *Biomass and Bioenergy*, **2012**, *41*, 34–43. https://doi.org/10.1016/j.biombioe.2012.01.033.

[129] Gray, M.; Johnson, M. G.; Dragila, M. I.; Kleber, M. Water Uptake in Biochars: The Roles of Porosity and Hydrophobicity. *Biomass and Bioenergy*, **2014**, *61*, 196–205. https://doi.org/10.1016/j.biombioe.2013.12.010.

[130] Haas, T. J.; Nimlos, M. R.; Donohoe, B. S. Real-Time and Post-Reaction Microscopic Structural Analysis of Biomass Undergoing Pyrolysis. *Energy Fuels*, **2009**, *23* (7), 3810–3817. https://doi.org/10.1021/ef900201b.

[131] Navarathna, C. M.; Bombuwala Dewage, N.; Keeton, C.; Pennisson, J.; Henderson, R.; Lashley, B.; Zhang, X.; Hassan, E. B.; Perez, F.; Mohan, D.; et al. Biochar Adsorbents

with Enhanced Hydrophobicity for Oil Spill Removal. *ACS Appl. Mater. Interfaces*, **2020**, *12* (8), 9248–9260. https://doi.org/10.1021/acsami.9b20924.

[132] Sidik, S. M.; Jalil, A. A.; Triwahyono, S.; Adam, S. H.; Satar, M. A. H.; Hameed, B. H. Modified Oil Palm Leaves Adsorbent with Enhanced Hydrophobicity for Crude Oil Removal. *Chemical Engineering Journal*, **2012**, *203*, 9–18. https://doi.org/10.1016/j.cej.2012.06.132.

[133] Sengupta, S.; Ray, D.; Mukhopadhyay, A.; Sengupta, S.; Kar, T. Lauric Acid Coated Fly Ash as a Reinforcement in Recycled Polymer Matrix Composites. *Journal of Applied Polymer Science*, **2015**, *132* (10). https://doi.org/10.1002/app.41586.

[134] Masek, A.; Cichosz, S.; Piotrowska, M. Biocomposites of Epoxidized Natural Rubber/Poly(Lactic Acid) Modified with Natural Fillers (Part I). *International Journal of Molecular Sciences*, **2021**, *22* (6), 3150. https://doi.org/10.3390/ijms22063150.

[135] Madhubashani, A. M. P.; Giannakoudakis, D. A.; Amarasinghe, B. M. W. P. K.; Rajapaksha, A. U.; Pradeep Kumara, P. B. T.; Triantafyllidis, K. S.; Vithanage, M. Propensity and Appraisal of Biochar Performance in Removal of Oil Spills: A Comprehensive Review. *Environmental Pollution*, **2021**, *288*, 117676. https://doi.org/10.1016/j.envpol.2021.117676.

[136] Nduka, J. K.; Ezenweke, L. O.; Ezenwa, E. T. Comparison of the Mopping Ability of Chemically Modified and Unmodified Biological Wastes on Crude Oil and Its Lower Fractions. *Bioresource Technology*, **2008**, *99* (16), 7902–7905. https://doi.org/10.1016/j.biortech.2008.01.066.

[137] Raj, K. G.; Joy, P. A. Coconut Shell Based Activated Carbon–Iron Oxide Magnetic Nanocomposite for Fast and Efficient Removal of Oil Spills. *Journal of Environmental Chemical Engineering*, **2015**, *3* (3), 2068–2075. https://doi.org/10.1016/j.jece.2015.04.028.

[138] Ahamad, T.; Naushad, Mu.; Ruksana; Alshehri, S. M. Ultra-Fast Spill Oil Recovery Using a Mesoporous Lignin Based Nanocomposite Prepared from Date Palm Pits (Phoenix Dactylifera L.). *International Journal of Biological Macromolecules*, **2019**, *130*, 139–147. https://doi.org/10.1016/j.ijbiomac.2019.02.038.

[139] Shokry, H.; Elkady, M.; Salama, E. Eco-Friendly Magnetic Activated Carbon Nano-Hybrid for Facile Oil Spills Separation. *Sci Rep*, **2020**, *10* (1), 10265. https://doi.org/10.1038/s41598-020-67231-y.

[140] Paleri, D. M.; Rodriguez-Uribe, A.; Misra, M.; Mohanty, A. K. Preparation and Characterization of Eco-Friendly Hybrid Biocomposites from Natural Rubber, Biocarbon, and Carbon Black. *Express Polymer Letters*, **2021**, *15* (3), 236–249. http://dx.doi.org/10.3144/expresspolymlett.2021.21.

[141] Li, Q.; Li, X.; Lee, D.-H.; Fan, Y.; Nam, B.-U.; Lee, J.-E.; Cho, U.-R. Hybrid of Bamboo Charcoal and Silica by Tetraethoxysilane Hydrolysis over Acid Catalyst Reinforced Styrene-Butadiene Rubber. *Journal of Applied Polymer Science*, **2018**, *135* (19), 46219. https://doi.org/10.1002/app.46219.

[142] Bartoli, M.; Giorcelli, M.; Jagdale, P.; Rovere, M. Towards Traditional Carbon Fillers: Biochar-Based Reinforced Plastic. In *Fillers*; IntechOpen: London, United Kingdom, 2020. https://doi.org/10.5772/intechopen.91962.

[143] Liu, W.; Li, K.; Xu, S. Utilizing Bamboo Biochar in Cement Mortar as a Bio-Modifier to Improve the Compressive Strength and Crack-Resistance Fracture Ability. *Construction and Building Materials*, **2022**, *327*, 126917. https://doi.org/10.1016/j.conbuildmat.2022.126917.

[144] FAO Crop Information: Maize https://www.fao.org/land-water/databases-and-software/crop-information/maize/en/ (accessed May 17, 2022).

[145] Bell, J.; Paula, L.; Dodd, T.; Németh, S.; Nanou, C.; Mega, V.; Campos, P. EU Ambition to Build the World's Leading Bioeconomy—Uncertain Times Demand Innovative and Sustainable Solutions. *New Biotechnology*, **2018**, *40*, 25–30. https://doi.org/10.1016/j.nbt.2017.06.010.

[146] Fu, P.; Bai, X.; Li, Z.; Yi, W.; Li, Y.; Zhang, Y. Fast Pyrolysis of Corn Stovers with Ceramic Ball Heat Carriers in a Novel Dual Concentric Rotary Cylinder Reactor. *Bioresource Technology*, **2018**, *263*, 467–474. https://doi.org/10.1016/j.biortech.2018.05.033.

[147] Liu, X.; Zhang, Y.; Li, Z.; Feng, R.; Zhang, Y. Characterization of Corncob-Derived Biochar and Pyrolysis Kinetics in Comparison with Corn Stalk and Sawdust. *Bioresource Technology*, **2014**, *170*, 76–82. https://doi.org/10.1016/j.biortech.2014.07.077.

[148] Pointner, M.; Kuttner, P.; Obrlik, T. Composition of Corncobs as a Substrate for Fermentation of Biofuels. *Agronomy Research*, **2014**, *12* (2), 391–396.

[149] Wanitwattanarumlug, B.; Luengnaruemitchai, A.; Wongkasemjit, S. Characterization of Corn Cobs from Microwave and Potassium Hydroxide Pretreatment. *Int J Chem Bio Eng*, **2012**, *6*, 354–358.

[150] Palanisamy, C. P.; Cui, B.; Zhang, H.; Jayaraman, S.; Kodiveri Muthukaliannan, G. A Comprehensive Review on Corn Starch-Based Nanomaterials: Properties, Simulations, and Applications. *Polymers*, **2020**, *12* (9), 2161. https://doi.org/10.3390/polym12092161.

[151] Aggarwal, P.; Dollimore, D.; Heon, K. Comparative Thermal Analysis Study of Two Biopolymers, Starch and Cellulose. *Journal of Thermal Analysis*, **1997**, *50* (1–2), 7–17. https://doi.org/10.1007/BF01979545.

[152] Ourania A. Ioannidou; George G. Stauropoulos; Anastasia A. Zabaniotou. Use of Biogenic Solids for Activated Carbon via Pyrolysis: The Case of Corn Cob. *High Temperature Materials and Processes*, **2008**, *27* (5), 355–360. https://doi.org/10.1515/HTMP.2008.27.5.355.

[153] Jordan, K.; Battista, J. A Stable Black-Refractive-Index-Matching Liquid for Optical CT Scanning of Hydrogels. *J. Phys.: Conf. Ser.*, **2009**, *164*, 012045. https://doi.org/10.1088/1742-6596/164/1/012045.

[154] Singh, B.; Camps-Arbestain, M.; Lehmann, J. *Biochar: A Guide to Analytical Methods*; CRC Press/Taylor and Francis Group, LLC: Boca Raton, FL, 2017.

[155] Medalia, A. I.; Kraus, G. 8 - Reinforcement of Elastomers by Particulate Fillers. In *Science and Technology of Rubber (Second Edition)*; Mark, J. E., Erman, B., Eirich, F. R., Eds.; Academic Press: San Diego, 1994; pp 387–418. https://doi.org/10.1016/B978-0-08-051667-7.50013-5.

[156] Lukens, Wayne W.; Schmidt-Winkel, P.; Zhao, D.; Feng, J.; Stucky, G. D. Evaluating Pore Sizes in Mesoporous Materials: A Simplified Standard Adsorption Method and a Simplified Broekhoff−de Boer Method. *Langmuir*, **1999**, *15* (16), 5403–5409. https://doi.org/10.1021/la990209u.

[157] Zheng, Y. Evaluation of a New Method to Estimate the Micropore Volume and External Surface Area of Single-Walled Carbon Nanotubes. Master's Thesis, University of Tennessee: Knoxville, Tennessee, 2008.

[158] Kumar, M.; Gupta, R. C.; Sharma, T. X-Ray Diffraction Studies OfAcacia AndEucalyptus Wood Chars. *J Mater Sci*, **1993**, *28* (3), 805–810. https://doi.org/10.1007/BF01151261.

[159] Singh, B.; Raven, M. D. Chapter 21: X-Ray Diffraction Analysis of Biochar. In *Biochar: A Guide to Analytical Methods*; CRC Press/Taylor and Francis Group, LLC: Boca Raton, FL, 2017; pp 245–251.

[160] Yoo, S.; Kelley, S. S.; Tilotta, D. C.; Park, S. Structural Characterization of Loblolly Pine Derived Biochar by X-Ray Diffraction and Electron Energy Loss Spectroscopy. *ACS Sustainable Chem. Eng.*, **2018**, *6* (2), 2621–2629. https://doi.org/10.1021/acssuschemeng.7b04119.

[161] Zhou, P.; Lee, R.; Claye, A.; Fischer, J. E. Layer Disorder in Carbon Anodes. *Carbon*, **1998**, *36* (12), 1777–1781. https://doi.org/10.1016/S0008-6223(98)00126-2.

[162] Kercher, A. K.; Nagle, D. C. Microstructural Evolution during Charcoal Carbonization by X-Ray Diffraction Analysis. *Carbon*, **2003**, *41* (1), 15–27. https://doi.org/10.1016/S0008-6223(02)00261-0.

[163] Pusceddu, E.; Santilli, S. F.; Fioravanti, G.; Montanaro, A.; Miglietta, F.; Foscolo, P. U. Chemical-Physical Analysis and Exfoliation of Biochar-Carbon Matter: From Agriculture Soil Improver to Starting Material for Advanced Nanotechnologies. *Mater. Res. Express*, **2019**, *6* (11), 115612. https://doi.org/10.1088/2053-1591/ab4ba8.

[164] Keiluweit, M.; Nico, P. S.; Johnson, M. G.; Kleber, M. Dynamic Molecular Structure of Plant Biomass-Derived Black Carbon (Biochar). *Environ. Sci. Technol.*, **2010**, *44* (4), 1247–1253. https://doi.org/10.1021/es9031419.

[165] Rao Penki, T.; Kishore;N. Munichandraiah, B.; Shanmughasundaram, D. High Rate Capability Of Coconut Kernel Derived Carbon As An Anode Material For Lithium-Ion Batteries. *Adv. Mater. Lett.*, **2014**, *5* (4), 184–190. https://doi.org/10.5185/amlett.2013.8530.

[166] Roychoudhury, A.; De, P. P. Elastomer–Carbon Black Interaction: Influence of Elastomer Chemical Structure and Carbon Black Surface Chemistry on Bound Rubber Formation. *Journal of Applied Polymer Science*, **1995**, *55* (1), 9–15. https://doi.org/10.1002/app.1995.070550102.

[167] Cantrell, K. B.; Hunt, P. G.; Uchimiya, M.; Novak, J. M.; Ro, K. S. Impact of Pyrolysis Temperature and Manure Source on Physicochemical Characteristics of Biochar. *Bioresource Technology*, **2012**, *107*, 419–428. https://doi.org/10.1016/j.biortech.2011.11.084.

[168] Kloss, S.; Zehetner, F.; Dellantonio, A.; Hamid, R.; Ottner, F.; Liedtke, V.; Schwanninger, M.; Gerzabek, M. H.; Soja, G. Characterization of Slow Pyrolysis Biochars: Effects of Feedstocks and Pyrolysis Temperature on Biochar Properties. *Journal of Environmental Quality*, **2012**, *41* (4), 990–1000. https://doi.org/10.2134/jeq2011.0070.

[169] Kizil, R.; Irudayaraj, J.; Seetharaman, K. Characterization of Irradiated Starches by Using FT-Raman and FTIR Spectroscopy. *J. Agric. Food Chem.*, **2002**, *50* (14), 3912–3918. https://doi.org/10.1021/jf011652p.

[170] Abdullah, A. H. D.; Chalimah, S.; Primadona, I.; Hanantyo, M. H. G. Physical and Chemical Properties of Corn, Cassava, and Potato Starchs; IOP Publishing Ltd, 2018; Vol. 160, p 012003. https://doi.org/10.1088/1755-1315/160/1/012003.

[171] Iizuka, K.; Aishima, T. Starch Gelation Process Observed by FT-IR/ATR Spectrometry with Multivariate Data Analysis. *Journal of Food Science*, **1999**, *64* (4), 653–658. https://doi.org/10.1111/j.1365-2621.1999.tb15104.x.

[172] Santha, N.; Sudha, K. G.; Vijayakumari, K. P.; Nayar, V. U.; Moorthy, S. N. Raman and Infrared Spectra of Starch Samples of Sweet Potato and Cassava. *J Chem Sci*, **1990**, *102* (5), 705–712. https://doi.org/10.1007/BF03040801.

[173] Cael, J. J.; Koenig, J. L.; Blackwell, J. Infrared and Raman Spectroscopy of Carbohydrates. Part VI: Normal Coordinate Analysis of V-Amylose. *Biopolymers*, **1975**, *14* (9), 1885–1903. https://doi.org/10.1002/bip.1975.360140909.

[174] Budai, A.; Calucci, L.; Rasse, D. P.; Strand, L. T.; Pengerud, A.; Wiedemeier, D.; Abiven, S.; Forte, C. Effects of Pyrolysis Conditions on Miscanthus and Corncob

Chars: Characterization by IR, Solid State NMR and BPCA Analysis. *Journal of Analytical and Applied Pyrolysis*, **2017**, *128*, 335–345. https://doi.org/10.1016/j.jaap.2017.09.017.

[175] Taherymoosavi, S.; Joseph, S.; Munroe, P. Characterization of Organic Compounds in a Mixed Feedstock Biochar Generated from Australian Agricultural Residues. *Journal of Analytical and Applied Pyrolysis*, **2016**, *120*, 441–449. https://doi.org/10.1016/j.jaap.2016.06.017.

[176] Wu, W.; Yang, M.; Feng, Q.; McGrouther, K.; Wang, H.; Lu, H.; Chen, Y. Chemical Characterization of Rice Straw-Derived Biochar for Soil Amendment. *Biomass and Bioenergy*, **2012**, *47*, 268–276. https://doi.org/10.1016/j.biombioe.2012.09.034.

[177] Yuan, J.-H.; Xu, R.-K.; Zhang, H. The Forms of Alkalis in the Biochar Produced from Crop Residues at Different Temperatures. *Bioresource Technology*, **2011**, *102* (3), 3488–3497. https://doi.org/10.1016/j.biortech.2010.11.018.

[178] Chun, Y.; Sheng, G.; Chiou, C. T.; Xing, B. Compositions and Sorptive Properties of Crop Residue-Derived Chars. *Environ. Sci. Technol.*, **2004**, *38* (17), 4649–4655. https://doi.org/10.1021/es035034w.

[179] Pastorova, I.; Botto, R. E.; Arisz, P. W.; Boon, J. J. Cellulose Char Structure: A Combined Analytical Py-GC-MS, FTIR, and NMR Study. *Carbohydrate Research*, **1994**, *262* (1), 27–47. https://doi.org/10.1016/0008-6215(94)84003-2.

[180] Lehmann, J.; Joseph, S. *Biochar for Environmental Management: Science, Technology and Implementation*, 2nd Edition.; Routledge: New York, NY, 2015.

[181] Krishnan, K. A.; Haridas, A. Removal of Phosphate from Aqueous Solutions and Sewage Using Natural and Surface Modified Coir Pith. *Journal of Hazardous Materials*, **2008**, *152* (2), 527–535. https://doi.org/10.1016/j.jhazmat.2007.07.015.

[182] Asai, S.; Kaneki, H.; Sumita, M.; Miyasaka, K. Effect of Oxidized Carbon Black on the Mechanical Properties and Molecular Motions of Natural Rubber Studied by Pulse NMR. *Journal of Applied Polymer Science*, **1991**, *43* (7), 1253–1257. https://doi.org/10.1002/app.1991.070430706.

[183] Luo, W.; Yin, B.; Hu, X.; Zhou, Z.; Deng, Y.; Song, K. Modeling of the Heat Build-up of Carbon Black Filled Rubber. *Polymer Testing*, **2018**, *69*, 116–124. https://doi.org/10.1016/j.polymertesting.2018.05.017.

[184] Liu, X.; Yu, L.; Liu, H.; Chen, L.; Li, L. Thermal Decomposition of Corn Starch with Different Amylose/Amylopectin Ratios in Open and Sealed Systems. *Cereal Chemistry*, **2009**, *86* (4), 383–385. https://doi.org/10.1094/CCHEM-86-4-0383.

[185] Liu, X.; Yu, L.; Xie, F.; Li, M.; Chen, L.; Li, X. Kinetics and Mechanism of Thermal Decomposition of Cornstarches with Different Amylose/Amylopectin Ratios. *Starch - Stärke*, **2010**, *62* (3–4), 139–146. https://doi.org/10.1002/star.200900202.

[186] Liu, X.; Wang, Y.; Yu, L.; Tong, Z.; Chen, L.; Liu, H.; Li, X. Thermal Degradation and Stability of Starch under Different Processing Conditions. *Starch - Stärke*, **2013**, *65* (1–2), 48–60. https://doi.org/10.1002/star.201200198.

[187] Stephen, A. M.; Phillips, G. O.; Williams, P. A. *Food Polysaccharides and Their Applications*, 2nd Edition.; CRC Press Taylor and Francis Group LLC, 2006.

[188] Abdullah, S.; Suzana, Y.; Ahmad, M.; Ramli, A.; Ismail, L. Thermogravimetry Study on Pyrolysis of Various Lignocellulosic Biomass for Potential Hydrogen Production. *World Academy of Science, Engineering and Technology*, **2010**, *72*, 129–133.

[189] Di Blasi, C. Modeling Chemical and Physical Processes of Wood and Biomass Pyrolysis. *Progress in Energy and Combustion Science*, **2008**, *34* (1), 47–90. https://doi.org/10.1016/j.pecs.2006.12.001.

[190] Kawamoto, H. Lignin Pyrolysis Reactions. *J Wood Sci*, **2017**, *63* (2), 117–132. https://doi.org/10.1007/s10086-016-1606-z.

[191] Qiao, Y.; Wang, B.; Ji, Y.; Xu, F.; Zong, P.; Zhang, J.; Tian, Y. Thermal Decomposition of Castor Oil, Corn Starch, Soy Protein, Lignin, Xylan, and Cellulose during Fast Pyrolysis. *Bioresource Technology*, **2019**, *278*, 287–295. https://doi.org/10.1016/j.biortech.2019.01.102.

[192] Malucelli, L. C.; Silvestre, G. F.; Carneiro, J.; Vasconcelos, E. C.; Guiotoku, M.; Maia, C. M. B. F.; Carvalho Filho, M. A. S. Biochar Higher Heating Value Estimative Using Thermogravimetric Analysis. *J Therm Anal Calorim*, **2020**, *139* (3), 2215–2220. https://doi.org/10.1007/s10973-019-08597-8.

[193] Sun, Y.; Gao, B.; Yao, Y.; Fang, J.; Zhang, M.; Zhou, Y.; Chen, H.; Yang, L. Effects of Feedstock Type, Production Method, and Pyrolysis Temperature on Biochar and Hydrochar Properties. *Chemical Engineering Journal*, **2014**, *240*, 574–578. https://doi.org/10.1016/j.cej.2013.10.081.

[194] Yi, Q.; Qi, F.; Cheng, G.; Zhang, Y.; Xiao, B.; Hu, Z.; Liu, S.; Cai, H.; Xu, S. Thermogravimetric Analysis of Co-Combustion of Biomass and Biochar. *J Therm Anal Calorim*, **2013**, *112* (3), 1475–1479. https://doi.org/10.1007/s10973-012-2744-1.

[195] Rafiq, M. K.; Bachmann, R. T.; Rafiq, M. T.; Shang, Z.; Joseph, S.; Long, R. Influence of Pyrolysis Temperature on Physico-Chemical Properties of Corn Stover (Zea Mays L.) Biochar and Feasibility for Carbon Capture and Energy Balance. *PLOS ONE*, **2016**, *11* (6), e0156894. https://doi.org/10.1371/journal.pone.0156894.

[196] Conti, R.; Fabbri, D.; Vassura, I.; Ferroni, L. Comparison of Chemical and Physical Indices of Thermal Stability of Biochars from Different Biomass by Analytical Pyrolysis and Thermogravimetry. *Journal of Analytical and Applied Pyrolysis*, **2016**, *122*, 160–168. https://doi.org/10.1016/j.jaap.2016.10.003.

[197] Dick, J. S.; Pawlowski, H.; Scheers, E. Alternate Instrumental Methods of Measuring Scorch and Cure Characteristics. *Polymer Testing*, **1995**, *14* (1), 45–84. https://doi.org/10.1016/0142-9418(95)90615-N.

[198] De Falco, A.; Marzocca, A. J.; Corcuera, M. A.; Eceiza, A.; Mondragon, I.; Rubiolo, G. H.; Goyanes, S. Accelerator Adsorption onto Carbon Nanotubes Surface Affects the Vulcanization Process of Styrene–Butadiene Rubber Composites. *Journal of Applied Polymer Science*, **2009**, *113* (5), 2851–2857. https://doi.org/10.1002/app.30261.

[199] Saatchi, M. M.; Shojaei, A. Effect of Carbon-Based Nanoparticles on the Cure Characteristics and Network Structure of Styrene–Butadiene Rubber Vulcanizate. *Polymer International*, **2012**, *61* (4), 664–672. https://doi.org/10.1002/pi.4132.

[200] Sadequl, A. M.; Ishiaku, U. S.; Ismail, H.; Poh, B. T. The Effect of Accelerator/Sulphur Ratio on the Scorch Time of Epoxidized Natural Rubber. *European Polymer Journal*, **1998**, *34* (1), 51–57. https://doi.org/10.1016/S0014-3057(97)00067-0.

[201] Rabiei, S.; Shojaei, A. Vulcanization Kinetics and Reversion Behavior of Natural Rubber/Styrene-Butadiene Rubber Blend Filled with Nanodiamond – the Role of Sulfur Curing System. *European Polymer Journal*, **2016**, *81*, 98–113. https://doi.org/10.1016/j.eurpolymj.2016.05.021.

[202] Weber, K.; Quicker, P. Properties of Biochar. *Fuel*, **2018**, *217*, 240–261. https://doi.org/10.1016/j.fuel.2017.12.054.

[203] Vélez, J. S.; Velásquez, S.; Giraldo, D. Mechanical and Rheometric Properties of Gilsonite/Carbon Black/Natural Rubber Compounds Cured Using Conventional and Efficient Vulcanization Systems. *Polymer Testing*, **2016**, *56*, 1–9. https://doi.org/10.1016/j.polymertesting.2016.09.005.

[204] Coran, A. Y. Vulcanization. In *Science and Technology of Rubber*; Elsevier, 1994; pp 339–385. https://doi.org/10.1016/B978-0-08-051667-7.50012-3.

[205] Rattanasom, N.; Saowapark, T.; Deeprasertkul, C. Reinforcement of Natural Rubber with Silica/Carbon Black Hybrid Filler. *Polymer Testing*, **2007**, *26* (3), 369–377. https://doi.org/10.1016/j.polymertesting.2006.12.003.

[206] Sholeh, M.; Rochmadi, R.; Sulistyo, H.; Budhijanto, B.; Virdhian, S. Nanostructured Silica From Bagasse Ash: The Importance of Mixing Parameters on Its Reinforcing Role in Natural Rubber Composite. *Arab J Sci Eng*, **2021**. https://doi.org/10.1007/s13369-021-05647-y.

[207] Fang, S.; Wu, S.; Huang, J.; Wang, D.; Tang, Z.; Guo, B.; Zhang, L. Notably Improved Dispersion of Carbon Black for High-Performance Natural Rubber Composites via Triazolinedione Click Chemistry. *Ind. Eng. Chem. Res.*, **2020**, *59* (48), 21047–21057. https://doi.org/10.1021/acs.iecr.0c04242.

[208] Tang, Z.; Zhang, C.; Wei, Q.; Weng, P.; Guo, B. Remarkably Improving Performance of Carbon Black-Filled Rubber Composites by Incorporating MoS2 Nanoplatelets. *Composites Science and Technology*, **2016**, *132*, 93–100. https://doi.org/10.1016/j.compscitech.2016.07.001.

[209] Dillon, J. H.; Prettyman, I. B.; Hall, G. L. Hysteretic and Elastic Properties of Rubberlike Materials Under Dynamic Shear Stresses. *Journal of Applied Physics*, **1944**, *15* (4), 309–323. https://doi.org/10.1063/1.1707434.

[210] Hentschke, R. The Payne Effect Revisited. *Express Polymer Letters*, **2017**, *11* (4), 278–292. https://doi.org/10.3144/expresspolymlett.2017.28.

[211] Warasitthinon, N.; Genix, A.-C.; Sztucki, M.; Oberdisse, J.; Robertson, C. G. The Payne Effect: Primarily Polymer-Related or Filler-Related Phenomenon? *Rubber Chemistry and Technology*, **2019**, *92* (4), 599–611. https://doi.org/10.5254/rct.19.80441.

[212] Gent, A. N. Extensibility of Rubber under Different Types of Deformation. *Journal of Rheology*, **2005**, *49* (1), 271–275. https://doi.org/10.1122/1.1835343.

[213] Smith, T. L.; Dickie, R. A. Effect of Finite Extensibility on the Viscoelastic Properties of a Styrene–Butadiene Rubber Vulcanizate in Simple Tensile Deformations up to Rupture. *Journal of Polymer Science Part A-2: Polymer Physics*, **1969**, *7* (4), 635–658. https://doi.org/10.1002/pol.1969.160070404.

[214] Huang, M.-F.; Yu, J.-G.; Ma, X.-F. Studies on the Properties of Montmorillonite-Reinforced Thermoplastic Starch Composites. *Polymer*, **2004**, *45* (20), 7017–7023. https://doi.org/10.1016/j.polymer.2004.07.068.

[215] Ge, X. C.; Li, X. H.; Zhu, Q.; Li, L.; Meng, Y. Z. Preparation and Properties of Biodegradable Poly(Propylene Carbonate)/Starch Composites. *Polymer Engineering & Science*, **2004**, *44* (11), 2134–2140. https://doi.org/10.1002/pen.20219.

[216] Xu, T.; Jia, Z.; Li, J.; Luo, Y.; Jia, D.; Peng, Z. Study on the Dispersion of Carbon Black/Silica in SBR/BR Composites and Its Properties by Adding Epoxidized Natural Rubber as a Compatilizer. *Polymer Composites*, **2018**, *39* (2), 377–385. https://doi.org/10.1002/pc.23946.

[217] Warasitthinon, N.; Robertson, C. Interpretation of the Tand Peak Height for Particle-Filled Rubber and Polymer Nanocomposites with Relevance to Tire Tread Performance Balance. *Rubber Chemistry and Technology*, **2018**, *91*. https://doi.org/10.5254/rct.18.82608.

[218] Bashir, M. A. Use of Dynamic Mechanical Analysis (DMA) for Characterizing Interfacial Interactions in Filled Polymers. *Solids*, **2021**, *2* (1), 108–120. https://doi.org/10.3390/solids2010006.

[219] Jiang, C.; Zhang, Y.; Ma, L.; Zhou, L.; He, H. Tailoring the Properties of Ground Tire Rubber/High-Density Polyethylene Blends by Combining Surface Devulcanization and

in-Situ Grafting Technology. *Materials Chemistry and Physics*, **2018**, *220*, 161–170. https://doi.org/10.1016/j.matchemphys.2018.08.040.

[220] Sattar, M. A.; Patnaik, A. Role of Interface Structure and Chain Dynamics on the Diverging Glass Transition Behavior of SSBR-SiO2-PIL Elastomers. *ACS Omega*, **2020**, *5* (33), 21191–21202. https://doi.org/10.1021/acsomega.0c02929.

[221] Scurati, A.; Lin, C. J. The Hysteresis Temperature and Strain Dependences in Filled Rubbers. *Rubber Chemistry and Technology*, **2006**, *79* (1), 170–197.

[222] Flanigan, C. M.; Beyer, L.; Klekamp, D.; Rohweder, D.; Stuck, B.; Terrill, E. R. Comparative Study of Silica, Carbon Black and Novel Fillers in Tread Compounds; Cleveland, OH, 2011; p 32.

[223] Shim, T.; Yoo, J.; Ryu, C.; Park, Y.-K.; Jung, J. Effect of Steam Activation of Biochar Produced from a Giant Miscanthus on Copper Sorption and Toxicity. *Bioresource Technology*, **2015**, *197*, 85–90. https://doi.org/10.1016/j.biortech.2015.08.055.

[224] Shao, J.; Zhang, J.; Zhang, X.; Feng, Y.; Zhang, H.; Zhang, S.; Chen, H. Enhance SO2 Adsorption Performance of Biochar Modified by CO2 Activation and Amine Impregnation. *Fuel*, **2018**, *224*, 138–146. https://doi.org/10.1016/j.fuel.2018.03.064.

[225] Pallarés, J.; González-Cencerrado, A.; Arauzo, I. Production and Characterization of Activated Carbon from Barley Straw by Physical Activation with Carbon Dioxide and Steam. *Biomass and Bioenergy*, **2018**, *115*, 64–73. https://doi.org/10.1016/j.biombioe.2018.04.015.

[226] Xu, Z.; He, M.; Xu, X.; Cao, X.; Tsang, D. C. W. Impacts of Different Activation Processes on the Carbon Stability of Biochar for Oxidation Resistance. *Bioresource Technology*, **2021**, *338*, 125555. https://doi.org/10.1016/j.biortech.2021.125555.

[227] Ahiduzzaman, Md.; Sadrul Islam, A. K. M. Preparation of Porous Bio-Char and Activated Carbon from Rice Husk by Leaching Ash and Chemical Activation. *SpringerPlus*, **2016**, *5* (1), 1248. https://doi.org/10.1186/s40064-016-2932-8.

[228] Ma, Y.; Chen, S.; Qi, Y.; Yang, L.; Wu, L.; He, L.; Li, P.; Qi, X.; Gao, F.; Ding, Y.; et al. An Efficient, Green and Sustainable Potassium Hydroxide Activated Magnetic Corn Cob Biochar for Imidacloprid Removal. *Chemosphere*, **2022**, *291*, 132707. https://doi.org/10.1016/j.chemosphere.2021.132707.

[229] Peng, H.; Gao, P.; Chu, G.; Pan, B.; Peng, J.; Xing, B. Enhanced Adsorption of Cu(II) and Cd(II) by Phosphoric Acid-Modified Biochars. *Environmental Pollution*, **2017**, *229*, 846–853. https://doi.org/10.1016/j.envpol.2017.07.004.

[230] Sun, J.; He, F.; Pan, Y.; Zhang, Z. Effects of Pyrolysis Temperature and Residence Time on Physicochemical Properties of Different Biochar Types. *Acta Agriculturae Scandinavica, Section B — Soil & Plant Science*, **2017**, *67* (1), 12–22. https://doi.org/10.1080/09064710.2016.1214745.

[231] Coran, A. Y. Chapter 7 - Vulcanization. In *The Science and Technology of Rubber (Fourth Edition)*; Mark, J. E., Erman, B., Roland, C. M., Eds.; Academic Press: Boston, 2013; pp 337–381. https://doi.org/10.1016/B978-0-12-394584-6.00007-8.

[232] Lewis, C.; Buanpa, R.; Kiatkamjornwong, S. Effect of Rubber Ratio, Carbon Black Level, and Accelerator Level on Natural Rubber/Bromobutyl Rubber Blend Properties. *Journal of Applied Polymer Science*, **2003**, *90* (11), 3059–3068. https://doi.org/10.1002/app.13036.